Test the potential of using riparian forests to reduce wave load and optimize dike design

B.T.F. Scheel

Delft University of Technology

MSc Thesis - Hydraulic Engineering

TUDelft

Deltares

Test the potential of using riparian forests to reduce wave load and optimize dike design

By

B.T.F. Scheel

in partial fulfilment of the degree of Master of Science at the

Delft University of Technology

Faculty of Civil Engineering and Geosciences

Thesis committee:	Dr. ir. B.K. van Wesenbeeck	TU Delft, Deltares	Chair
	Dr. ir. B. Hofland	TU Delft	Supervisor
	Ir. S. Kalloe	TU Delft	(Daily) Supervisor
	Dr. Ir. J.P. Aguilar-López	TU Delft	Supervisor

Student number:	4717252	
Project duration:	September, 2023 - August, 2024	

Preface

I am pleased to present the results of my research into the potential of using riparian forests to reduce wave loads and optimize dike design. This thesis has been submitted in partial fulfilment of the degree of Master of Science in Hydraulic Engineering at Delft University of Technology. The research was carried out in collaboration with Deltares, a knowledge institute for innovative solutions in the field of water and subsurface.

In particular, I would like to thank Su Kalloe for her weekly supervision meetings to brainstorm about all the different angles of approach, and for the excellent guidance and inspiration she provided during these meetings. I'm also very grateful to Bregje van Wesenbeeck for her professional and precise feedback and for giving me the opportunity to carry out this research within Deltares. I would also like to thank Bas Hofland for his professional view on the topics studied and his enthusiasm during the meetings to discuss the progress and results of the work done. Finally, I would like to thank Juan Pablo Aguilar-López for sharing his knowledge on the probabilistic and programming parts of this research and for the most useful explanations and sparring sessions on the methods to be used.

Finally, I would like to thank my parents and my sister for their love, support and belief in me. This has helped me to achieve the goals I have set for my thesis and to make it a success. I would also like to thank my friends for their daily support and for keeping my spirits up. Finally, I'd like to thank my girlfriend for her endless support and love throughout this journey. Her patience and encouragement throughout this process has been a constant source of motivation and strength for me.

Bart Scheel
Delft, August 2024

Summary

Known for its low-lying, flood-prone geography and rivers that find their way to the sea, the Netherlands has a history of flooding. The flood events of the 1990s, which resulted in large-scale evacuations, led to a change in focus from primarily strengthening dikes to creating more space for the river to flow and storing water to prevent repetition of these events. With changing climate conditions, rising water levels, land subsidence and sediment supply issues, there is a need to periodically assess the safety level of these primary flood defences. The last periodical assessment of the safety level of the dikes using the new assessment methodology, which tests the dikes based on the probability of flooding, identified numerous dikes that do not meet the required safety level. These insufficiently safe sections will need to be redesigned and reinforced, providing opportunities for innovative and environmentally friendly solutions.

Previous research has extensively investigated the ability of different types of ecosystems, such as salt marshes, mangroves and willow forests, to attenuate incoming waves and reduce wave loading on coastal and riverine structures. Various approaches have been used to model wave attenuation, including field studies, laboratory experiments and numerical simulations. These studies have found that vegetation can significantly dissipate wave energy, thereby reducing the impact on flood defences. The difficulty with using vegetation as a protective measure is its dynamic and uncertain behaviour, which created the need to improve the reliability of using vegetation.

While a general agreement can be observed in the literature on the beneficial effects of vegetation on wave attenuation, the reliability of these effects on failure probabilities remains an area requiring further investigation. This thesis investigates the potential of using riparian forests for wave attenuation and dike design optimisation. The main objective is to investigate how wave attenuation by riparian forests can improve dike safety and to identify the sensitive variables that most significantly affect the probability of flooding. The key research questions in this thesis are therefore related to 'How can wave attenuation contribute to dike design and safety assessment?', and, 'What are the key variables that influence the probability of flooding?'

Vegetated foreshores can reduce the wave height of incoming waves. Therefore, implementation of vegetated foreshores in the calculation of failure probabilities of wave-related failure mechanisms, can have a positive effect on the dike design and safety assessment. Erosion of the outer slope of a grass dike due to wave impact and wave run-up could potentially benefit from the protection of a forest. To test this, a model is created that combines the current used models for wave impact and run-up with the wave energy balance including the energy dissipation term due to vegetation. The combined models are subjected to a Monte Carlo simulation to produce the probability of failure for erosion of the outer grass slope due the two wave load mechanisms. The model also determines the sensitivity for each input parameter to identify the key variables of the system. The model analyses a dike section of route 10.3, a dike near the town of Kampen.

The results indicate that the presence of riparian forests can significantly reduce the impact of waves on dikes, mainly through the effects of the frontal-surface area, which contributes for 50 % to the result of the model, and the length of the forest, which contributes between 15% and 25%. To be effective, the combination of forest length, frontal-surface area and stiffness must be large enough. The results suggest that by strategically placing trees with the largest frontal-surface area at the height where the highest probability of failure, e.g. wave loading, occurs, the probability of failure can be significantly reduced. For the case study carried out, the results show that a forest on the foreshore is able to bring a dike section to the required level of safety, where it is not safe in the absence of a forest.

However, the challenges posed by the dynamic and uncertain nature of ecosystems are important points for further research. Different models can be used to investigate the importance of variables that were left out of the scope, or modelling different case studies and scenarios can lead to greater support for the results of this research. Despite these challenges, this research shows that riparian forests can be an effective complement to traditional dike strengthening measures. By reducing the reliance on hard revetments, these green solutions offer a more sustainable and cost-effective approach to flood protection.

In conclusion, this thesis provides an insight into the use of riparian forests to increase the level of dike safety. The research confirms that vegetated foreshores have the potential to be integrated into the current flood defence framework and provide a viable solution for dike sections that do not meet safety standards due to wave related failure mechanisms. The results support the potential of riparian forests to optimise dike design and contribute to a more resilient and environmentally friendly flood protection strategy in the Netherlands.

Contents

<div align="right">

1

</div>

Introduction

The topic of this research is the effect of riparian forests on waves, and thereby wave loads and dike design. First a theoretical analysis is performed on the method of dike design in the Netherlands, and which mechanisms are affected by the appearance of riparian forests in front of river dikes. Additionally, a probabilistic model of a riparian forest on the foreshore of a dike is made to get insight in the sensitive components of forests, waves and dikes. This chapter describes and defines the problem on which this research is based and the objectives of this research.

1.1. Relevance of research

The Netherlands is a low-lying, flood-prone country, where rivers find their way to the sea (RWS 2022a; Gerritsen 2005). In 1993 and 1995, extreme rainfall and high amounts of melt water caused very high water levels in the Dutch rivers (RWS n.d. Burgers 2014). The fear of failure of the dike led to evacuation of thousands of citizens in 1993. Two years later, in 1995, high water levels in the Meuse river flooded large areas in the province of Limburg (RWS n.d.). The high water events in the Dutch rivers led to the Law for Temporary Dike Enhancements (Burgers 2014), to help prevent repetition of the events in the 90s. From 2000 onwards, a new method of high water protection was introduced. Instead of just looking at dike strengthening, creating more room for the river to flow and store water formed the new starting point for future projects (RWS n.d.).

Each location along the Dutch rivers provides different opportunities to create more room for the river to flow, or the enhance the strength of the dike(RWS n.d.). For example, at one location dikes can be moved in landward directions, where at other locations lowering the foreshore is more effective. Although more room for the river is created, the safety level of the dikes still need to be large enough to withstand extreme events.

Therefore, periodically assessment of the safety level of the dike trajectories are performed (de Bruin et al. 2016). Studies such as Mapping Safety in the Netherlands (Dutch: Veiligheid Nederland in Kaart) (Vergouwe et al. 2014), and projects as the Flood Protection Program (Dutch: Hoogwaterbeschermingsprogramma [HWBP]) have assessed the probability of flooding along the dikes in the Netherlands and focused on how to decrease this probability for the dikes that do not meet the required safety standard (HWBP 2023).

Dike trajectories that do not meet the required safety standard require strengthening and need to be redesigned, which creates opportunities for innovative and greener solutions that help reduce the probability of flooding and increase their value as green infrastructure (Schoonees et al. 2019). The assessment and design of these trajectories are performed following the standards and guidelines provided by the Assessment and Design Instrument (Dutch: Beoordelings- en Ontwerp Instrumentarium [BOI]) (IPLO 2023).

Various methods are being researched to increase the strength of the dike, e.g. new revetment types,

or to reduce the load on the dike, e.g. detached structures or forests in front of the original dike. Reducing loads on a dike can be a promising measure to decrease the flood probability of a dike trajectory without the need of using expensive, eco-unfriendly reconstructions of the existing dike. The ability of forests to attenuate incoming waves, and reduce the wave load on dikes, is a topic that has been studied from different perspectives over the last decade. Hasselmann and Collins (1968) focused on predicting wave attenuation by vegetation fields by increasing the soil friction coefficient. Another approach was introduced by Dalrymple et al. (1984), who modelled the vegetation as an array of cylinders and assessed the wave force on these cylinders.

Möller et al. (2002) were one of the first researchers to investigate the effect of salt marsh vegetation on wave dissipation using a combination of field and numerical studies. van Wesenbeeck et al. (2022) showed that for willow forests under extreme wave conditions, the reduction of wave impact and run-up depends on: (i) wave height and length, (ii) vegetation surface area, and (iii) movement of vegetation branches. Kalloe et al. (2022) demonstrated the need for a more thorough quantification of vegetation parameters, such as frontal surface area, in the process of determining wave attenuation under extreme conditions. Vuik, van Vuren, et al. (2018) focused on the method for assessing the probability of failure of a hybrid flood defence consisting of a dike with a vegetated foreshore, and Vuik, Suh Heo, et al. (2018) added a failure mode to vegetation by modelling stem break.

The different effects and the degree of effectiveness of, for example, salt marshes, riparian forests and vegetated foreshore systems have been extensively studied. The results of these studies, e.g. by Vuik, van Vuren, et al. (2018), proved that salt marsh vegetation on a foreshore does influence the incident waves approaching a flood defence. This formed the foundation to further research the effects that different vegetation types can have on the wave height of incident waves, and the probability of failure as a result of wave-related failure mechanisms.

1.2. Problem definition

Previous research has provided many promising insights in the application of vegetation on the foreshore of flood defences to reduce the wave load, and probability of failure of the defence. Further research into the effects on failure probabilities is necessary in order to, in the end, incorporate the effects of vegetated foreshore into dike design and flood risk assessment standards. Therefore, a more thorough reliability assessment and testing to engineering standards for flood probability is required (Bilkovic et al. 2017; van Wesenbeeck et al. 2014). The research carried out on the effect of nature-inclusive coastal protections by Bilkovic et al. (2017) has led to the following problem definition:

Incorporating the protective services of riparian forests into the assessment methodology of flood defences is difficult because the dynamic and uncertain character of ecosystems reduces the reliability of the defence system.

The problems stated above created the foundation for the scope of this research, since the reliability of a nature-inclusive flood defences can be improved by performing probabilistic assessments of the probability of flooding. These assessments provide insight into the sensitive elements of a flood defence and the statistical and physical correlation between the different strength or load parameters. This helps to identify where and how vegetation can have the most significant impact on the design of a hybrid flood defence and where they can be incorporated into the existing design methodology.

Clarification of mentioned elements:

- **Ecosystem-based flood defence:** is a flood defence that by creation or restoration of an ecosystem can provide an alternative or additional protection against floods (Temmerman et al. 2013). In other words, ecosystem-based flood defences use the protective ecosystem services to decrease the probability of flooding. The applicability of these defences are depending on the location of the defence and the normative load case for that location.
- **Probabilistic assessment:** is the method used to assess the probability of flooding of a flood defence system using the various failure mechanisms of the system and to identify which components contribute most to these mechanisms.
- **Statistical correlation:** describes the correlation between model variables and data sets. This type of correlation may be the result of similar underlying principles or common use of the variables (Atmanspacher et al. 2019).
- **Physical correlation:** describes the interaction of different physical components that influence each other's behaviour (Oestges et al. 2001). An example of this phenomenon may be that a reduction in crest height due to subsidence may result in more overtopping discharge, or more related to this research, wave heights that exceed the occurring water depths.

1.3. Research questions and approach

The scope of this research is to *to test the potential of using riparian forests to reduce wave load and optimize dike design*. This is done by performing a literature study the dike design and assessment process in the Netherlands, to show how the effect of vegetation fits into the process, and how to model the wave load taking vegetation into account.

Combining the literature on dike design/assessment with the literature on wave dampening by vegetation, a model is created and validated to model erosion of the outer slope due to the incoming waves, comparing the situation with and without a forest. The model is used to perform a probabilistic analysis to investigate the effects that a willow forest can have on the wave load on the dike slope, and the probability of failure due to wave related failure mechanisms. The probabilistic analysis consists of the assessment of the erosion of the outer grass slope of a river dike in the Netherlands. The modelled forest in front of the dike consist of willow trees due to their relative high occurrence in the Netherlands, and the large amount of knowledge of there behaviour during (extreme) wave load events (van Wesenbeeck et al. 2022).

A more clear overview of each approach with their according research questions are defined below:

1. Perform a literature study to the current design methodology, the design/implementation requirements for vegetated foreshores and the methodologies for probabilistic risk assessment.

   (a) What is the current methodology for designing dikes in the Netherlands?
   (b) How is the probability of flooding for a dike modeled?
   (c) How does vegetation attenuate wave load on a dike?
   (d) How can wave attenuation due to vegetation be incorporated in the design/assessment standards?

2. Develop a model to model the probability of failure of a hybrid river dike under wave loading.

3. Perform a probabilistic analysis for a river dike with a vegetated foreshore

   (a) What are the distributions for the model variables?
   (b) What are the sensitive variables, that have the greatest impact on the probability of flooding?
   (c) How is the probability of failure of the dike influenced by the presence of a forest?

1.4. Report outline

Chapter 2	**Literature study**	This chapter introduces the following subjects for understanding the performed research: dike design/assessment methods used in the Netherlands, assessment of the grass revetment due to wave impact and wave run-up, the theory behind wave attenuation, and the theory used to perform a probabilistic analysis.
Chapter 3	**Methodology**	This chapter describes the designed model by means of the framework as presented in figure 3.1. Secondly, the model input used in this case is presented, and finally the case location for the assessment is described.
Chapter 4	**Model validation**	This chapter compares the results of the model with the current-used software for grass revetment erosion to validate the model. Furthermore, the wave energy dissipation model is validated using the results from the large-scale flume tests performed on willow trees.
Chapter 5	**Results**	This chapter provides the results for simulation that is performed in this research. This is divided into the analysis of the probability of failure due to erosion of the grass revetment, and the sensitivity analysis of the input parameters.
Chapter 6	**Discussion**	This chapter discusses the meaning and significance of the results presented in the chapter 5. Followed by a discussion of how vegetated foreshores can be implemented in safety assessments and dike design.
Chapter 7	**Conclusion**	In the conclusion, the main research questions are answered to come to a conclusion on the main objective of this research.
Chapter 8	**Recommendations**	The conclusion is followed by the recommendations for further research related to the scope of this research, and implementation of vegetated foreshores in the safety assessment.

Literature study

The Netherlands continues to enhance its methodology for designing dikes to remain protected against rising sea levels and increased flood risks. This literature study studies the current methodology for dike design in the Netherlands, focusing on the key design parameters, the role that vegetation can fulfil within that methodology, and the theory of probabilistic modelling of flood risks. Research towards these aspects results in a comprehensive understanding of how innovative solutions to flood probability using natural elements can improve the safety of flood protections bordering the Dutch rivers.

2.1. Dike design/assessment methods

Designing a dike is not a straightforward method. There are many iterative steps, and a lot of different stakeholders involved in the process. The primary function of a dike is on the other hand rather clear: prevent the hinterland from flooding. In this section, the history behind the creation of the Dutch dike system is introduced first. Secondly, the different dike components of a standard dike cross-section are introduced and the failure mechanisms related to a standard dike are addressed. Finally, the current-used design method for flood defences in the Netherlands, and how it is formed to be as it is today, is described.

2.1.1. History

The Netherlands has been in a battle with water for as far as history goes back. The behaviour of rivers and sea have always been of large influence on the formation of the land, but also on the society (Tockner et al. 2002). Through the years, the appearance of flood defences and the way of they are designed changed a lot, and to be resilient against future threats, it will keep on changing and improving in the future.

Around 500 BCE, the Northern parts of the Netherlands started to create artificial dwelling mounds and small soil bodies around farmland. Early in the 12th century, these individual soil bodies were slowly connected to each other, which created the first dike rings in the Netherlands (van Baars 2009). Most were too steep, too low, contained too much peat or had insufficient slope protection (van Baars 2009). The size of these relative small dike rings increased through time, and eventually outgrew the management capabilities of the villages, which resulted in the establishment of the first waterboards in the Netherlands (Arnold et al. 2009).

A step forward in time to 1900, studies were performed on the closing of the Southern Sea (Dutch: Zuiderzee) with as main goal the effects on land reclamation, flood protection and shortening of the coastline. In 1916 the Southern Sea flood changed the perspective on the effects on flood protection found in the studies, and in 1918 the decision to close the Southern Sea and reclaim certain areas was made. This resulted the Southern Sea defence (Dutch: Zuiderzeewerken) with the Afsluitdijk (English: Closing barrier) as the best-known structure.

Not only the coastal areas of the Netherlands are prone to flooding, also the flood safety of the river areas is of major importance. Rivers tend to change path regularly, which can still be observed in the soil structure around the current river paths (van Baars 2009). From history, the waterboards tried to manage water towards the river by placing dikes perpendicular to the flow path of smaller streams. Through time, these dikes connected and created larger defence structures that are still maintained and improved today (HWBP 2023). A good example of managing the behaviour of the river is the Pannerdensch Canal, which had the original purpose of transporting more water from the Upper-Rhine to the Lower-Rhine and IJssel river. Initially, more water was going into the canal, resulting in dike breaches along the Lower-Rhine. To cope with this, another canal (the Bijlands Canal), an extra IJssel estuary and the Pannerdensche Kop (a bifurcation splitting the Upper-Rhine into the Waal river and the Pannerdensch canal) were created. These measures created a more stable distribution of water over the Waal and Pannerdensch canal.

Two of the most well-known coastal floods in the Netherlands are the Saint-Elizabeths flood from 1421, which was the result of dike breaches and floods in South-Holland and Zeeland, and the North Sea flood from 1953, which was the result of a storm surge hitting the coastline of Zeeland (Gerritsen 2005).
The 1953 flood resulted in the establishment of the Delta Committee and Delta Program. The committees, and program, primary tasks was to prevent similar flood events to happen in the future (HWBP 2023). Based on the advise of this committee the Delta defence (Dutch: Deltawerken) were constructed, consisting of multiple dams and flood barriers, from which the Eastern Scheldt barrier (Dutch: Oosterscheldekering) is one of the most well-known barriers (HWBP 2023).

During the 90s, due to extreme rainfall and run-off due to melt water, high water levels occurred in the Dutch river areas (RWS n.d. Burgers 2014). In 1993, it did not come to a flood event, but the fear of flooding of the neighbouring areas led to evacuation of 12,000 citizens (RWS n.d.). Two years later, a similar high water event resulted in flooding of large areas of the province of Gelderland. Close to 250,000 citizens and 1 million animals needed to be evacuated.

To help prevent against repetition of these high water flood events, the government implemented the Law or Temporary Dike Enhancements (Burgers 2014). Following this low, from the 00s onwards, a new point of view towards high water protection was formed. The focus shifted from reinforcing the river dikes, to also create more room for the river to flow and store its excess water (RWS n.d.).

Figure 2.1: The village of Itteren (Limburg) during the 1995 flood event (Eyck 1995)

2.1.2. Dike components
Flood defences are long, interconnected systems with multiple trajectories that can fail due to different failure mechanisms. The term flood defence is a broad concept including all types of structures designed to retain water and prevent against flood events. The primary flood defence systems, in the Netherlands referred to as *dike rings*, are flood prone areas under protection of flood defences or higher grounds. Dike rings are divided into smaller parts, called *dike trajectories*, defined as a collection of smaller dike sections for which failure of a section results in a similar type of flooding/amount of casualties. These *dike sections* are parts of a trajectory with more or less uniform characteristics (e.g.

geometry, orientation, hydraulic load, etc.). For the assessment of a dike, a 2D representation of the uniformity of a dike section is used, referred to as *cross-sections* (Jonkman, Jorissen, et al. 2021). An overview of the individual components of a dike ring is presented in figure 2.2.
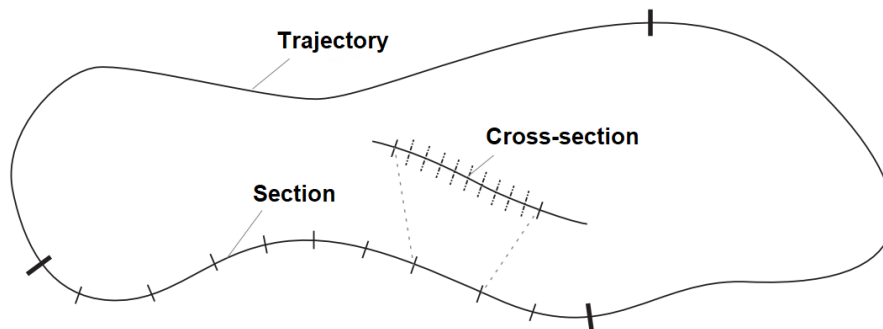
Figure 2.2: Clarification dike ring components (van der Krogt 2022)

Every type of flood defence has different applications and consists of many components, and each component has different properties adding different strengths (or weaknesses) to a flood defence. In this study, the focus lies specifically on the design of river dikes. To assess the level of safety, or in other words, probability of flooding, it is important to define the different components in advance.

A dike is a flood defence and should therefore be conform the safety norm against flooding in order to withstand extreme hydraulic loads that could lead to severe flood events. Sufficient stability and impermeability are necessities for a dike in order to reach the safety norm. Hydraulic loads can be high water levels, wave attack (wave impact, wave run-up and overtopping) (Jonkman, Jorissen, et al. 2021).

In general, the outer parts of a dike (dike cover) consist of a revetment from hard (concrete/rock) or soft (grass/bush) revetment components, to protect the dike core from wave load. Since the focus of this study is erosion of the outer slope, the type of revetment on the outer dike slope is of great importance. To test the potential of a riparian forest, it is desired to test the effect on soft revetments first, in order to prevent the use of harder revetments. Reducing the amount of load can influence the choice between the harder and soft revetments, affecting the costs of the defence (van Zelst et al. 2021).

The inner parts of the dike can also be protected with a revetment to protect against instability, piping and overtopping (Jonkman, Jorissen, et al. 2021).
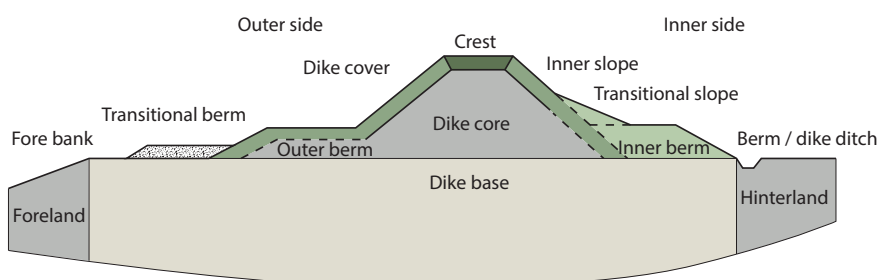
Figure 2.3: General dike anatomy with the most important components (based on (Jonkman, Jorissen, et al. 2021))

The core and base of the dike properties are related to the type of soil present. There is no soil type that possesses all the properties needed for a solid dike (Jonkman, Jorissen, et al. 2021). For stability, sand and gravel are the most suitable soil type, but the downside is their high permeability. Peat and clay on

the other hand possess a low permeability, but are unstable, and for peat the possibility of shrinkage is a danger when it gets dry (van Baars 2004). This makes them less suited for dike structures. Accordingly, the best solution is to use the strengths and weaknesses of different soil types, to strengthen each other (Jonkman, Jorissen, et al. 2021). This type of enforcing can be compared to reinforced concrete, where both materials have opposing characteristics, but together result in a stronger material.

2.1.3. Failure mechanisms

Dikes and other flood defences all serve the same purpose, but are all implemented in different environments. This results in different load and resistance combinations for each structure. The differences in load and resistance results in a variety of failure mechanisms that can occur (Jonkman, Jorissen, et al. 2021). Most of the failure mechanisms are related to hydraulic loads (water level or wave attack), but soil-related instabilities may also occur. Knowing which failure mechanism is induced by which load or related to certain strengths or weaknesses of dike components is important information for the assessment the probability of flooding.In figure 2.4 the most encountered failure mechanisms for dikes are displayed based on Jonkman, Jorissen, et al. (2021).
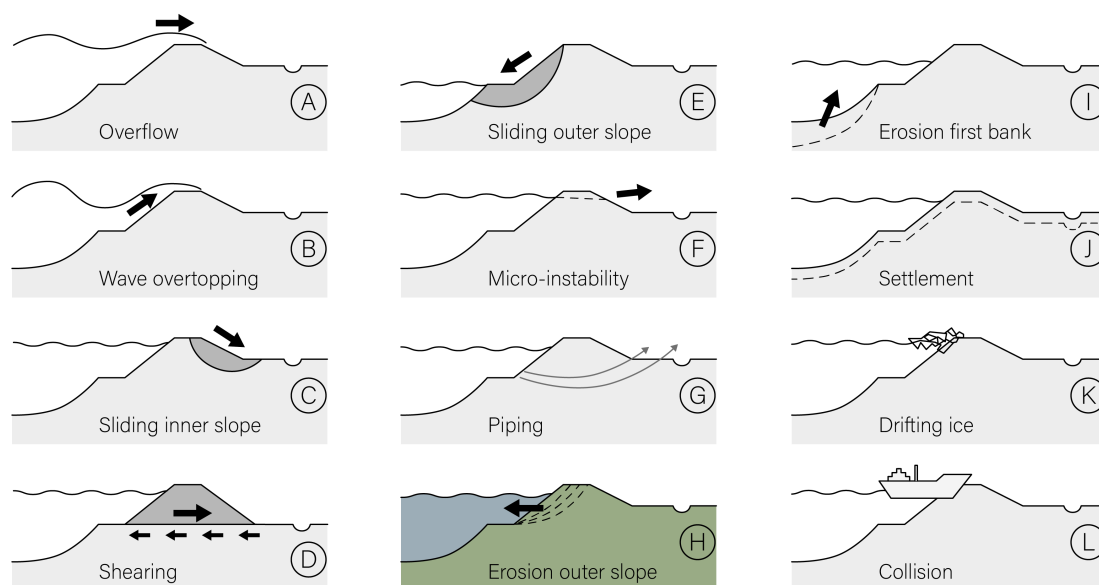
Figure 2.4: Overview of the most encountered failure mechanisms (Jonkman, Jorissen, et al. 2021)

The schematic overview in figure 2.4 illustrates how each failure mechanism behaves, and some more extensive information is given on each mechanism below.

A. **Overflow:** occurs when the still water level exceeds the crest level of the defence.
B. **Overtopping:** occurs when the water level is below the crest level, but the wave run-up rolls over the defence.
C. **Sliding (inner slope):** the soil of the inner slope becomes saturated, pore pressure increases, effective stress reduces and unstable sliding planes can occur.
D. **Shearing:** is a similar mechanism to sliding of the inner slope, but the sliding plane occurs along the base of the dike.
E. **Sliding (outer slope):** this can occur when the water level drops relatively quick, which leaves the pore pressure high and effective stress low. The same sliding planes as sliding of the inner slope now occur on the outside.
F. **Micro-instability:** is a mechanism that can occur when the phreatic surface in the body of the dike rises and seepage water reaches the inner slope of the dike.
G. **Piping:** also called internal erosion, is the mechanism where seepage paths flow under/through the dike body towards the water. This can result in collapse or sliding of the structure.

H. **Erosion (outer slope):** is a mechanism that may occur over time, when the revetment of the structure is eroded away and the loads slowly weaken the structure.

I. **Erosion (first bank):** when the water erodes the foreshore a structure, the slopes can become to steep, making the structure unstable.

J. **Settlement:** some areas can be prone to subsidence and consolidation. When the structure settles to much, the crest level can become too low and overflow and overtopping may occur to often.

K. **Drift ice:** excessive amounts of ice can block rivers and streams, leading to an increase of the water level, which leads to overflowing and overtopping.

L. **Collision:** a ship colliding with a dike is a possibility, but in most assessments and designs left outside the scope, since it is more relevant for locks and sluices. (Jonkman, Jorissen, et al. 2021)

Each of the described failure mechanisms contributes for a part to the probability of flooding of a structure. Therefore, the probability of flooding is distributed over the failure mechanisms using the probability factor ω (Jongejan, Diermanse, et al. 2020). For dike trajectories in the Netherlands, the distribution of failure probability factor ω is as presented in table 2.1.

Table 2.1: Distribution of failure probability factor ω (RWS 2017)

Flood defence	Failure mechanism	ω
Dike	Overflowing and Overtopping	0.24
	Piping and Micro-instability	0.24
	Macro-stability inner slope	0.04
	Erosion and Damage revetment	0.10
Structure	Closure fail	0.04
	Piping	0.02
	Construction fail	0.02
	Other	0.30
Total		**1.00**

Since the study is focused on testing the potential of vegetation to attenuate wave load and how it can optimize dike design, the failure mechanisms due to wave load on the outer slope: (i) wave impact and (ii) wave run-up are analysed further in this study.
Erosion of the outer slope is part of the probability factor for damage and erosion to the revetment. For grass revetments, the 0.10 from table 2.1 is distributed even further into 0.012 for failure of asphalt revetments, 0.045 for erosion of the grass revetment, 0.005 for sliding of the grass revetment, and 0.03 for instability of rock placements (de Bruin et al. 2016).

The components of flood defence structures and dike cross-sections and the failure mechanisms that results in failure of these structures are important in their assessment and design. The methods for assessment and design are described in the following section 2.1.4.

2.1.4. Safety standard
The method of design and assessment of a dike or other flood defence structure is a process that is constantly evolving. This is because the load and strength conditions for which a design is made, or on which it is based, are also constantly evolving. These changing conditions lead to outdated and obsolete methods, and are therefore required to be updated from time to time. In this section the previous-used assessment methods for flood defence structures in the Netherlands are explained.

The 1953 North Sea flood changed the perspective on flood safety. Before the flood, safety for structures relied on intuition or experience, setting dike crest levels based on the highest observed water levels plus a margin (Jonkman, Voortman, et al. 2018). After the flood, the Delta Committee proposed a uniform safety standard, aiming for a 1/125,000 annual risk in Central Holland, considering the potential losses of capital, lives, and societal breakdown (Jonkman 2007). This led to a shift in safety norm towards exceedance frequencies depending on each region's economic risk and flood consequences

(TAW 2000). This was incorporated in the 2006 Hydraulic Boundary Conditions, the predecessor of the current method.

The current used method emphasizes the probability of flooding due to various failure mechanisms rather than just water level exceedance (Jonkman, Voortman, et al. 2018). The current method, the 2017 Statutory Assessment Instrument (WBI2017), incorporates statistical uncertainties in hydraulic load predictions within probabilistic models, acknowledging the inherent uncertainties in extreme event forecasting (de Waal 2018).

The shift in flood safety standards from exceedance probabilities directly connected to risk towards implementing the maximum allowable probability of flooding between them creates a clearer connection between exceedance probabilities of load conditions and acceptable (societal) risk, as shown in Figure 2.5 (Jongejan and Calle 2013).
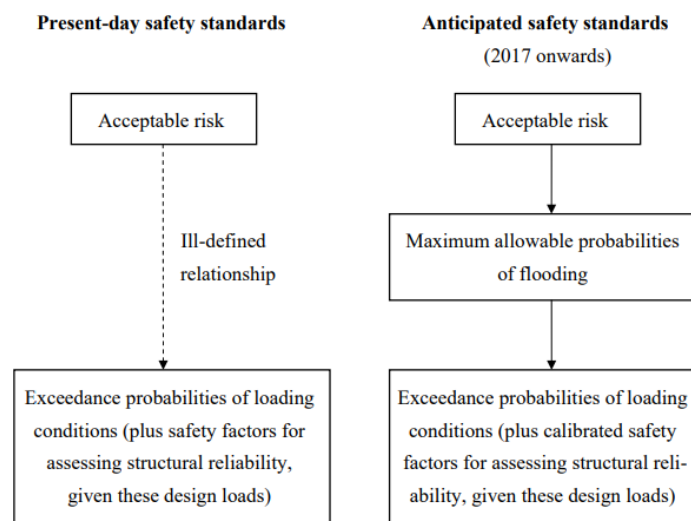
Figure 2.5: From acceptable risk to probabilities of flooding and probabilities of exceedance (Jongejan and Calle 2013)

So, currently the safety standards are expressed in terms of probability of flooding. The new safety standards are a result of a nationwide flood risk assessment in the Netherlands. In this risk assessment three criteria were assessed (Jonkman, Voortman, et al. 2018).

1. **Individual Risk:** areas with an individual risk above 10^{-5} per annum are considered insufficient safe, and higher safety standards were assigned in these areas (Jonkman, Voortman, et al. 2018). Individual risk is the annual probability of being killed by a flood at a certain location (Jonkman, Voortman, et al. 2018)

2. **Societal Risk:** research was done to find the areas with the highest contribution to national societal risk. For these areas a higher safety standard was proposed (Jonkman, Voortman, et al. 2018). Societal risk is generally expressed as the exceedance probability of an event that results in a certain number of fatalities (Jonkman, Voortman, et al. 2018).

3. **Economic Risk:** for every flood defence, an optimal level of protection was determined (Eijgenraam 2006), taking costs and decreasing risk into account. The economic risk is generally expressed as the likelihood of economic damages (Jonkman, Voortman, et al. 2018).

The assessment of the risks by Vergouwe et al. (2014) based on flood hazard analysis, reliability analysis of flood defence systems, breaching analysis, damage and loss of life estimations, and risk quantification created the foundation to the new safety standard (Jonkman, Voortman, et al. 2018).

The safety standard is used for two main purposes, and described in the Assessment- and Design Instrument [BOI], which is based on theory from the previous used instruments, and are further developed to meet the current requirements to assess and design with regards to the probability of flooding (BOI 2019).

    i **Statutory Assessment Instrument (WBI2017):** Assessment of the probability of flooding of a dike trajectory (de Waal 2018).

ii **Design Instrument (OI2014):** Designing a new dike section that meets the required safety level (RWS 2017).

The WBI is used to assess the safety of an existing flood defence by providing a procedure for determining the loads for different failure mechanisms and calculation regulations (de Waal 2018). The OI is used to design new flood defences or redesign defences that fail to meet the required safety standard by providing procedures to design dike elements for specific probabilities of failure per failure mechanism (RWS 2017).

The methods can either be used separately to assess or design a flood defence, but they can also be used in serie when the assessment shows that a flood defence does not meet the required safety level. This connection between the instruments is visualised in figure 2.6 by the dashed line.

In figure 2.6 the process diagram shows for each instrument what information is needed as input, what steps are taken and what the result of the process is.

Step A and B in the OI block are mentioned separately, because not every mechanism is designed according to the OI's new standard regarding probabilities of flooding. There are still some mechanisms of flood defences that need to be designed using the old guidelines, and are therefore represented by B in the figure (RWS et al. 2016).
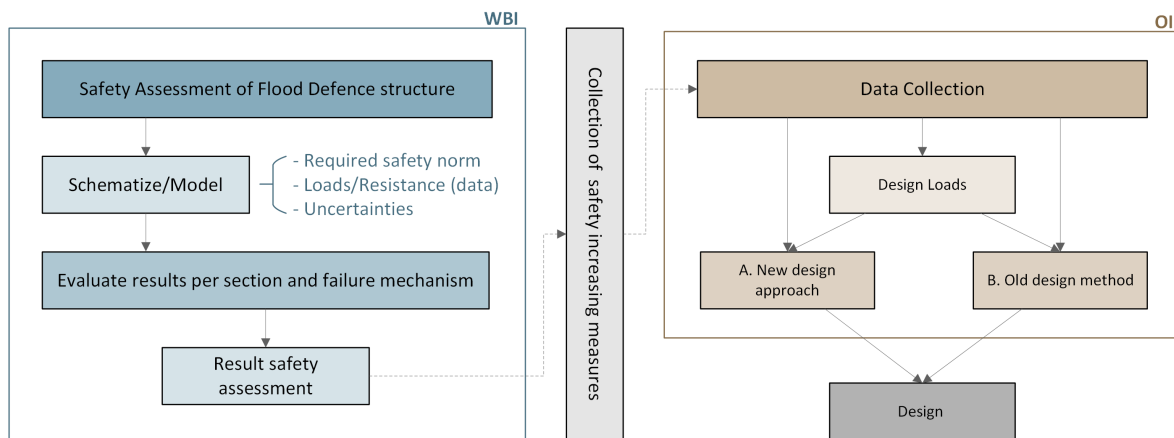
Figure 2.6: Process overview of WBI (based on (de Waal 2018)) and OI (based on (Kok et al. 2016; RWS et al. 2016; RWS 2017))

2.1.5. Probability of Flooding

The assessment or design of a flood defence, as a river dike, is all connected to the safety standard for the particular dike trajectory. This safety standard is referred to as a lower threshold (figure 2.7) of probability of flooding (D) that a dike trajectory may reach. Therefore, each dike trajectory is also assigned a signal value (B), from which preparations to reinforcement of the dike section need to start as soon as possible. Point (A) is a point where a decline in probability of flooding is noticed, but no measures need to be taken right away. The decline in safety is due to the increase of load, which is related to climate change (Kok et al. 2016), but also due to a decrease in strength of the structure, because of ageing. Point (C) is the point where the work on dike reinforcement commences, and point (E) is the new probability of flooding immediately after reinforcement (Kok et al. 2016). Points A-D can be linked to the assessment of dike trajectories by WBI in figure 2.6, and point E can be seen as the design standard for which a dike is designed by OI in the same figure.
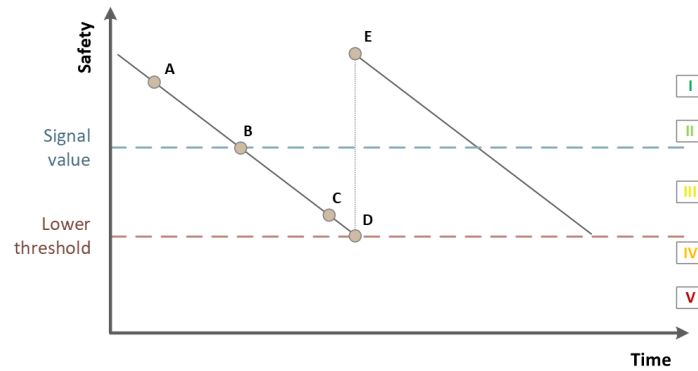
Figure 2.7: Visualisation of the probability of flooding (based on Kok et al. (2016))

For the assessment of a trajectory, the most efficient way is to dismantle the maximum probability of flooding into requirements for smaller independent elements, such as the different failure mechanisms and dike sections/cross-sections (van der Krogt 2022). Dismantling the probability of flooding is done by distributing the probability using the failure probability factor ω and the length-effect parameter N.

$$P_{req,section} = \frac{P_{max} \cdot \omega}{N} \tag{2.1}$$

Where $P_{req,cs}$ is the probability of failure per failure mechanism per cross-section (per year), P_{max} is the maximum allowed probability of flooding for a dike trajectory, (bottom line per year), ω is the failure probability factor, and N is the length-effect factor.

The probability factor ω, the distribution of probability of flooding, is already described in section 2.1.2. The length-effect parameter N is the other component that is used in the distribution of the probability of flooding and accounts for the weaker spots in a dike trajectory. The longer a trajectory becomes, the more sections it contains, which increases the probability that the trajectory contains a weaker section. The probability of flooding for a long dike trajectory is therefore higher than for a small dike trajectory, this is the definition of the length effect (Kok et al. 2016). The importance of the length effect is based on the spatially correlated loading conditions (Jongejan, Diermanse, et al. 2020), so for erosion-related failure the length effect is relative low with respect to geotechnical-related failure, because the loading conditions for erosion are less spatially correlated (Jongejan, Diermanse, et al. 2020). In other words, erosion related failure is a result of a more weakly spatial correlated load (waves) than, e.g., piping which is strongly spatial correlated due to the variability in soil properties (Jongejan, Diermanse, et al. 2020). The described method results in a distribution of the maximum allowed probability of flooding down to the failure probability per failure mechanism on cross-section level, which is visualised in figure 2.8.
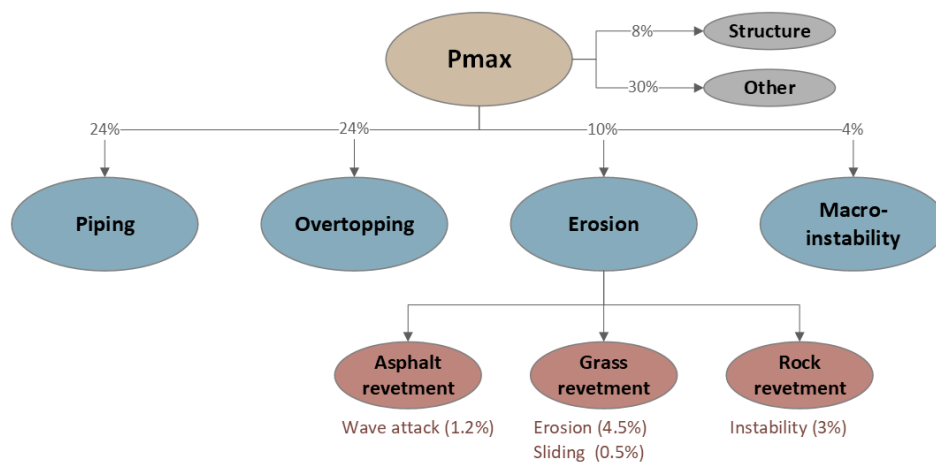
Figure 2.8: Generic fault tree for dikes in the Netherlands (Kok et al. 2016)

To categorize the safety of a dike section the WBI different categories of safety are described by de Waal (2018). These categories are found back in the nationwide flood risk assessment performed by Vergouwe et al. (2014), and are shown in table 2.2. These safety categories are also shown in figure 2.7, to indicate how the safety categories correspond to the signal value and the lower threshold.

Table 2.2: Category boundaries for the safety assessment on dike section level (de Waal 2018)

Category	Description	Lower boundary				Upper boundary
I	Meets signal value by a margin	0	$\leq$	$P_{req,section}$	$\leq$	$1/30 * \omega *$ signal value
II	Meets signal value	$1/30 * \omega *$ signal value	$\leq$	$P_{req,section}$	$\leq$	$\omega *$ signal value
III	Meets lower threshold, but not the signal value	$\omega *$ signal value	$\leq$	$P_{req,section}$	$\leq$	$\omega *$ lower threshold
IV	Does not meet signal value and lower threshold	$\omega *$ lower threshold	$\leq$	$P_{req,section}$	$\leq$	lower threshold
V	Does not meet signal value and lower threshold by a margin	lower threshold	$\leq$	$P_{req,section}$	$\leq$	$30 *$ lower threshold

To assess the probability of failure of grass revetments, the WBI includes an assessment method called the Grass Erosion Outer Slope (GEBU) that provides guidelines for modelling loading conditions on grass revetments. Two different loading conditions of particular interests for this research are loading due to wave impact (de Waal and Hoven 2015a) and wave run-up (de Waal and Hoven 2015b).

The modelling of wave impact and wave run-up as described in the GEBU, includes different equations and input parameters. To create more insight in these processes, they are explained in detail in the following section (section 2.2.1).

2.2. Assessment of grass revetments

The assessment of a dike regarding the erosion of the outer slope requires the calculation of the amount of load on, and the strength of the revetment. This is done following the guidelines from the GEBU as described by the WBI (de Bruin et al. 2016). In this section the assessment of erosion of grass revetments due to wave impact and wave run-up are described in detail.

The design of a dike against wave-related failure depends on three wave-structure interaction processes: wave impact, wave run-up/run-down and wave overtopping.

Figure 2.9 shows the transformation of (1) incident waves approaching the dike towards the processes where they can induce damage and eventually failure. The first interaction of a wave with the structure is when it breaks on the slope of the dike and results in (2) impact on the dike slope. After the breaking of incident waves and impact on the slope, the waves (3) run up the slope and either reach a certain run-up height and run back down the slope, or the wave reaches the crest height of the dike and (4) flow over the top of the dike. When overtopping occurs, the water starts to (5) run down the landward slope of the dike.

For these different wave-structure interactions, the WBI describes different levels of assessment. For this research, the considered processes for erosion of the outer slope of the dike are wave impact and wave run-up, explained in detail in section 2.2.1.
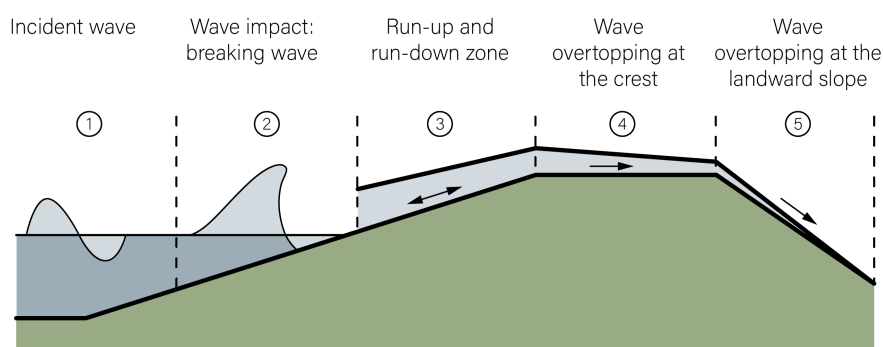
Figure 2.9: The main wave-structure interactions on a dike (van der Meer et al. 2018; Schüttrumpf 2001)

The WBI describes three steps of assessment, in increasing order of detail in calculation:

- **Elementary assessment:** contains a simple assessment of three key characteristics: (i) wave height, (ii) grass quality, and (iii) type of soil in dike core (de Waal 2018). If these characteristics do not fulfil, e.g., the wave height is already too large, the WBI moves on to the detailed assessment.
- **Detailed assessment:** takes prescribed calculations that need to be performed and contains defined standards that conclude whether the assessed location is sufficiently safe or not (de Waal 2018). The equations and theory from the detailed assessment are used in this study to perform the main objective of this research.
- **Customized assessment:** when the detailed assessment concludes that the location does not meet the required safety standards, a customized assessment can be carried out to perform additional calculations to investigate in more detail if the revetment does meet requirements (de Waal 2018).

2.2.1. Wave impact

The first interaction between incident waves and the dike is wave breaking, the result is a significant pressure on the dike slope which can lead to damage of the dike revetment. The magnitude of the damage depends on the force that waves are able to exert on the slope, and the strength of the revetment (e.g. which material covers the dike slope). For this research. the wave impact on grass slopes is the most relevant, and is explained in detail in this section.

For wave impact, the assessment is based on the resistance-duration curve shown in figure 2.10. This curve shows the relation between the significant wave height H_{m0} and the durationtime that the grass revetment can withstand that wave load. When the duration exceeds this value, damage to the revetment layers start to occur. Erosion of grass revetments due to wave impact is described by de Waal and Hoven (2015a), and adjusted with additional parameters by Vuik (2019). The calculation method described by de Waal and Hoven (2015a) is used in the assessment software BM Grass Revetment (*BM Gras Buitentalud*) (Deltares 2019) which is created for the WBI.
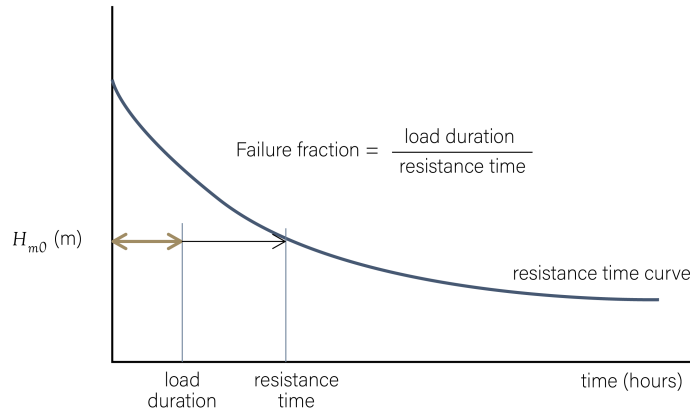
Figure 2.10: Resistance-duration curve (based on de Bruin et al. (2016))

The load and resistance for the process of wave impact is described in time, so accordingly the loading time and resistance time. The resistance duration described by de Waal and Hoven (2015a) is split in the time needed to erode the top layer (grass revetment layer) and the time needed to erode the sub layer (the layer between the top layer and the core layer). A cross-sectional view of the described layers is shown in figure 2.11.
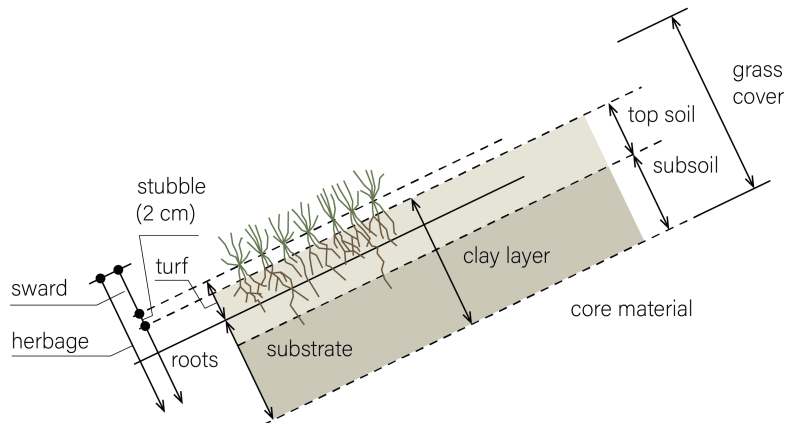
Figure 2.11: Structure and division of a grass cover (Muijs 1999)

The resistance time for the top t_{top} and sub layer t_{sub} are defined by de Waal and Hoven (2015a) in equation 2.2 and 2.3. The resistance time of the top layer depends on the empirical parameters c_a, c_b, c_c, and the significant wave height H_{m0}, expressed in the following equation by Vuik (2019):

$$t_{top} = f_\alpha \frac{1}{c_b} ln \left[\frac{max((H_{m0} - c_c); 0)}{c_a} \right]$$
(2.2)

The duration time of the sub layer depends on the thickness of the top and sub layer combined d_{tot},

sand fraction f_{sand} through constant c_d ($c_d = 1.1 + 8 * max((f_{sand} - 0.7); 0))$, and the significant wave height H_{m0}, expressed in the equation by Vuik (2019):

$$t_{sub} = f_\alpha \left[\frac{max((d_{tot} - 0.2); 0)}{c_d(\frac{1}{3})^{1.5} max((H_{m0} - 0.5); 0)} \right] \tag{2.3}$$

A linear correction factor for slope angles between 1:3 and 1:6 is defined by Kruse (2010), to account for differences in erosion duration for different slopes. The equation is expressed as follows, and depends on the ratio r_α between 1:6 and 1:3 slopes, and is on average 1.51.

$$f_\alpha = \frac{\frac{(r_\alpha - 1)}{3}}{tan(\alpha)} + 2 - r_\alpha \tag{2.4}$$

2.2.2. Wave run-up

After breaking of the incident waves, all the impact on the dike slope is exerted, and the wave front runs over the dike slope. The wave front runs up the slope until a certain run-up height R_u, after which it starts to runs down the slope as well. If the run-up height exceeds the crest height, overtopping occurs and water flows down in the crest and inner slope, which lies out of the scope of this research. Erosion due to wave run-up is only assessed above the wave impact zone. This is done because it is assumed that the load due to wave impact is governing over the load due to wave run-up (de Bruin et al. 2016).

Erosion due to wave run-up is assessed by comparing the critical overload D_{crit} with the cumulative overload $D_{load,z}$. The critical cumulative overload represents the strength of the grass revetment, and depends on the level of damage/failure. de Waal and Hoven (2015b) stated two different values for damage and failure of the grass revetment.

$D_{crit,damage}$ = 4000 m^2/s^2
$D_{crit,failure}$ = 7000 m^2/s^2

The cumulative overload $D_{load,z}$, as presented by de Waal and Hoven (2015b) for a stationary storm event (constant still water level z_{swl}) is calculated using the following equation:

$$D_{load,z} = \sum_{i=1}^{N} max\left[(\alpha_m U_{i,z}^2 - \alpha_s U_{crit}^2); 0 \right]) \tag{2.5}$$

As shown in equation 2.5, the front velocity $U_{i,z}$ of the wave run-up for a single wave i on the evaluation level z is compared to the critical velocity U_{crit}. The front- and critical velocity are accompanied by two factors, α_m is a correction factor for increased load, and α_s a correction factor for decreased strength, at transitions and objects (e.g. stairs, roads, asphalt tot grass, etc.). When no objects are present, both α-factors equal 1. Overload occurs when the front velocity $U_{i,z}$ exceeds the critical velocity U_{crit}, and adding every occurrence of overload results in the cumulative overload $D_{load,z}$. The critical front velocity U_{crit} describes the grass quality and takes lower values for weaker grass revetments (de Waal and Hoven 2015b), which is 6.60 m/s for stronger grass revetments, and 4.30 m/s for weaker grass revetments.

In this formulation, the number of waves N during a time interval can be calculated by dividing the load duration ΔT of a stationary event (constant still water level) by the mean wave period T_m, as presented in equation 2.6

$$N = \frac{3600 \Delta T}{T_m} \tag{2.6}$$

To calculate the front velocity of a single wave $U_{i,z}$, equation 2.7 shows that it depends on the maximum front velocity $U_{i,max}$ along the slope of wave run-up i at a certain evaluation level above the still water level ($z = z_{eval} - z_{swl}$, and the run-up level Ru_i of run-up event i with respect to the water level (shown in equation 2.9. The maximum front velocity depends on the constant c_u (by default 1.10) defined by de Waal and Hoven (2015b), and the run-up level Ru_i of run-up event i with respect to the water level.

$$U_{i,z} = U_{i,max} \cdot max\left(0; min\left(1; \frac{Ru_i - z}{0.25 Ru_i} \right) \right) \tag{2.7}$$

Where the maximum front velocity $U_{i,max}$ is defined as:

$$U_{i,max} = c_u \sqrt{g Ru_i} \tag{2.8}$$

The run-up level Ru_i of run-up event i with respect to the water level takes a couple of steps to calculate and are described in detail in de Waal and Hoven (2015b) and results in equation 2.9. Equation 2.9 takes as input the 2% run-up level $Ru_{2\%}$, the run-up level that is exceeded by 2% of incident waves and the number of waves N.

$$Ru_i = Ru_{2\%} \sqrt{\frac{ln\left(1 - \frac{i}{N+1}\right)}{ln(0.02)}} \tag{2.9}$$

With the 2% run-up level $Ru_{2\%}$ described in van der Meer et al. (2018) by equation 2.10 and 2.11:

$$\frac{R_{u2\%}}{H} = a \cdot \gamma_b \cdot \gamma_f \cdot \gamma_\beta \cdot \xi \tag{2.10}$$

With a maximum of:

$$\frac{R_{u2\%}}{H} = b \cdot \gamma_f \cdot \gamma_\beta \left(4 - \frac{1.5}{\sqrt{\gamma_b \cdot \xi}}\right) \tag{2.11}$$

The 2% run-up level $Ru_{2\%}$ depends on: a and b, which are stochastic normal-distributed variables, γ_b, γ_f and γ_β, which are influence factors for the: influence of a berm, influence of roughness elements, and oblique wave attack, respectively. The equations or values of the influence factors are retrieved from van der Meer et al. (2018). The Iribarren number ξ, as presented in equation 2.12, is an important factor in describing the behaviour of waves on a slope. It is also called the breaker parameter or surf similarity parameter. It plays an important role in describing the interaction of waves approaching a structure. This behaviour is primarily influenced by the slope steepness and deep water wave steepness, which connects the structural parameter to the hydraulic parameter (Battjes 1974), see equation 2.12.

$$\xi = \frac{\tan\alpha}{\sqrt{\frac{H}{L_0}}} \tag{2.12}$$

With the deep water wave length L_0:

$$L_0 = \frac{gT^2}{2\pi} \tag{2.13}$$

Where:

α Slope angle [°].
H Wave height [m].
g Gravitational acceleration [m/s^2].
T Significant wave period [s].

2.3. Wave attenuation

To protect against erosion of the outer slope, two types of measures can be applied (i) the revetment can be protected against the wave load, or (ii) the wave load can be reduced. Different types of protection can be implemented in a design, e.g., harder revetment types as asphalt or rock placement. Studies have shown that vegetation in front of dikes can be a good way to design an eco-friendly and cost-effective dikes. Vegetation on the foreshore can significantly reduce wave energy during storm conditions, resulting in lower wave heights (Vuik, van Vuren, et al. 2018). Vegetation has different parameters that results in wave energy dissipation or enhance the general wave attenuation mechanisms, which are important for building a wave attenuation model.

Many studies predicted wave attenuation by vegetation, each using a different approach. Predicting the amount of attenuation by using an increase of the bottom friction coefficient was introduced by Hasselmann and Collins (1968) and elaborated on by Quartel et al. (2007). Dalrymple et al. (1984) and Kobayashi et al. (1993) modelled vegetation, by representing the vegetation as an array of cylinders, and assessed the wave forcing on those cylinders. Simulating the effects using cylinders, has more resemblance to the geometry of vegetation, which is now the preferred method of modelling wave attenuation by vegetation.

The study by Dalrymple et al. (1984) focused on vegetation on a flat bottom, subjected to regular incident waves. His study found an analytical solution for the wave height evolution through a vegetation field. The findings from Dalrymple et al. (1984) were extended by Mendez et al. (2004), that studied the wave height evolution through a vegetation field with sloping bottom and irregular waves. The study by Mendez et al. (2004) resulted in the following equation for wave energy dissipation due to vegetation:

$$\langle \varepsilon_v \rangle = \frac{1}{2\sqrt{\pi}} \rho \tilde{C}_d b_v N_v \left(\frac{kg}{2\sigma} \right)^3 \frac{\sinh^3 k\alpha h + 3\sinh k\alpha h}{3k\cosh^3 kh} H_{rms}^3 \tag{2.14}$$

Where:

ρ	Fluid density $[kg/m^3]$.
$\tilde{C}_D$	Bulk drag coefficient $[-]$.
b_v	Cylinder (plant) diameter $[m]$.
N_v	Number of cylinders (plants) per unit area $[1/m^2]$.
k	Wave number $[1/m]$.
g	Gravitational acceleration $[m/s^2]$.
α	Stem height to water depth ratio $[-]$.
h	Water depth $[m]$.
H_{rms}	Root mean square wave height $[m]$.

The formula created by Mendez et al. (2004) did not take into account differences in the vegetation parameters over the height, so more or less straight cylinders with a diameter b_v and a bulk drag coefficient $\tilde{C}_D$. Looking at the geometry of a willow tree, modelling the tree as a cylinder with the same properties over the height, will give inadequate results. Willows have different properties distributed over the height of the tree, which needed more research to improve the existing formulae and models by Mendez et al. (2004). Suzuki (2011) performed one of the first studies towards layered vegetation types to add vertical layers to the energy dissipation term for vegetation by Mendez et al. (2004) (equation 2.14.

Research into the effects of a willow forest, and thereby the different properties of a willow tree, has been conducted in the Delta flume of Deltares (van Wesenbeeck et al. 2022). The flume has a length of 300 m, a width of 5 m and a depth of 9.5 m. The wave board in the flume is capable of producing a wave field with a significant wave height up to 2.0 m. The flume created the perfect facility to perform large-scale physical model tests of a willow forest (van Wesenbeeck et al. 2022). The experimental setup used in the Delta flume is shown in figure 2.12. A dike with a horizontal foreshore was constructed out of concrete and extended with plywood. The dike section consists of two parts: the lower part with a slope of 1:3.6 and the upper part with a slope of 1:3. The dike had a crest height of +11.75m above the bottom of the flume. The toe of the dike had an elevation of +2.33 m above the flume bottom. The

foreshore was situated +2.33 m from the bottom and contained a 40 m long willow forest. The top of the foreshore was covered with a concrete layer to prevent the willows from rooting up due to the wave load (Çete 2019).

The results of the large-scale physical model test in the Delta flume were used to obtain more insight in the influence of vegetation on incoming waves, and improve the numerical equations and models that were used before.
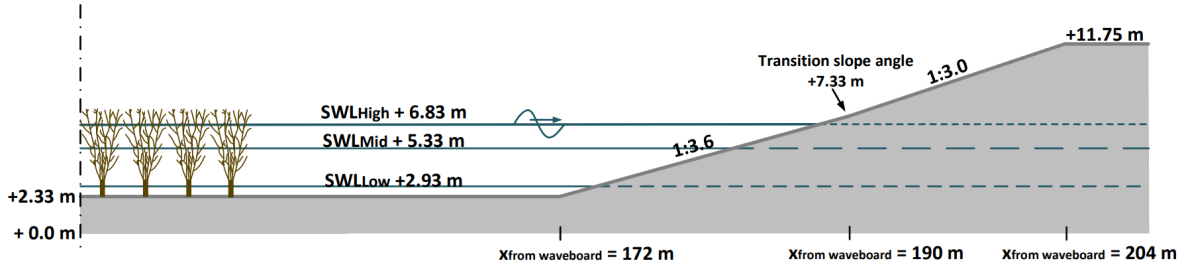
Figure 2.12: Schematization of the set-up of the dike and forest in the Delta flume (Çete 2019)

The results of the physical test facilitated modifications for the existing formula, Kalloe et al. (2022) modified the formula of Mendez et al. (2004) and Suzuki (2011) to take into account different vegetation properties per vertical vegetation layer, resulting in the following formulation of the dissipation due to vegetation term of the wave energy balance (Equation 2.16).

$$\langle \varepsilon_v \rangle = \sum_{i=1:I} \frac{1}{2\sqrt{\pi}} \rho \tilde{C}_d \left(\frac{g k_p}{2\sigma} \right)^3 A_{v,i} \frac{(\sinh^3 k_p \alpha_i h - \sinh^3 k_p \alpha_{i-1} h) + 3 (\sinh k_p \alpha_i h - \sinh k_p \alpha_{i-1} h)}{3 k_p \cosh^3 k_p h} H_{rms}^3$$

(2.15)

Where:

k_p	Wave number $[1/m]$.
$\tilde{C}_D$	Bulk drag coefficient $[-]$.
$A_{v,i}$	Total front width of vegetation per horizontal area perpendicular to the waves for layer i $[m]$.
α_i	Ratio between the depth at the top of layer i and the total water depth h $[]$.
h	Water depth $[m]$.
H_{rms}	Root mean square wave height $[m]$.

To conclude, numerous studies have already been conducted on the wave attenuating properties of willow forests (e.g. (Dalrymple et al. 1984), (Mendez et al. 2004), (van Wesenbeeck et al. 2022) and (Kalloe et al. 2022)). These studies created various equations to quantify the amount of wave height reduction and validated them with physical tests (e.g. small-/large-scale flume tests). The resulting equations create the opportunity to use them to model vegetation effects on waves and analyse the effects that attenuated waves may have on the probability of failure by wave-related failure mechanisms.

Wave energy balance

Vegetation on the foreshore is not the only wave energy influencing processes. Incoming waves approaching a flood defence structure are influenced by a variety of processes that increase or decrease the load that is exerted on the structure. The transformation of these waves, including dissipation of energy due to wave breaking (Thornton et al. 1983), bottom-friction (Bertotti et al. 2000) and vegetation (Mendez et al. 2004; Kalloe et al. 2022), is described by an energy flux balance equation. For straight, parallel contours the energy conservation equation for normal incident waves including dissipation due to breaking $\langle \varepsilon_{br} \rangle$, bottom-friction $\langle \varepsilon_f \rangle$, and vegetation $\langle \varepsilon_v \rangle$ is given by Booij et al. (1999):

$$\frac{\partial E c_g}{\partial x} = -\langle \varepsilon_{br} \rangle - \langle \varepsilon_f \rangle - \langle \varepsilon_v \rangle$$

(2.16)

The average rate of dissipation due to breaking $\langle \varepsilon_{br} \rangle$ is determined by Thornton et al. (1983), and depends on the adjusting parameters B and γ_b, and the average frequency f_p corresponding to the peak period T_p, as shown in equation 2.17.

$$\langle \varepsilon_{br} \rangle = \frac{3\sqrt{\pi}}{16} \rho g \frac{B^3 f_p}{\gamma_b^4 h^5} H_{rms}^7 \tag{2.17}$$

The dissipation due to bottom-friction is formulated by (Bertotti et al. 2000) and shown in equation 2.18. It depends on the bottom-friction coefficient C_{bottom}, wave number k, and the relative frequency σ.

$$\langle \varepsilon_f \rangle = C_{bottom} \frac{\sigma^2}{g^2 \sinh^2 kh} \tag{2.18}$$

Since the wave energy is directly related to the height of the wave (Bryan et al. 2020), shown in equation 2.19, the wave energy balance equation (equation 2.16 can be used to model the change in wave height as a result of the described energy dissipation processes. Since all wave heights in the balance equation are root means square wave heights H_{rms}, the wave height [1] in the formula needs to be converted using the formula as stated in Thornton et al. (1983), being $H = 1.42 * H_{rms}$.

$$E = \frac{1}{8} \rho g (1.42 H_{rms})^2 \tag{2.19}$$

---

[1]The distribution from which the wave heights were sampled in the model of this research represented significant wave heights, instead of root mean square wave heights. Therefore the outcomes of the failure probability calculation are considered slight underestimations, since the used wave heights should be larger.

2.4. Probabilistic analysis

The design and assessment of a flood defence depends for a large amount of uncertainties, which as stated in the problem definition, created the base for this study. To work with uncertainties in a design, different approaches are used to come to a safe structure or design. In this section, different approaches to perform probabilistic analyses are introduced, the use of a limit state function is explained, and which probabilistic reliability analysis methods are suited to deal with limit state functions as used in this study.

2.4.1. Uncertainty

The presence of uncertainty in the design process of any structure, flood defences included, can be a challenging factor. The magnitude of the load on the structure, and the magnitude of the resistance of the structure consist of many uncertainties. This is the reason why the standard and guidelines are defined as probabilities, because without uncertainty the probability of flooding would either be one or null (flood or no flood) (Diermanse et al. 2016). Uncertainties can be reduced with the help of research and measurements.

Between the design process of a new/reinforced defence and the assessment of an existing defence, there is a minor difference. The difference is whether one takes into account the design lifetime. For the assessment of an existing flood defence structure, only the current resistance of the structure is assessed, while for the design of a new structure, the resistance over the lifetime is taking into account. The types of uncertainty can be divided into two types: (i) aleatory uncertainties, and (ii) epistemic uncertainties. Aleatory uncertainties are natural uncertainties, e.g. the inconsistency in the yearly-discharge of a river, resulting in variable water levels (Diermanse et al. 2016). Epistemic uncertainties are the uncertainties originating from incomplete knowledge about a process, e.g. limited amounts of measurements or models that do not give an accurate representation of reality (Diermanse et al. 2016).

To assess the probability of flooding for a flood defence structure, uncertainties must be quantified accurately or minimized. This involves conducting measurements or using models to predict loads and strengths. However, since neither measurements nor models are flawless, probabilistic analyses incorporate uncertainty by using probability distributions rather than using single values, so taking a variability of the values into account. Using distributed values and techniques like Monte Carlo simulations (see Section 2.4.4) to calculate the probability of occurrence of failure due to a failure mechanisms makes it possible to take the uncertainty and dynamic behaviour of input parameters into account in assessment and design projects.

Taking the uncertainty of input parameters into account in the probabilistic analysis is important for the scope of this thesis, and to analyse how much influence the uncertainty has on the probability of failure. By quantifying these influences of the parameters on the probability of failure. In figure 2.13 the different sources of uncertainty in the calculation of the failure probability are shown to get insight where uncertainty is introduced in the calculation.
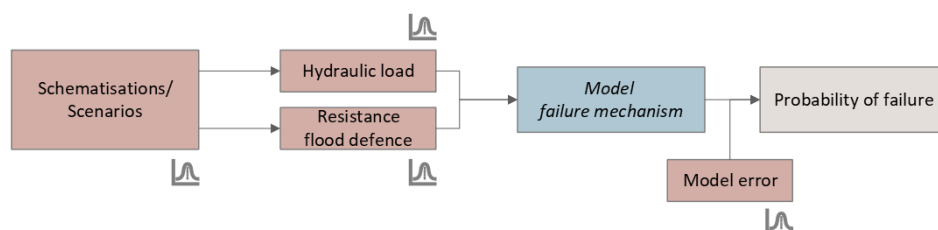
Figure 2.13: Sources of uncertainty (based on Diermanse et al. (2016))

2.4.2. Deterministic to Probabilistic methods

Between the design methods, four levels can be distinguished from deterministic towards full probabilistic. In table 2.3 the different levels are discussed in brief. In this study, the level III approach (fully probabilistic) is used to assess the effect of a riparian forest on wave attenuation and design of dike elements. Previous studies, as performed by de Bruijn (2020), has focused on the similar objective,

but using a mpre deterministic approach. This can be used as a reference and possible validation of more probabilistic models in the future.

<div align="center">Table 2.3: Overview of probabilistic methods (Schiereck et al. 2019)</div>

Level	Approach	Explanation
0	Deterministic	Characteristic loads are chosen from observations/studies and a certain threshold is chosen as characteristic strength
I	Quasi-probabilistic	Every load/strength parameter is multiplied with a safety factor
II	Approximate probabilistic	The probability of flooding/failure is approached by simplified functions
III	Fully probabilistic	The probability of flooding/failure is determined by numerical integration of the probability distributions and functions or by random drawn realisations of the probability functions

2.4.3. Limit state function

To assess the reliability of a flood defence structure, the two most important elements are the loads on the structure, and the resistance against the load. With these elements, and their uncertainties, the limit state function can be formulated and analysed, as shown in equation 2.20. For different loads and resistances, different failure mechanisms will occur. To get an overview of the failure mechanisms and the corresponding interdepencies for a dike section, a fault tree, like figure 2.8, can be made for each section.

$$Z = R - S = R(x_1, x_2, \ldots, x_m) - S(x_{m+1}, \ldots, x_n) \tag{2.20}$$

Where:
Z	Limit State function
R	Strength (French: *Résistance*)
S	Load (French: *Sollicitation*)
$x_1, \ldots, x_m, \ldots, x_n$	All random variables involved in strength and load

The main elements of loads on a flood defence structure are in general: the water pressure, wave forces and water flowing along, over, through and under the structure. These main loads set in motion different load effects on a structure which results in losses in strength or stability. The loads contain a certain level of uncertainties, for example the magnitude of a load or the water level that is only exceeded once every couple of year.

The resistance is the strength of the flood defence structure against the occurring loads. In general, these resistance elements are the height of the structure, the friction angle between the soil particles in the core of the structure and the cover layer of a structure. The resistance of a structure is also prone to uncertainties (Kok et al. 2016).

Uncertainties in load and resistance elements, results in the expression of the load and strength elements in terms of probability. To work with uncertainties in a design, probabilities are assigned to the different elements of load and strength.

For design or assessment, the strength of a structure is generally determined using models. The accuracy depends on the amount of simplification in the model and physical knowledge of the occurring phenomena. In most designs it is preferable to work from rough and simple models in the beginning, towards more detailed and refined models further in the process. When more data and knowledge is gathered on specific topics, the assigned probabilities and models can be adjusted accordingly (Kok et al. 2016).

2.4.4. Probabilistic methods

The probability of flooding, or the probability of failure due to a specific failure mechanism, is based on a significant amount of uncertainty. To improve the reliability of a model, a full probabilistic method enables analysis of the failure probability. Several methods can be applied to perform the assessment,

each with their own advantages and disadvantages.

The First Order Reliability Method (FORM) and the Monte Carlo (MC) method are two of the best known methods. FORM is a slightly more complex method than MC, but is more accurate in less computations. The only disadvantages, is that all the variables need to be expressed as a Normal (Gaussian) distribution (Sekhavatian et al. 2018). The Monte Carlo method on the other hand, can sample from different distributions, but takes more computations to come to an accurate result (Sekhavatian et al. 2018). Since not all the input variables have a Normal distribution, the MC method is preferred over FORM. In the following section the Monte Carlo method is explained in detail, and how it is applied in the model.

Monte Carlo simulations

The Monte Carlo simulations is a relative simple method that is able to evaluate a problem many times using random sampled input parameters every computation. The parameters are sampled from their specific distribution, which do not need to be a Normal distribution. The more computations the MC method performs, the higher the accuracy of the results.

The method is based on a definition of failure, which is in most cases similar to the limit state function, as in equation 2.20, but can also be expressed in the form of a Factor of Safety or Reliability Index (Gibson 2011). This definition of failure behaves as a threshold that determines whether the structure fails or not.
This is computed by performing a specified minimal amount of computations N, which can be calculated using equation 2.21. The minimum amount of computations assures that the results from the model are accurate, but also prevents from overestimating the amount of computations, optimizing the computations time.

$$N = \left(\frac{d}{\alpha}\right)^2 \frac{1-p}{p} \tag{2.21}$$

Where, d is the normal standard deviation estimated from figure 2.14b, α is the acceptable error in the analysis to assess the probability of failure, p is the probability of failure. The probability of failure p is not known in advance, since this is the wanted outcome of the model, so iterative computations can be necessary to analyse whether more computations are needed.

Each individual computation, the input variables are sampled from the according distribution, and the limit state function Z is calculated. For all the computation the number of failures n_{fails}, where $Z < 0$, are added up. Dividing the number of failures over all computations n_{fails}, by the total amount of computations, expresses the probability of failure in percentages, as shown in equation 2.22.

$$P_f = \frac{n_{fails}}{N} \cdot 100\% \tag{2.22}$$
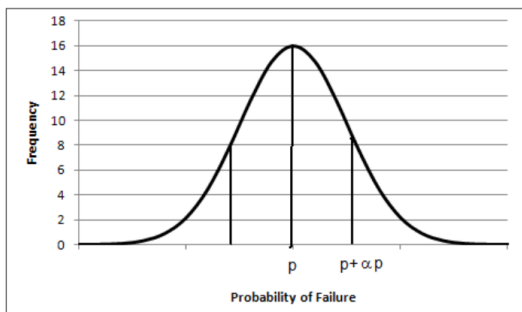
(a) PDF of P_f

Percentage of Confidence (%)	Normal Standard Deviate (d)
80	1.28
85	1.44
90	1.64
95	1.96
99	2.57

(b) Percentage of Confidence and according Normal Standard Deviation

Figure 2.14: PDF, Percentage of Confidence and Normal Standard Deviation (Gibson 2011)

Sensitivity analysis

Performing a Monte Carlo simulation as described in the previous section uses a lot of different generated input parameters to produce the different limit state outcomes. Each parameter influences the outcome, but the magnitude of influence differs heavily. To analyse this magnitude of influence a sensitivity analysis (SA) is used to rank the input parameters according to their contribution to the outcome (Saltelli and Annoni 2010).

Distinction is made between *local* and *global* SA methods. When the input of a model is linear and no interactions between input parameters are expecred, a *local* method is applied to examine the effect of small changes around a fixed point in the input space (Saltelli and Annoni 2010). When there are interactions between the input parameters and non-linear effects can occur, a *global* method captures the entire input space and examines the influence of input variability on the outcomes of the model (Saltelli and Annoni 2010).

For the model used in this research, a *global* SA method should be used, since the physical model of wave attenuation and revetment erosion is non-linear and a lot of parameters interact with each other. *Variance-based sensitivity analysis* (VB-SA) is a method that makes it possible to rank input parameters based on their contribution to the models outcome. The most used method of VB-SA is described by Sobol (Sobol' 2001), introducing the first-order Sobol indices S_i that are calculated for each parameter (equation 2.23). Saltelli, Ratto, et al. (2008) used this theory to introduce total sensitivity indices S_{total} or S_T, described in equation 2.24.

$$S_i = \frac{V[E(Y|X_i)]}{V(Y)} \tag{2.23}$$

The first-order index describes the main effect contribution of each input factor to the variance of the output. In equation 2.23, Y is the output of the model with the input parameters X_i, so $Y = f(X_i)$. The conditional expectation $E(Y|X_i)$ is the value of Y derived by averaging over all factors X_i, and $V[E(Y|X_i)]$ is the variance of that function over X_i.
The value of S_i can be seen as a measure of how good $E(Y|X_i)$ fits the outcome. Higher absolute values for S_i ($S_i \approx 1$) indicate that input parameter X_i has a relative large influence on the outcome of the model (Saltelli and Annoni 2010).

$$S_{T_i} = \frac{E[V(Y|X_i)]}{V(Y)} = 1 - \frac{V[E(Y|X_i)]}{V(Y)} \tag{2.24}$$

The value of S_{T_i} corresponds to the fraction of $V(Y)$ that can be assigned to X_i and all the interactions of X_i with other input parameters. For models where all the input parameters X_i are independent and not interacting with each other, the first-order and total sensitivity indices are equal (Saltelli and Annoni 2010). For interacting parameters the difference between S_{T_i} and S_i is an indicator for the magnitude of interaction.

This SA method makes it possible to analyse the influence of the different hydraulic, forest and dike parameters that are part of the model used in this study. Further explanation of the implementation of this method in the model is described in section 2.4.

2.5. Summary of Literature

To create a foundation of knowledge, this literature review investigates the role vegetation can take in wave attenuation on the dike foreshore and its connection to erosion of the outer slope of a grass dike. The summary addresses the following questions:

(a) What is the current methodology for designing dikes in the Netherlands?
(b) How does vegetation attenuate wave load on a dike?
(c) How is the probability of flooding for a dike modeled?
(d) How can wave attenuation due to vegetation be incorporated in the design/assessment standards?

To research the effects of willow forests on dike design, understanding the current dike design methods in the Netherlands is essential. The Delta Committee and Delta Program, introduced the use of safety standards and exceedance frequencies to assess and design flood defence structures, which have evolved into using the probability of flooding considering the probability of failure of different failure mechanisms. This approach allows for consideration of factors beyond just high water levels, distributing the allowed probability of flooding over various failure mechanisms.

Reducing the probability of flooding involves either increasing dike strength or decreasing the load on the dike. Vegetated foreshores can reduce incoming wave height, potentially allowing for less revetment material and resulting in more eco-friendly and cost-effective designs. However, incorporating vegetation into dike design is challenging due to the uncertainties related to forest properties, such as geometry, spatial distribution, seasonal variations, and vegetation failure.

Among potential failure mechanisms, erosion of the outer slope highly related to wave load and can be mitigated by a forest on the foreshore. Erosion due to wave impact occurs below the still water level, and erosion due to wave run-up above the still water level. When the probability of failure due to erosion is insufficient, usually hard revetment types are placed to increase the resistance against erosion. Implementing a forest to reduce the wave height can decrease the load on the grass, and reduce the call for increased resistance by harder revetment types.

Modeling the forest effect on the probability of flooding involves using parameters for hydraulic load, forest geometry, and dike dimensions as input for the calculation. This results in wave height reduction scenarios, which are then used to calculate wave impact and wave run-up at different evaluation levels on the dike. By determining the probability of failure for each mechanism through Monte Carlo simulations, a comprehensive overview of a willow forest's impact on dike design can be created.
Using this model, the method for detailed designs or assessments can determine whether a forest can be used on the foreshore as a load reduction factor, and after further research, design codes can make it possible to use vegetated foreshores more widely.

3

Methodology

This chapter explains the research methodology. This research uses a structured framework for the model to go from incoming waves towards the probability of failure due to wave load. The model is generated to model and analyse the effect of willow forests in two different ways: (i) produce the probability of failure for different water levels, and (ii) to analyse the sensitivity of the different parameters on the outcome. The created model combines physical modelling and probabilistic modelling to test the potential of applying riparian vegetation in dike design.

3.1. General framework

To be able tot test this potential, different analyses and assessments are performed using a computational model that is able to (i) model the wave attenuation by a willow forest, (ii) calculate the load due to wave run-up and wave impact, and (iii) use the limit state for both load cases to calculate the probability of failure using Monte Carlo simulations. Additional to these calculations a sensitivity analysis connects the different input to the generated output to analyse how much a certain input parameters affects the output (Saltelli, Ratto, et al. 2008). In this section the general framework of the created model is explained in more detail, and visualised by the workflow as presented in figure 3.1. The workflow is partially based on the failure assessment performed in Vuik, van Vuren, et al. (2018), with the addition of the wave attenuation theory due to vegetation by Kalloe et al. (2022), and the sensitivity analysis using variance-based sensitivity analysis as described by Saltelli and Annoni (2010). After clarification of the different modules in the workflow, the different input parameters are described, and it is clarified how the data and input is collected.

As described, the model is able to perform four different calculations/analysis: (i) reduced wave heights, (ii) wave load due to impact and run-up, (iii) the probability of failure and at last (iv) the sensitivity of each parameter. The outline of the described framework is shown in figure 3.1.
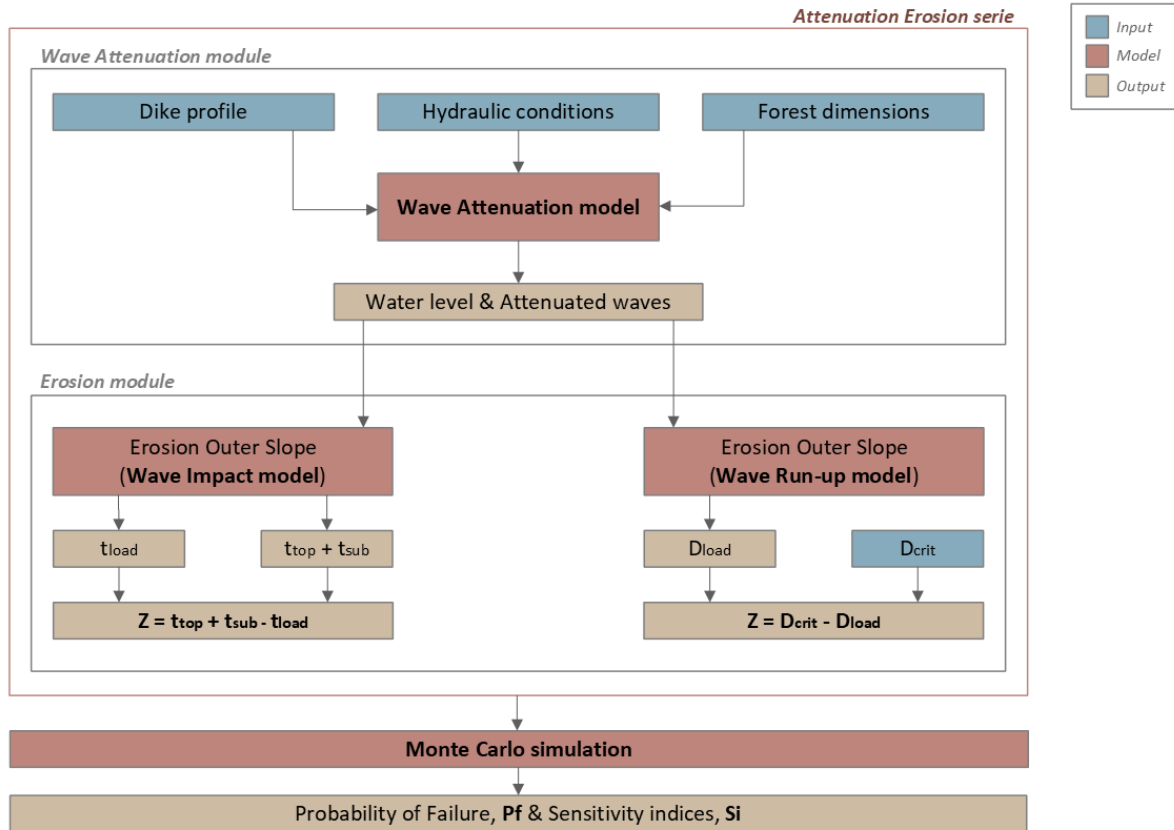
Figure 3.1: Workflow of the attenuation-erosion model

The model starts by calculating the attenuated wave height, introduced in section 3.1.1. The attenuated wave height is used as input for the wave load calculation modules, described in section 3.1.2, where both modules calculate the limit state function. This serie of calculations are all part of the overarching probabilistic module that uses them to perform Monte Carlo simulations, introduced in section 3.1.3. The results of these simulations is that many different wave-forest configurations are tested to analyse the effect on the limit state function, and to analyse how the different vegetation parameters influence the outcome, which is described in section 3.1.3.

3.1.1. Wave attenuation module

The first module of the Attenuation-Erosion (AE) model performs the wave attenuation. The *wave attenuation module* is used to produce the attenuated wave height H_{noveg} and H_{veg} after an incoming wave has passed the forest on the foreshore of the dike. The wave height of a wave travelling towards the shore is direct related by the wave energy flux balance (Equation 2.16). The wave energy flux balance can be solved over a certain length $L_{foreshore}$ using an ordinary differential equation (ODE), each spatial step the change in wave energy, and therefore wave height, is determined. The energy of the incoming wave is affected by the shoaling $\langle \varepsilon_{sh} \rangle$, breaking $\langle \varepsilon_{br} \rangle$, bottom-friction $\langle \varepsilon_f \rangle$ and vegetation term $\langle \varepsilon_v \rangle$, described in section 2.3. Each process is able to change the energy and shape of the wave and the final load on the slope of the structure.

In figure 3.2 a simple overview of the input and output is presented to create insight in the process of the model. As shown in the general workflow (Figure 3.1) the output of the wave attenuation module is used as input for the Erosion module. The solved ODE takes the vegetation input parameters (A_v, h_{tree}, L_f and C_D) to determine the energy dissipation term due to the forest. The constant and variable input parameters are described in table 3.1 and 3.2, accordingly.
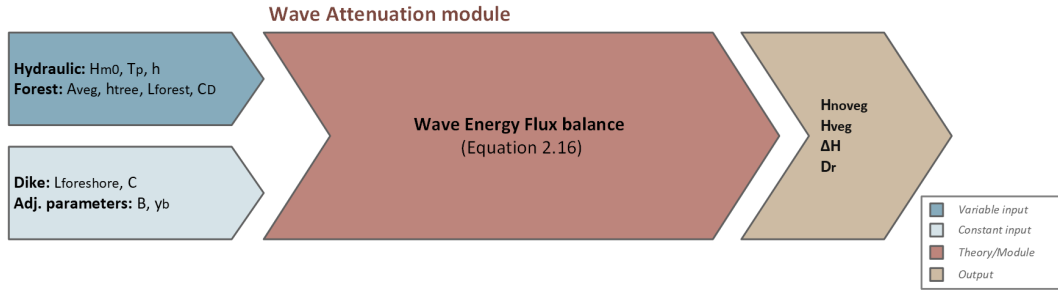
Figure 3.2: Simple overview of the wave attenuation module

As described, the wave attenuation module produces the input for the following modules in the workflow. The attenuated wave height H_{noveg}, where no forest is present on the foreshore, and the attenuated wave height with the presence of a forest H_{veg}. Both of the attenuated wave heights are calculated to be able to compare both outcomes and conclude about the effect that a forest has on the wave height, but also on the probability of failure due to the different erosion mechanisms.

The difference between the two attenuated wave heights ΔH shows the total amount of wave height reduction due to the forest by subtracting H_{veg} from H_{noveg}, and is also returned by the wave attenuation module. The difference in wave heights is used to calculate the damping ratio D_r, which is calculated using the following equation.

$$D_r = \frac{\Delta H}{H_{m0}} = \frac{H_{noveg} - H_{veg}}{H_{m0}} \tag{3.1}$$

3.1.2. Erosion module

As described in the workflow of the Attenuation-Erosion model, the erosion module consists of two different sub-modules that describe the failure mechanisms: (i) erosion due to *wave impact*, and (ii) erosion due to *wave run-up*. Both sub-modules are designed to determine the limit state function in such a way that they can be used in the Monte Carlo simulation to produce the probability of failure for the according mechanism.

Wave impact

The *wave impact module*, as a part of the erosion module, uses the attenuated wave heights (H_{noveg} and H_{veg}) that resulted from the wave attenuation module as input to calculate the limit state function. The module uses different hydraulic and dike related input parameters. Another important hydraulic parameter that is related to the wave heights, is the duration of loading t_{load} by the particular waves. The theory for assessing grass revetments described in by RWS (2022b) describes that for the largest part of the Netherlands, a small amount of intertidal areas excluded, a duration time of 12 hours is taken for a constant water level. This means that the water level with the highest wave load is the normative loading area (RWS 2022b).

Furthermore, dike related constants and variables are used as input to calculate the resistance time for the top-layer t_{top} (Equation 2.2 and sub-layer t_{sub} (Equation 2.3). The grass strength parameters C_a, C_b and C_c describe the quality of the grass revetment (Vuik, van Vuren, et al. 2018). A difference in grass quality is made in the assessment guidelines, differing between open and closed grass sods. The original equations used for analysing the resistance times where based on $1:3$ slope angles. Vuik, van Vuren, et al. (2018) added a correction factor f_{α_d} (Equation 2.4) to the existing resistance time equations, which is valid for slopes between $1:3$ and $1:6$. This equation is based on the slope angle $\tan \alpha$ and the slope angle factor r_α. In figure 3.3 a simple overview of how the model takes the input to the equations, and how the output is generated.
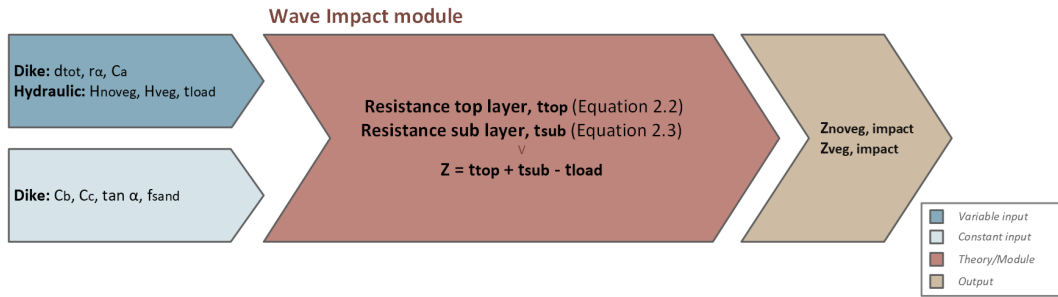
Figure 3.3: Simple overview of the wave impact module

The output of the wave impact module are the limit state values, calculated using the load and resistance time for the given input. Since the module takes both attenuated wave heights (H_{noveg} and H_{veg}), the limit state values ($Z_{noveg,impact}$ and $Z_{veg,impact}$) are calculated for the scenario with and without vegetation on the foreshore, as shown in the right arrow in figure 3.3. The module is designed to be able to be used in the Monte Carlo simulation, so all the limit state outcomes can be collected to calculate the probability of failure due to wave impact, and perform a sensitivity analysis towards the influence of the input parameters.

Wave run-up

The *wave run-up module* is the other part of the erosion module, and uses the similar attenuated wave heights (H_{noveg} and H_{veg}) as input, to produce the limit state values for the situation with and without vegetation ($Z_{noveg,runup}$ and $Z_{veg,runup}$). The model uses the same hydraulic parameters as the wave impact module, with the addition of the peak wave period T_p, which is needed to calculate the number of waves N (Equation 2.6). To determine the cumulative overload $D_{load,z}$ for a level z above the still water line, the 2% run-up level is calculated using equation 2.10.

The occurrence of overload is dependent on the grass quality by means of the critical wave front velocity u_{crit}, which differs for open and closed grass sods in the same way as it differs for wave impact. Overload does not mean that the revetment fails for the first wave i with a wave front velocity u_i higher than the critical velocity. Failure or damage occurs when the cumulative overload $D_{load,z}$ exceeds the critical cumulative overload D_{crit}, which is shown in the limit state function in figure 3.4. The input values for the constant and variable parameters are presented in table 3.1 and 3.2, accordingly.
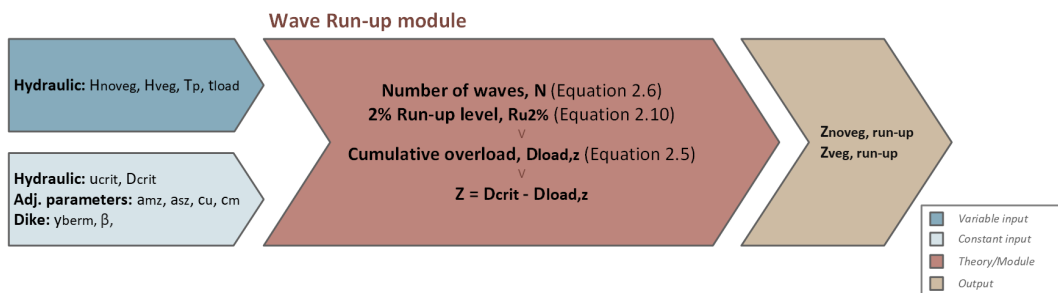
Figure 3.4: Simple overview of the wave run-up module

The run-up module is designed in the same way as the impact module, in order to be able to be used in the Monte Carlo simulation, so again all the limit state outcomes can be collected to calculate the probability of failure due to wave impact, and perform a sensitivity analysis towards the influence of the input parameters.

3.1.3. Monte Carlo module

The *Monte Carlo module* is the overarching module that takes a specific amount of samples n for the variable parameters, and run the three described modules in serie, to produce the limit state value for each combination of samples i, for both wave impact and wave run-up for the situation with and without

vegetation. The conditional probability of failure for the assessed water level is calculated by dividing the total of limit state values that lead to failure $|Z_i < 0|$ by the total number of samples n, as shown in equation 3.2.

$$P(F|h) = \frac{|Z_i < 0|}{n} \tag{3.2}$$

Since the probability is calculated for a certain water level, it is considered a conditional probability of failure. This means that it is the probability of failure due to wave attack given that the water level occurs, denoted as $P(F|h)$. To come from a conditional probability of failure towards the total probability of failure P_f for the whole slope, the conditional probability of failure (cumulative density function/CDF) is multiplied by the marginal probability of occurrence of the water level $P(h)$ (probability density function/PDF), integrated over the vertical step Δz.

$$P_f = \int P(F|h)P(h)\Delta z \tag{3.3}$$

As shown in figure 3.5, the Monte Carlo module uses 3.2 for both erosion types and the situation with and without vegetation. In the blue boxes on the right the constant and variable input parameters are shown. Some differences are made between sampled values, taken into account in the sensitivity analysis, some are not taken into account in the sensitivity analysis, and the water level h, foreshore length $L_{forshore}$, and bulk drag coefficient C_D are changed between simulations, but constant for the particular simulation. This is done to be able to: (i) analyse the probability of failure over the height of the dike (by running simulations for different water levels), and (ii) to be able to analyse the difference in stiffness of the vegetation by performing the simulations for different water levels for different values of drag coefficient.
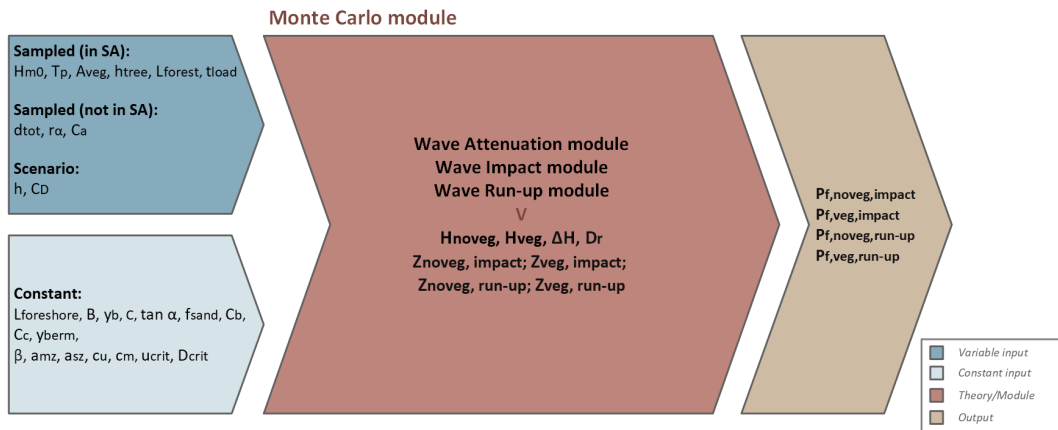
Figure 3.5: Simple overview of the Monte Carlo module

The sensitivity analysis (SA) is performed inside of the Monte Carlo module. The SA analyses the effects that changes in the input parameters have on the variance of the limit state outcomes. This analysis makes it possible to conclude about which input parameters contribute the most to the outcome. As shown in figure 3.5, the analysis are performed for all the limit state outcomes ($S_{noveg,impact}$, $S_{veg,impact}$, $S_{noveg,runup}$ and $S_{veg,runup}$).

3.1.4. Model input
The described modules are all part of the Attenuation Erosion model as shown in figure 3.1. Each module depends on different input parameters. Some are constant for each simulation, while others vary from simulation to simulation. This section describes the origin of the parameters and, if they are collected using data or software, explains how this is done.

Constants
The constant parameters of the modules are displayed in the light blue boxes of the module overviews in figure 3.2 (wave attenuation), figure 3.3 (impact), figure 3.4 (run-up) and figure 3.5 (monte carlo).

The Monte Carlo module sums up all the parameters that are used in the assessment of the dike in this research. In table 3.1 these parameters are displayed with the according reference or source. Some of the parameters show a C as value (or distribution for the variable parameters) for the $Case$-dependent parameters. Collecting the input for the case-dependent parameters is explained further on.

Table 3.1: Constant input parameters for Attenuation Erosion model. Parameters with the value C or S are considered case-/scenario-dependent and need to be specified accordingly

		Description	Value	Unit	Reference
General	g	Gravitational acceleration	9.81	m/s^2	-
	$tan(\alpha)$	Angle of outer slope	C	m/m	AHN (2019)
Attenuation	B	Adjusting parameter of Thornton et al. (1983) model	1	$-$	Thornton et al. (1983)
	C	Bottom-friction coefficient	0.07	$-$	Hasselmann, Barnett, et al. (1973)
	y_b	Adjusting parameter of Thornton et al. (1983) model	0.73	$-$	Thornton et al. (1983)
	$L_{foreshore}$	Foreshore length	S	m	*Google Earth*
Impact	C_b	Parameter grass strength	-0.035	$1/h$	Vuik, van Vuren, et al. (2018)
	C_c	Parameter grass strength	0.25	m	Vuik, van Vuren, et al. (2018)
	f_{sand}	Sand fraction	0.35	m	Vuik, van Vuren, et al. (2018)
Run-up	u_{crit}	Critical front velocity	6.60	$-$	RWS (2022b)
	D_{crit}	Critical cumulative overload	7,000	m^2/s^2	de Waal and Hoven (2015b)
	y_{berm}	Influence factor for a berm	1	$-$	van der Meer et al. (2018)
	β	Angle of wave attack	C	$\circ$	*Hydra-NL*
	a_{mz}	Factor for increased load	1	$-$	de Waal and Hoven (2015b)
	a_{sz}	Factor for decreased strength	1	$-$	de Waal and Hoven (2015b)
	c_u	Relation run-up height and max. front velocity	1.10	$-$	de Waal and Hoven (2015b)
	c_m	Constant for ratio $T_{m0}/T_{m-1,0}$	0.92	$-$	de Waal and Hoven (2015b)

The angle of the outer slope $\tan(\alpha)$, the foreshore length $L_{foreshore}$ and the angle of wave attack β are the case-dependent parameters. The slope angle of the outer slope is derived from elevation data collected from the current altitude file of the Netherlands (Algemeen Hoogtebestand Nederland/AHN). In Appendix A the method for collecting the elevation levels for the profile of the structure is explained. The important parameters that are derived from the data are the elevation level of the toe and crest of the dike, and the horizontal locations of these points to calculate the (absolute) horizontal distance, to produce the outer slope angle by the following calculation. The data is also used to create an overview of the cross-section as shown in figure 3.8.

$$\tan(\alpha) = \frac{Z_{crest} - Z_{toe}}{|x_{crest} - x_{toe}|} \qquad (3.4)$$

The second case-dependent parameter is the length of the foreshore $L_{foreshore}$ (and equal to the maximum variable length of the forest L_{forest}), which is determined by analysing the length of the foreshore using satellite images (collected from Google Earth) and comparing it with the vegetationmonitor. The vegetationmonitor uses, as described in Appendix A, the vegetation chart in the Netherlands to conclude whether vegetation is not located in important flow paths of the river. Based on the two visual data sources, the length of the foreshore $L_{foreshore}$ can be measured.

Finally, the angle of wave attack β depends on the location of the cross-section. Hydra-NL is a probabilistic software program that models the statistics for hydraulic loads in the Netherlands, including the wind statistics. Based on these statistics it is able to determine the primary wind direction, in other words the direction where the highest wave loads will come from. For the wave impact module, the angle of attack is not included in the calculation conform WBI. For the wave run-up module, the angle of attack is included in the calculation of the wave run-up height (equation 2.10)). So, using Hydra-NL, the angle of wave attack β is determined for the location that is assessed.

Variables
The constant parameters of the modules are displayed in the darker blue boxes of the module overviews in figure 3.2 (wave attenuation), figure 3.3 (impact), figure 3.4 (run-up) and figure 3.5 (monte carlo). In table 3.2 these parameters are displayed with the according reference or source. Some of the parameters show a C or a S as value (or distribution for the variable parameters) for the $Case$-dependent parameters or the $Scenario$-dependent parameters. Collecting the input for the case-dependent parameters is explained further on.

Table 3.2: Variable input parameters for Attenuation Erosion model. Parameters with the value C or S are considered case-/scenario-dependent and need to be specified accordingly

		Description	Distribution	Unit	Reference
Hydraulic	H_{m0}	Significant wave height	$W(2.50, 0.90)$	m	Vuik, van Vuren, et al. (2018)
	T_p	Peak wave period	$5.30\sqrt{H_{m0}}$	s	-
	t_{load}	Storm/Load duration	$N(12, 0.68)$	h	RWS (2022b)
	h	Water level	S	$mNAP$	*Hydra-NL*
Dike	d_{tot}	Thickness of top and sub layer	$N(0.50, 0.10)$	m	Vuik, van Vuren, et al. (2018)
	r_a	Slope angle factor	$N(1.51, 0.11)$	$-$	Vuik, van Vuren, et al. (2018)
	C_a	Parameter grass strength	$N(1.82, 0.62)$	m	Vuik, van Vuren, et al. (2018)
Forest	L_{forest}	Forest length	$L_{foreshore} * B(8, 2)$	m	*Google Earth*
	$A_{v,trunk}$	Frontal-surface area (trunk)	$N(0.054, 0.003857)$	$m/tree$	Kalloe et al. (2022)
	$A_{v,c1}$	Frontal-surface area (layer 1)	$N(0.384, 0.02743)$	$m/tree$	Kalloe et al. (2022)
	$A_{v,c2}$	Frontal-surface area (layer 2)	$N(0.224, 0.016)$	$m/tree$	Kalloe et al. (2022)
	$A_{v,c3}$	Frontal-surface area (layer 3)	$N(0.136, 0.009714)$	$m/tree$	Kalloe et al. (2022)
	$A_{v,c4}$	Frontal-surface area (layer 4)	$N(0.0352, 0.002514)$	$m/tree$	Kalloe et al. (2022)
	$A_{v,c5}$	Frontal-surface area (layer 5)	$N(0.0192, 0.001371)$	$m/tree$	Kalloe et al. (2022)
	h_{tree}	Vegetation height (divided in layers)	$N(5.33, 0.38)$	m	Kalloe et al. (2022)
	C_D	Bulk drag coefficient	S	$-$	Kalloe et al. (2022) and van Wesenbeeck et al. (2022)

The water level h is another case-dependent parameter that is determined by Hydra-NL. The program, as described in Appendix A, uses the statistical data on water levels for the specific location of the cross-section and produces the water level with their according return period. Each water level is used as input for the model to calculate the conditional probability of failure due to wave attack for the specific water level $P(F|WL)$, and remains constant throughout the particular simulation. This probability of failure is used in the assessment of the total probability of failure for the dike revetment.

The scenario-dependent parameter bulk drag coefficient C_D is specified per simulation in order to analyse the effect that the stiffness of the vegetation has on the (conditional) probability of failure of the dike revetment. Based on the findings by van Wesenbeeck et al. (2022), to simulate stiffer vegetation branches are assigned a bulk drag coefficient of 1.20, and for flexible branches a bulk drag coefficient of 0.70 is set (Kalloe et al. 2022). The runs for each water level are performed for the situation without vegetation, stiff vegetation and flexible vegetation.

3.2. Case description

To show the effects that a forest can have on the safety level of a dike, the model is applied on a case in the Dutch river area. The selected case study area is the IJsseldijk bordering the lower part of IJssel river near Kampen, as shown in figure 3.6. Kampen is a city in the north-west of the province of Overijssel. This case was selected for its grass dike accompanied by a large green foreland with the potential to support a willow forest, and that the dike trajectory 10.3, where the IJsseldijk is part of, did not meet the required safety level during the national assessment by Vergouwe et al. (2014). Vergouwe et al. (2014) assessed every dike trajectory in the Netherlands on the probability of failure due to every failure mechanism, as described in section 2.1.3. For every assessment track the probability of failure on cross-sectional level was calculated, and for trajectory 10.3 the assessment of Grass Erosion of the Outer Slope (GEBU) was insufficient. The result for the grass revetment was considered to *not meet the signal value (*$1/10,000$*) and lower limit* $1/3,000$. This led to selection of this trajectory for the case study, since it has the potential to improve the safety level by applying a forest on the foreshore.
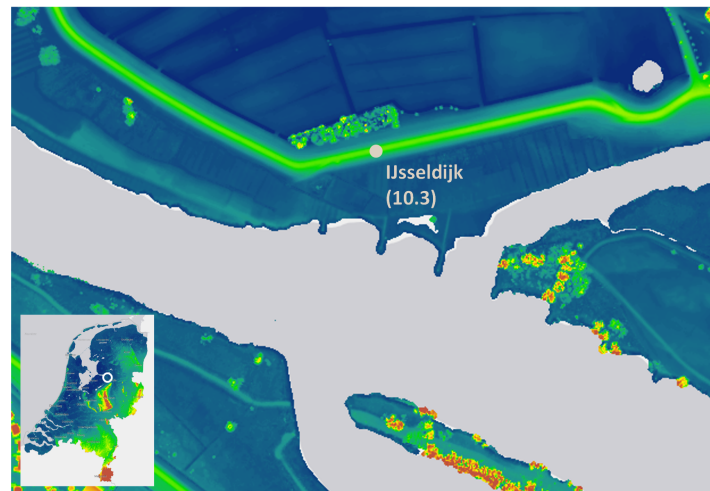
Figure 3.6: Location of the IJsseldijk (part of trajectory 10.3)

The second requirement to select this location is that the foreshore in front of the cross-section of the trajectory is sufficiently large to grow a forest. The length of the foreshore is one of the scenario-dependent input parameters of the model. In figure 3.7 the area for vegetation on the foreshore is mapped and measured to determine the foreshore length $L_{foreshore}$ of this case location. The foreshore lengths $L_{foreshore}$ are normal to the dike trajectory, as displayed in figure 3.7a by the white line. The foreshore length is a constant maximum value on which the forest length L_f is modelled variable.

(a) Measurement of the foreshore length $L_{foreshore}$. The modelled foreshore lengths are normal to the dike trajectory, and the direction is shown in the figure by the *white* line.

(b) Map of the in-situ vegetation areas by VegetationChart (2020). The *light green* areas are grass lands and fields, the *dark green* area is forest, the *purple* areas are reeds and brushwood, *light blue* is water, and *red* is built or paved area.

Figure 3.7: Overview of foreshore length (Google Earth) and vegetation area (VegetationChart 2020)

Figure 3.7a shows that the normal distance from the dike to the river is roughly 100 meter. The purple and darker green areas in 3.7b represent reeds/bushes and forest, respectively. Which indicates that vegetation is able to grow on this foreshore. Another case-dependent parameter depending on the dike geometry is the angle of the outer slope $\tan(\alpha)$, which is determined using the elevation level of the toe and crest of the dike. The source of the elevation levels is the current altitude file of the Netherlands (AHN 2019). For the assessed dike trajectory the elevation levels are shown in figure 3.8.
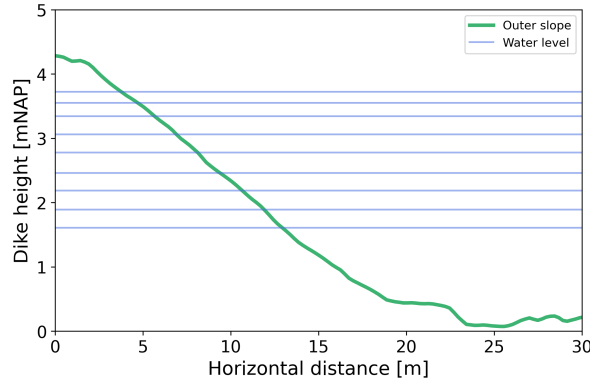
Figure 3.8: Cross-section of the elevation levels for trajectory 10.3

The hydraulic case-dependent input parameters are the angle of wave attack β and the water level h, both determined by Hydra-NL. This software program uses the statistics for the hydraulic loads in the Netherlands to produce load scenarios based on the required safety level of a trajectory. It is also possible to produce the water levels with return periods from $1/10$ years up to $1/100,000$ years. Calculating the probability of failure using the water levels with their according probability of exceedance of that water level, produces the conditional probability failure due to wave attack given that the specific water level occurs.

The angle of wave attack β is based on the wind statistics used in Hydra-NL. This makes it possible to determine the governing wave direction(s) that approach the dike. For the assessment of wave impact, the effect of this angle is not implemented in the assessment standard yet, and therefore left out of the wave impact module. When the model is expanded, the length of the foreshore and the length of the path that the waves travel through the forest become dependent on the angle of wave attack. For wave run-up, the angle of wave attack is in the equation for the wave run-up height (equation 2.10), and therefore the angle of wave attack is input for the model.

In table 3.3 and 3.4 the described case-dependent input parameters, which were left blank in the tables in section 3.1.4, are displayed. In the first table, the water levels with the according return periods are shown. The return periods are used in the analysis of the results to calculate the total probability of failure for the cross-section from the produced conditional probabilities of failure.

Table 3.3: Return period with the according water level (collected from Hydra-NL)

Description		Unit	Value								
Return period	R	$years$	10	30	100	300	1,000	3,000	10,000	30,000	100,000
Water level	h	m	1.607	1.891	2.188	2.46	2.779	3.062	3.341	3.551	3.723

In the second table with case-dependent parameters the angle of the outer slope $\tan(\alpha)$ is calculated from the profile in figure 3.8, resulting in a slope close to a $1:5$ slope. The angle of wave attack as a result from Hydra-NL, representing the most significant wave direction with respect to the dike normal. The other two parameters from table 3.4, the foreshore length and the bulk drag coefficient are important parameters, since they lead to the different scenarios that are analysed and compared in this case. The length of the foreshore $L_{foreshore}$ is split into a 40 meter forest (similar to the forest tested in the flume experiments) to be compared to the maximum possible forest length of 100 meter for the case location. The bulk drag coefficient C_D is also split up into two scenarios. Testing the influence of rigid vegetation

with a drag coefficient of 1.20, against more flexible branches with a drag coefficient of 0.70. Comparing the scenarios not only the percentage of contribution on the probability of failure as provided by the sensitivity analysis, but also absolute effects of the different scenario-dependent parameters.

Table 3.4: Case-dependent input parameters for dike trajectory 10.3

Description		Unit	Value		Source
Foreshore length	$L_{foreshore}$	m	40	100	*Google Earth*
Bulk drag coefficient	C_D	$-$	0.7	1.2	(Kalloe et al. 2022; van Wesenbeeck et al. 2022)
Angle of outer slope	$\tan(\alpha)$	m/m	0.1987		*AHN*
Angle of wave attack	β	$°$	75		*Hydra-NL*

To summarise the case description in brief. The model, as visualized and described in section 3.1, is used to assess the probability of failure for the outer slope of the dike of trajectory 10.3. This is done for every water level for the situation where no forest is present, and the situation with a forest on the foreshore of the dike. The forest is modelled for two different lengths $L_{foreshore}$ and two different bulk drag coefficients C_D. So for each water level, four calculations are made, from which the results are analysed and described in the next section.
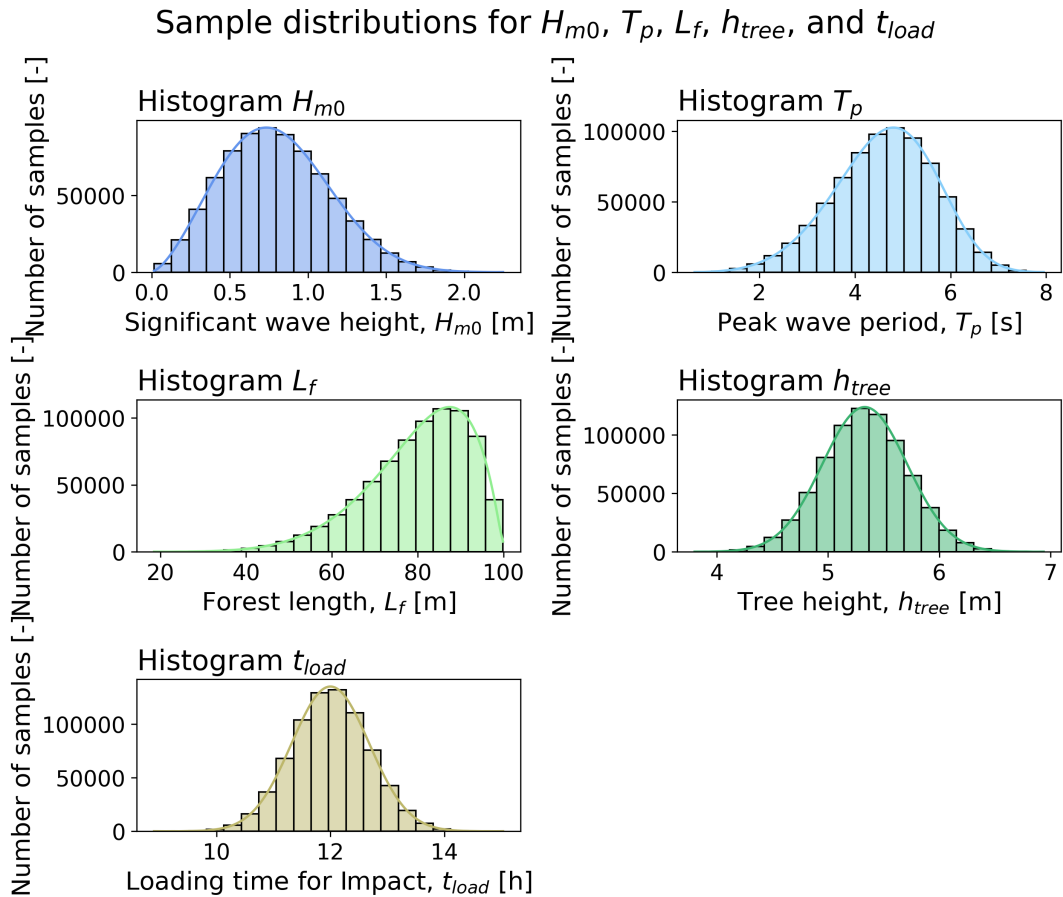
Figure 3.9: Distributions of the variable input parameters: wave height H_{m0}, peak wave period T_p, length of the forest L_{forest}, vegetation height h_{tree}, and the load duration t_{load}. These are the variables taken into account in the sensitivity analysis.

Sample distributions for A_v per layer
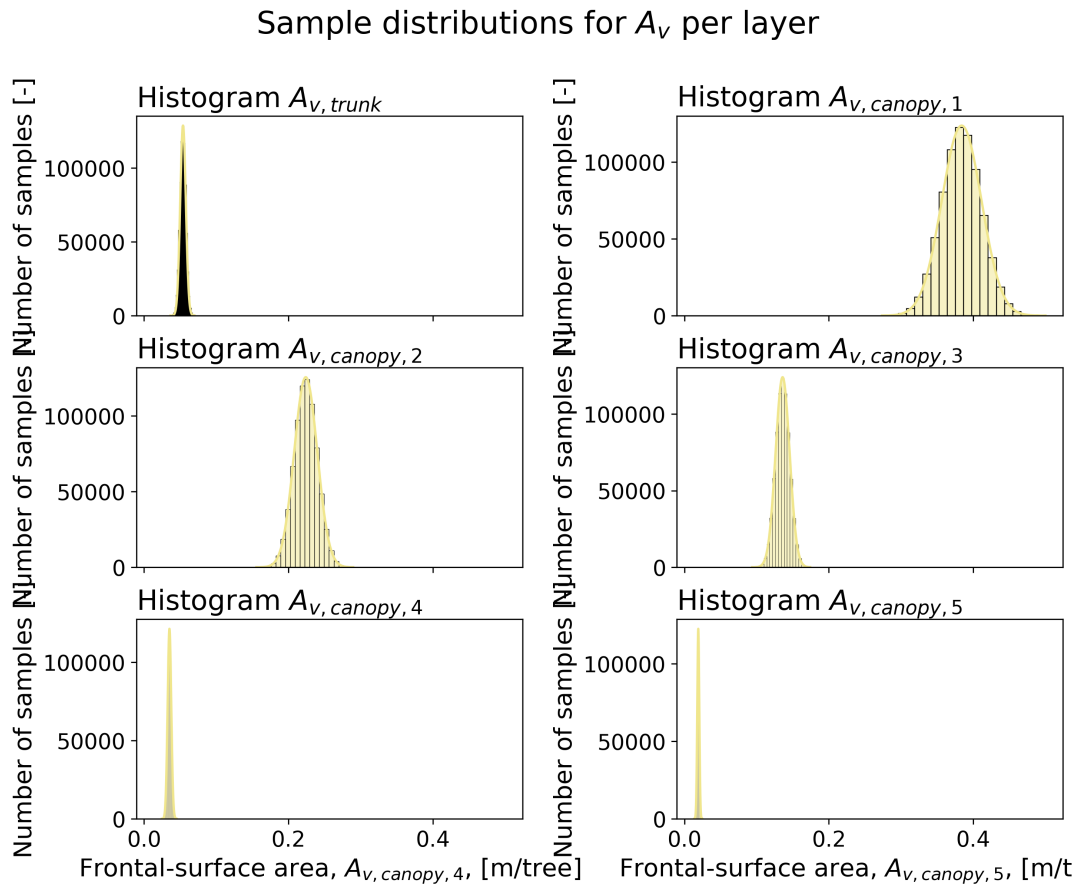
Figure 3.10: Distributions of the variable input parameters: grass strength parameters C_a, thickness of the top + sub layer of the soil d_{tot}, and the slope angle factor r_a. These are the variables not taken into account in the sensitivity analysis.
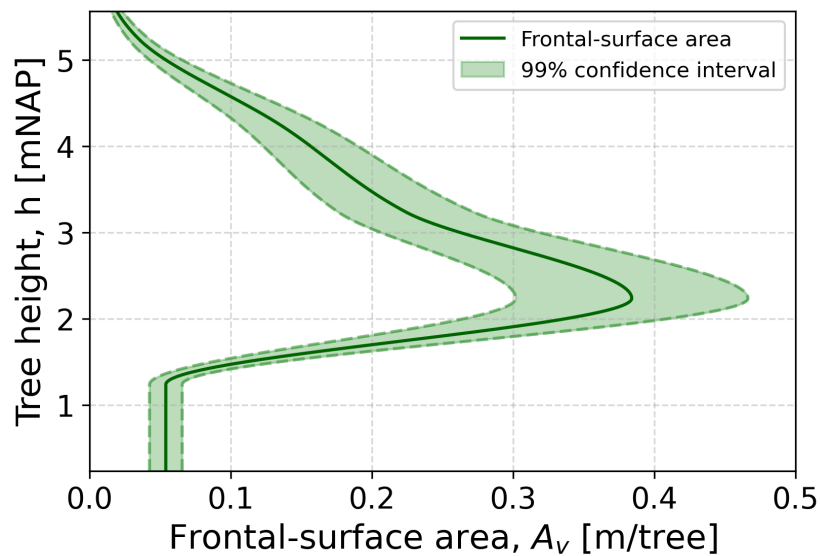
Figure 3.11: Distribution of frontal-surface area over height of a 15-year old tree, and 3 years since the last cut (with the 99% confidence interval as boundary).

Model validation

The Attenuation-Erosion model is constructed to increase the reliability for application of willow forests as dike protection against wave load. To make a reliable analysis of the magnitude of wave attenuation and the effect it has on the probability of failure P_f that the model produces, the output has to be validated. In this section the methodology to validate the model is described for the wave attenuation module and erosion module.

4.1. Outer Slope Erosion module

Model validation is a crucial step in the development of the Attenuation Erosion model to ensure the reliability of the output. First, the outer slope erosion is validated by performing similar calculations using the developed model and the software used by the WBI for grass dike assessments, BM Grass Outer Slope (BM Gras Buitentalud, as described in Appendix A). Both the model and the software are able to calculate the load due to wave impact and wave run-up on the grass revetment and generate the same type of output. To show the reliability of the model, the calculation is performed for 5 different locations in Dutch river branches.

The input used to validate the model is generated using Hydra-NL. As described in section 3.1.4, it is able to generate the water levels with their according return period. Hydra-NL is also capable of generating the wave load parameters due to wave impact and run-up that are used in BM Grass Outer Slope. It generates the significant wave height H_{m0}, peak wave period T_p, wave steepness s and the direction of wave attack for their according return period for a certain water level. In this section the validation for a cross-section of dike trajectory 10.3 is described. This dike cross-section borders the IJssel river and is located near Kampen. A limitation of the BM software for wave impact is that the slope angle $\tan(\alpha)$ is fixed on $1:3$ dikes, therefore this slope angle is also used in the model. The linear correction factor as used in the paper of Vuik, van Vuren, et al. (2018) is equal to one for a slope angle of $1:3$, so the model can still be validated using the equations described in section 2.2.1.

4.1.1. Wave impact validation

For the wave impact validation, the results from Hydra-NL are gathered for different water levels up to the maximum water level for the lower limit of the trajectory, $1/3,000$ for the assessed dike trajectory. The water level for the lower limit of trajectory 10.3 is 3.062 mNAP, so for the validation the water levels from 1.0 mNAP to 3.0 mNAP are assessed, with vertical steps of 0.25 meter. Each of the water levels will have different wave heights as result from Hydra-NL, and according to the assumptions made in WBI (RWS 2022b), these wave conditions will be constant over a timespan of 12 hours, so this is used as the load duration t_{load} in the validation.

The input gathered from Hydra-NL is shown in table 4.1, and are used together with the parameters for wave impact from table 3.1 and 3.2 to perform the calculations of the resistance time of the top layer and resistance time of the sub and top layer combined. The BM software uses the resistance times and calculates a failure fraction for them using equations 4.1 and 4.2.

$$F_{top} = \frac{t_{load}}{t_{top}} \tag{4.1}$$

When the cumulative failure fraction of the top layer F_{top} exceeds the value of 1, t_{top} becomes 0 in the calculation for the total failure fraction F_{total}, since the top layer is eroded it takes 0 hours to erode.

$$F_{total} = \frac{t_{load}}{t_{sub} + t_{top}} \tag{4.2}$$

The calculation of the failure fractions use the resistance times, in figure 4.1 the combined output of the resistance time equations 2.3 and 2.2 are plotted against different slope angles $\tan(\alpha)$ for different significant wave heights H_{m0}. This figure is used in the later part of this section to analyse the outcome of the validation calculations.
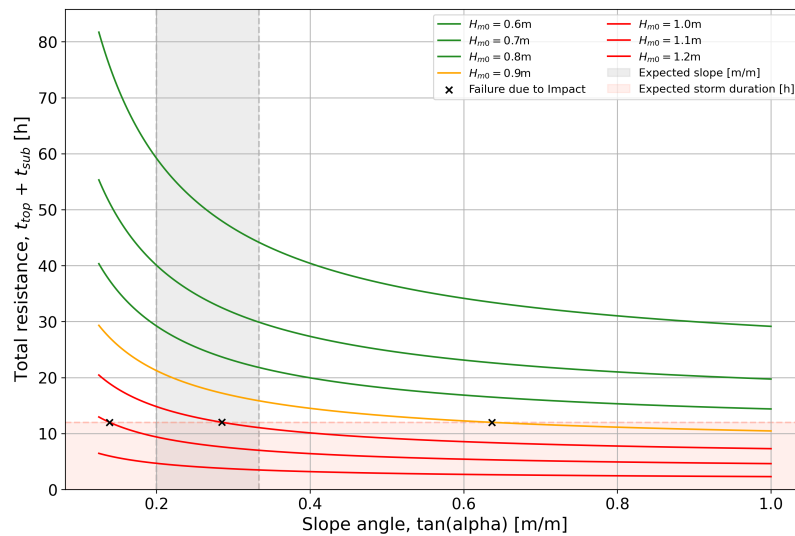
Figure 4.1: Total resistance time (sub + top layer) against slope angles for different wave heights

From Hydra-NL the hydraulic load for each water level with the return period of $1/3,000$ is displayed in ascending order in table 4.1. For a water level of 3.00 mNAP, the software resulted in *extrapolated*, which means that the output is a result of extrapolation, and is therefore less accurate and not included in this validation.

Table 4.1: Input (collected from Hydra-NL) for validation of the wave impact module

Water level [$mNAP$]	Sign. wave height [m]	Peak wave period [s]	Wave steepness [$-$]	Wave direction [$°N$]	Angle of attack [$°$]
1.00	0.33	2.51	0.0337	246.8	79.8
1.25	0.48	2.62	0.0449	246.9	79.9
1.50	0.63	2.76	0.0530	246.9	79.9
1.75	0.74	2.81	0.0596	247.4	80.4
2.00	0.73	2.82	0.0590	248.1	81.1
2.25	0.68	2.81	0.0551	249.0	82.0
2.50	0.63	2.80	0.0513	249.7	82.7
2.75	0.61	2.83	0.0489	250.2	83.2
3.00	*extrapolated*				

The input from the above table resulted in the following two tables of output, where table 4.2 shows the results from BM Grass Outer Slope, and table 4.3 shows the results from the Attenuation Erosion model. From the numbers alone it proofs that the model produces similar results as the BM software.

To visualize the accuracy, figure 4.2 shows the results from both tables plotted against each other, together with the line representing equality. The markers line up close to this line, and the R^2-error is close to 1, from which it can be concluded that the model produces similar outcomes as the software used by the WBI to assess grass revetments.

Table 4.2: Results for the wave impact calculation by BM Grass Outer Slope

Evaluation height $[mNAP]$	Failure fraction (top) $[-]$	Failure fraction (total) $[-]$
1.00	0.170	0.011
1.25	0.290	0.012
1.50	0.440	0.318
1.75	0.600	0.466
2.00	0.580	0.451
2.25	0.510	0.383
2.50	0.440	0.318
2.75	0.420	0.291
3.00	*extrapolated*	

Table 4.3: Results for the wave impact calculation by the Attenuation Erosion model

Evaluation height $[mNAP]$	Failure fraction (top) $[-]$	Failure fraction (total) $[-]$
1.00	0.166	0.000
1.25	0.286	0.000
1.50	0.434	0.311
1.75	0.589	0.457
2.00	0.572	0.442
2.25	0.498	0.375
2.50	0.434	0.311
2.75	0.411	0.285
3.00	*extrapolated*	

(a) Comparison between BM Grass Outer Slope and Attenuation Erosion model due to wave impact for the top layer

(b) Comparison between BM Grass Outer Slope and Attenuation Erosion model due to wave impact for the sub + top layer
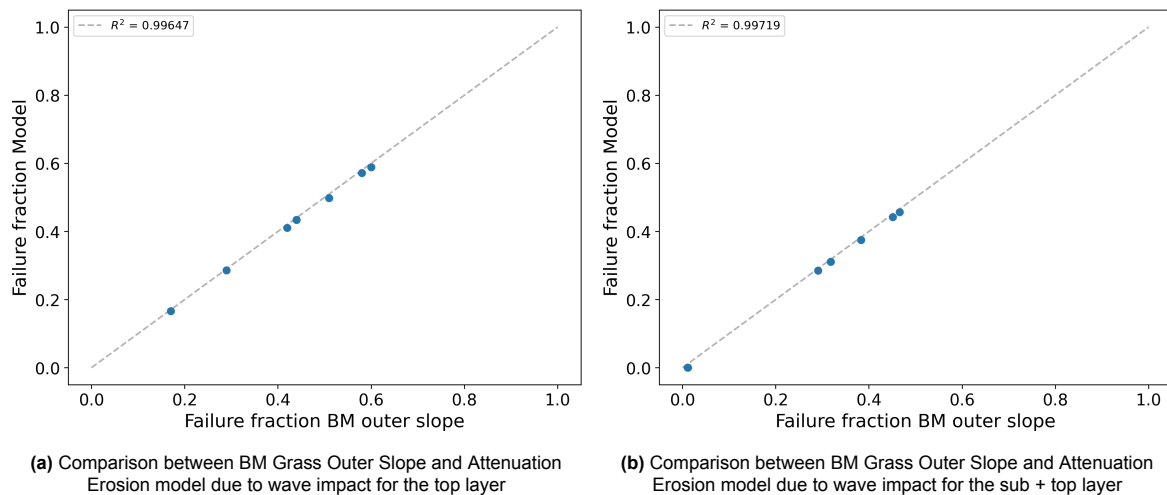
Figure 4.2: Analysis of the results for wave impact

4.1.2. Wave run-up validation

For the wave run-up validation, a similar approach is used to check the accuracy of the Attenuation Erosion model. The input data is gathered in the same way as described for the wave impact valdiation,

collecting the hydraulic load data according to the lower limit of trajectory 10.3 for each water level. The same assumption regarding the load duration of 12 hours is assumed for wave run-up. The BM Grass Outer slope software produces the cumulative overload $D_{load,z}$ for a specified evaluation level z. The same calculation is performed by the Attenuation Erosion model, using equation 2.5 to compare the results and test the accuracy of the model.

The results for the cumulative overload of equation 2.5 are plotted in figure 4.3 against the slope angle $\tan(\alpha)$ for different significant wave heights H_{m0} for a load duration of 12 hours, as assumed. The dashed line shows the critical value of overload D_{crit} of $7,000\ m^2/s^2$ and a critical front velocity u_{crit} of $6.60\ m/s$ (closed grass quality). The green lines show that for wave heights below 1 meter, no overload will come out of the model, since the critical flow velocity won't be exceeded. To still be able to assess the accuracy of the model, the critical flow velocity is lowered to the value for open grass quality ($u_{crit} = 4.30$) m/s and the load duration is increased to 24 and 36 hours.
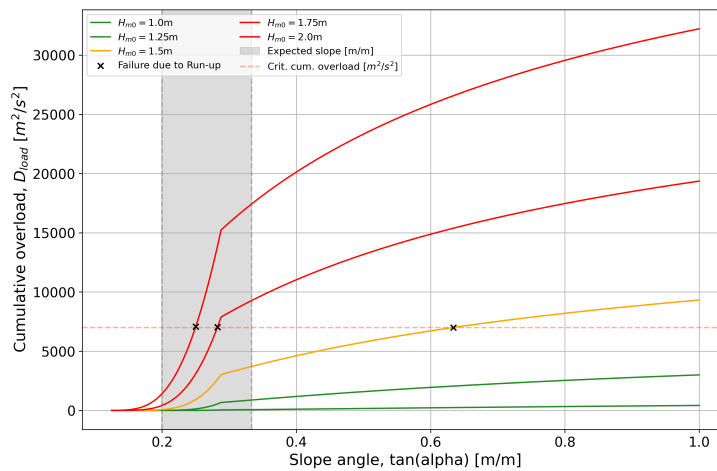
Figure 4.3: Cumulative overload against slope angles for different wave heights

Similar to the validation of the wave impact module, the input for the hydraulic load is gathered through Hydra-NL, which is displayed in ascending order in table 4.4. For a water level of 3.00 mNAP, the software resulted in *extrapolated*, which means that the output is a result of extrapolation, and is therefore less accurate and not included in this validation.

Table 4.4: Input (collected from Hydra-NL) for validation of the wave run-up module

Water level [$mNAP$]	Sign. wave height [m]	Peak wave period [s]	Wave steepness [$-$]	Wave direction [$°N$]	Angle of attack [$°$]
1.00	0.34	2.44	0.0362	236.4	69.4
1.25	0.50	2.33	0.0593	221.0	54.0
1.50	0.63	2.63	0.0584	235.0	68.0
1.75	0.73	2.68	0.0650	234.2	67.2
2.00	0.71	2.57	0.0685	234.9	67.9
2.25	0.69	2.82	0.0555	248.9	81.9
2.50	0.63	2.81	0.0514	249.7	82.7
2.75	0.61	2.83	0.0489	250.2	83.2
3.00	*extrapolated*				

The input from the above table resulted in the following two tables of output, where table 4.5 shows the results from BM Grass Outer Slope, and table 4.6 shows the results from the Attenuation Erosion model. From the numbers alone it shows that the model produces values of the some order of magnitude, but are not as accurate as the validation for wave impact. This is also visualized in figure 4.4 for a load duration of 24 and 36 hours. These load duration are assessed since the cumulative overload is zero for the load duration of 12 hours, as prescribed by the WBI (RWS 2022b). As observed in figure 4.3,

this is not an unexpected outcome. For this reason, the wave run-up calculation is assessed during the simulations, but it is highly expected to result in probabilities of zero. If the results are zero, the wave run-up will not be assessed in the results of the failure probability nor the sensitivity analysis.

The less accurate outcomes for the validation of wave run-up can be the result of small errors in one of the equations. The calculation of the cumulative overload is depending on more parameters in comparison to wave impact, where the resistance times are depending on one or two equations. The serie of equations for cumulative overload could be the origin of the difference. The tables show that the created model overestimates the cumulative overload when compared to the BM software results. Which is also indicated by the R^2-error, it is not close to one, meaning that there is some variance between the model output and assessment software. Therefore, the model can still be applied, provided it is taken into account that the results of the model can result in overestimation of the cumulative overload compared to the BM software used in the WBI.

Table 4.5: Results for the wave run-up calculation by BM Grass Outer Slope

Water level	Evaluation height	Cumulative Overload		
$[mNAP]$	$[mNAP]$	$t_{storm} = 12h$, $u_{crit} = 6.6m/s$ $[m^2/s^2]$	$t_{storm} = 24h$, $u_{crit} = 4.3m/s$ $[m^2/s^2]$	$t_{storm} = 36h$, $u_{crit} = 4.3m/s$ $[m^2/s^2]$
1.00	1.10	0.000	0.000	0.000
1.25	1.35	0.000	0.000	0.000
1.50	1.60	0.000	394.353	589.497
1.75	1.85	0.000	1,291.733	1,930.941
2.00	2.10	0.000	689.817	1,031.170
2.25	2.35	0.000	1,559.570	2,331.316
2.50	2.60	0.000	892.768	1,334.551
2.75	2.85	0.000	793.499	1,186.158

Table 4.6: Results for the wave run-up calculation by the Attenuation Erosion model

Water level	Evaluation height	Cumulative Overload		
$[mNAP]$	$[mNAP]$	$t_{storm} = 12h$, $u_{crit} = 6.6m/s$ $[m^2/s^2]$	$t_{storm} = 24h$, $u_{crit} = 4.3m/s$ $[m^2/s^2]$	$t_{storm} = 36h$, $u_{crit} = 4.3m/s$ $[m^2/s^2]$
1.00	1.10	0.000	0.000	0.000
1.25	1.35	0.000	0.000	0.000
1.50	1.60	0.000	235.273	354.977
1.75	1.85	0.000	1,524.926	2,290.645
2.00	2.10	0.000	769.844	1,157.514
2.25	2.35	0.000	1,373.336	2,063.239
2.50	2.60	0.000	499.090	751.133
2.75	2.85	0.000	367.097	552.967
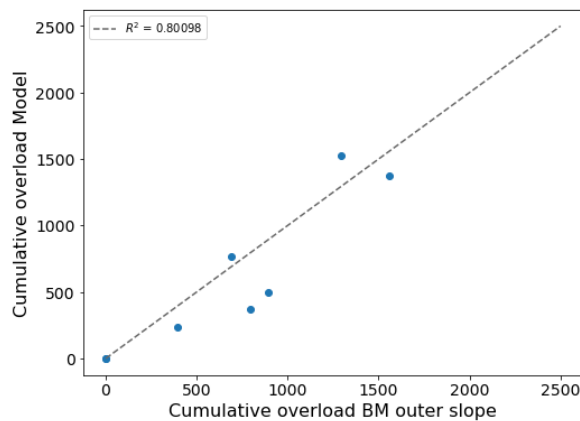
(a) Comparison between BM Grass Outer Slope and Attenuation Erosion model due to wave run-up for a load duration of 24 hours
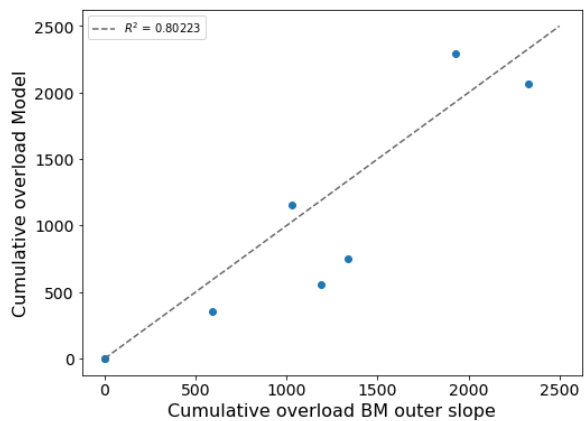
(b) Comparison between BM Grass Outer Slope and Attenuation Erosion model due to wave run-up for a load duration of 36 hours

Figure 4.4: Analysis of the results for wave run-up

4.2. Wave Attenuation module

The Wave Attenuation module of the Attenuation Erosion model is validated using the large-scale flume tests in the Delta flume of Deltares. As described in paragraph 2.3, the large-scale tests where performed on a willow forest of 40 meter long from which the wave heights were measured before and after passing through the forest. The Attenuation-Erosion model is built to produce the same type of wave attenuation, and it is based on equation 2.15 formed by (Kalloe et al. 2022). This makes it possible to validate the Wave Attenuation section of the model by recreating the large-scale test in the model using the same forest dimensions and hydraulic conditions as input parameters.

In the two figures below, the wave height results of the model are visualized by the two lines, the black constant for the situation without vegetation, the green dashed line for the wave height through the forest. The markers at the start and end of the forest represent the measurements from the flume. As shown, the results of the model are approach the measurements for both situations, which shows that for different wave climates the model gives an accurate outcome for the wave height after passing through a forest.
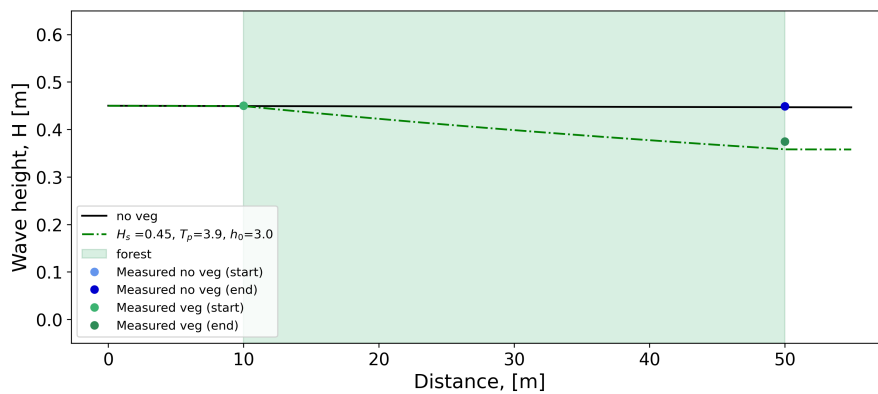
Figure 4.5: Validation of wave attenuation for the situation with $h = 3.0m$, $H_0 = 0.45m$ and $T_p = 3.9s$
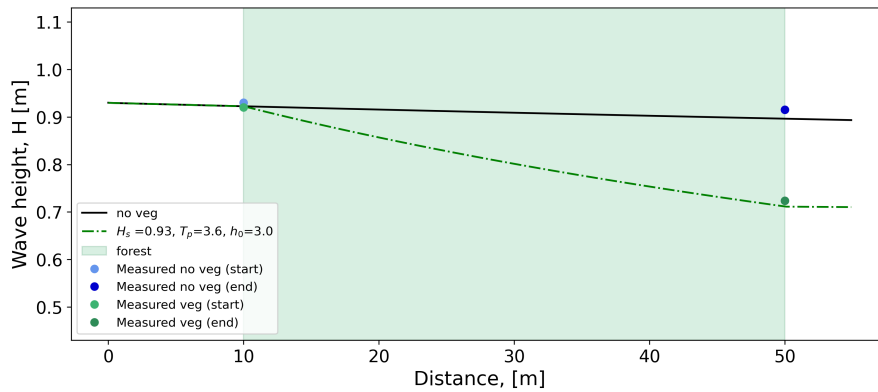
Figure 4.6: Validation of wave attenuation for the situation with $h = 3.0m$, $H_0 = 0.93m$ and $T_p = 3.6s$

5

Results

This chapter presents the findings of the research conducted to address the research questions as stated in the introduction (Chapter 1). The results are generated by applying the created general framework to model the probability of failure due to wave attack on the grass revetment of a dike cross-section of trajectory 10.3. First, the results from the probability assessment are described, followed by the results of the sensitivity analysis for the key input parameters related to wave-vegetation interaction..

5.1. Probability of Failure

The probability of failure due to wave impact and wave run-up is modelled using the constant and variable input parameters as described in chapter 3. The input for the model are the water levels from table 3.3, and the constant and variable input parameters from table 3.1 and 3.2, accordingly. From the distributions, a number of samples are taken to perform the Monte Carlo simulations and the sensitivity analysis. For the sensitivity analysis, the formula for the number of samples is $N \cdot (2D + 2)$, where N is a number of samples, and D is the number of variables analysed in the sensitivity analysis. The N needs to be a power of two, in this thesis 16.384 is used in order to get enough samples to get accurate results, even when the probability of failure becomes really small. For the situation without a forest, the variable input parameters are H_{m0}, T_p and t_{load}, creating a total amount of samples of 131.072. For the situation with a forest, more variables are used because of the addition of the layered vegetation parameters, resulting in 753.664 total samples.

The model produces the conditional probability of failure given the occurrence of that water level $P(F|h)$, based on the number of times that the limit state function is smaller than zero for each set of samples. The conditional failure probability is used in combination with the marginal probability of occurrence of that water level $P(h)$ to compute the combined probability of failure $P(F|h)P(h)$. As described in appendix B, performing this calculation for every water level Δz, and integrate over the water levels results in the total probability of failure P_f. The calculation of the total probability of failure P_f, as described above, is performed for two different foreshore lengths. For each foreshore length, the situation without a forest, and forest with two different tree types are modelled by means of different bulk drag coefficients. This is done to be able to analyse the effect of the vegetation flexibility, since the vegetation flexibility is one of the elements described by the bulk drag coefficient.

In this section, the results for the different forest lengths are shown side-by-side in the following figures, while the difference in drag coefficient is presented inside the figures, represented by the solid ($C_d = 0.70$) and dashed ($C_d = 1.20$) green line. The blue line in each plot represents the situation without a forest (vegetation) present on the foreshore.

An important result from the calculations is that for all the simulations, the conditional probability of failure due to wave run-up was zero. Therefore, wave run-up is not visibly represented in the figures in this section, and the following section (5.2) describing the sensitivity analysis. As visualised in figure 4.3, relative high waves are needed for erosion due to wave run-up to occur.

The results for the conditional probabilities of failure are shown in figure 5.1. From these figures it is observed that for the situation without a forest, the current situation, for water levels lower than 1.891 mNAP the conditional failure probability becomes zero for a foreshore of 100 meter. Higher water levels show a gradual increase towards a conditional probability of failure of 0.01 for the highest water level (3.723 mNAP). Modelling a shorter foreshore, a conditional probability of failure is present at a level of 1.607 mNAP. A similar gradual increase is found when the water level increases, and approaches also a probability of failure close to 0.01 for the higher water levels.

(a) Conditional probability of failure for the scenario with a foreshore length $L_{foreshore}$ of 100 meter.

(b) Conditional probability of failure for the scenario with a foreshore length $L_{foreshore}$ of 40 meter.
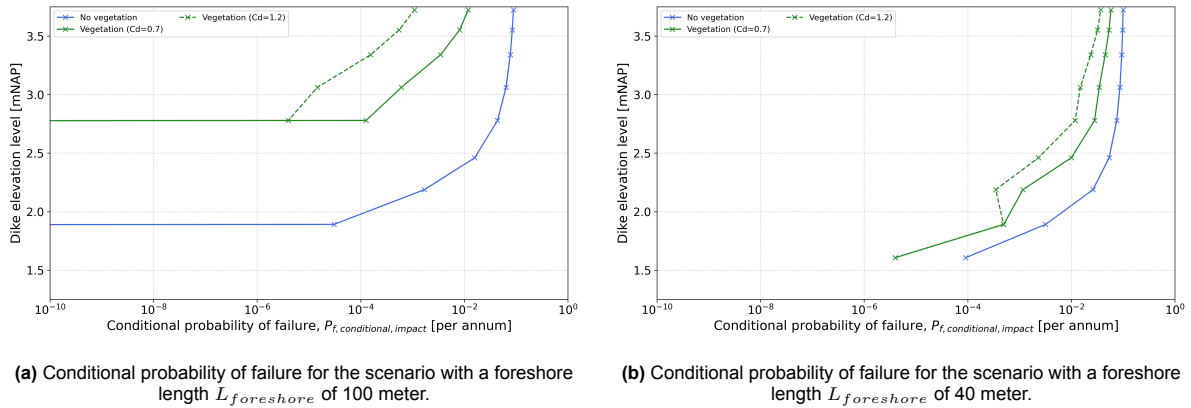
Figure 5.1: Conditional probability of failure for the forest lengths L_{forest} of 100 meter (left) and 40 meter (right). The crosses point out the modelled water levels from table 3.3.

When a forest is placed on both foreshores, it is observed that for the longer forest, the first conditional probability of failure occurs at a much higher water level than the scenario without a forest. For both drag coefficients, the first failure probability is observed at 2.779 mNAP. It is also observed that the forest on the foreshore is able to reduce the probability of failure significantly, where the forest with the higher drag coefficient (C_D = 1.20) is able to reduce more than the forest with the lower drag coefficient (C_D = 0.70). This is in line of expectation, the less drag is induced by the trees, the less wave energy is dissipated, resulting in higher wave heights and higher loads.

The shorter forest shows slightly different behaviour. For the lowest simulated water level (1.607 mNAP), the model does produce conditional failure probabilities, where the forest also shows a reduced conditional probability of failure. For the scenario without a forest, the probability increases when the water level increases. It is observed that for the water level of 2.188 mNAP, the probability is decreased compared to the lower water for the scenario with a higher drag coefficient, and for the lower drag forest the probability increases only by a small margin compared to the lower water level. This water level corresponds with the height of the tree with the largest frontal-surface area, as presented in figure 3.11.
In figure 5.1, both the left and right graph show that for increasing water levels, the effect of the forest on the conditional probability of failure reduces. This can be explained by the equations for the wave energy balance theory, which shows that for higher water levels, the waves interact less with the bottom, and travel through parts of the trees with less frontal-surface area. Less wave energy results in larger waves, which results in larger failure probabilities. This also explains the difference in conditional failure probability for the situation without a forest, for the longer foreshore the failure probability is lower, because the waves travel a longer distance and have more interaction with the bottom, resulting in more wave energy dissipation and lower conditional failure probabilities.

The straight connections between the model results are due to the relative large vertical distance between the water levels. When these large steps Δz are used in the calculation of the total probability of failure P_f, the result would be inaccurate. Therefore, the results are interpolated with a step size of 0.000001 meter, to get the most accurate outcome. This creates many water levels with according conditional failure probabilities based on the results from the simulations. The results of interpolation are shown in figure 5.2.
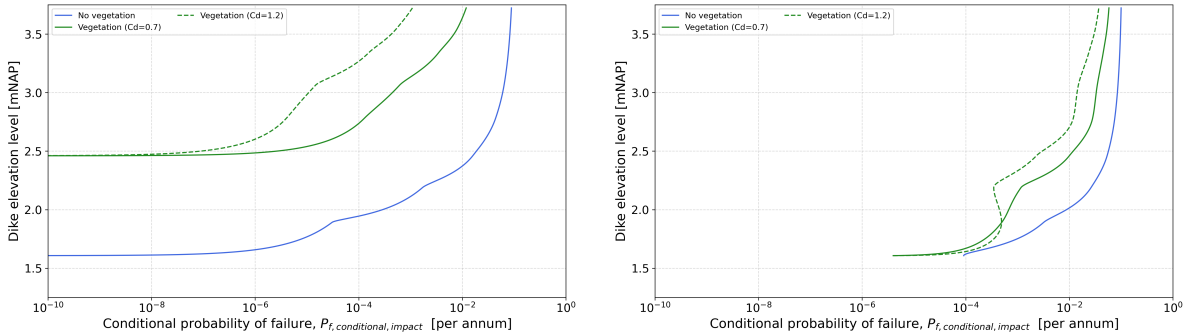
(a) Interpolated conditional probability of failure for the scenario with a foreshore length $L_{foreshore}$ of 100 meter.

(b) Interpolated conditional probability of failure for the scenario with a foreshore length $L_{foreshore}$ of 40 meter.

Figure 5.2: Interpolated conditional probability of failure for the forest lengths L_{forest} of 100 meter (left) and 40 meter (right)

The interpolated graphs shown above are still conditional probabilities of failure. To calculate the combined probability of failure $P(F|h)\,P(h)$ for each water level, the marginal probability of occurrence of a water level $P(h)$ is calculated using the steps as shown in Appendix B.

The conditional probability of failure for each water level from the interpolated results is multiplied with the marginal probability of the particular water level to get the combined probability of failure. The results of this calculation for both forest lengths are shown in figure 5.3.
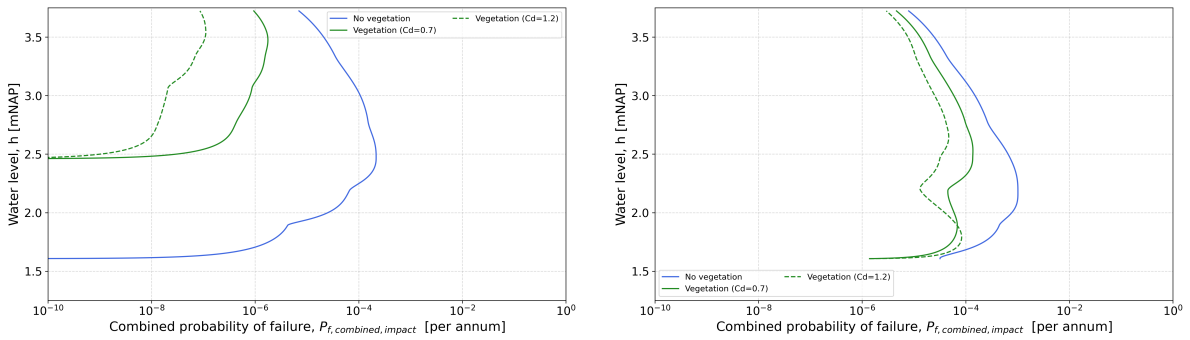
(a) Combined probability of failure for the scenario with a foreshore length $L_{foreshore}$ of 100 meter.

(b) Combined probability of failure for the scenario with a foreshore length $L_{foreshore}$ of 40 meter.

Figure 5.3: Combined probability of failure for the forest lengths L_{forest} of 100 meter (left) and 40 meter (right)

To assess the total probability of failure for the grass revetment due to wave attack, the derived combined probabilities of failure for each interpolated water level as presented above, are integrated over the dike height. Doing this for the different calculations, result in the total failure probability P_f for the assessed dike trajectory for each scenario as presented in table 5.1. The probabilities of failures are assigned the safety category based on the intervals shown in table 2.2, describing whether the signal value or lower limit is met or not. The safety categories make it possible to see at once whether measures are needed to increase the resistance against a certain failure mechanism, as shown in figure 2.7.

Table 5.1: Total probability of failure for the grass revetment due to wave-induced erosion for the scenarios with a 100 meter (left) and 40 meter long forest (right)

	$P_{f,impact,100}$	$P_{f,runup,100}$	$P_{f,total,100}$	**Safety category**	$P_{f,impact,40}$	$P_{f,runup,40}$	$P_{f,total,40}$	**Safety category**
No vegetation	$1.730E-04$	$0.00E+00$	$1.730E-04$	IV	$7.898E-04$	$0.00E+00$	$7.898E-04$	V
Vegetation (Cd = 0.70)	$1.197E-06$	$0.00E+00$	$1.197E-06$	II	$1.305E-04$	$0.00E+00$	$1.305E-04$	IV
Vegetation (Cd = 1.20)	$5.764E-08$	$0.00E+00$	$5.764E-08$	I	$6.374E-05$	$0.00E+00$	$6.374E-05$	IV
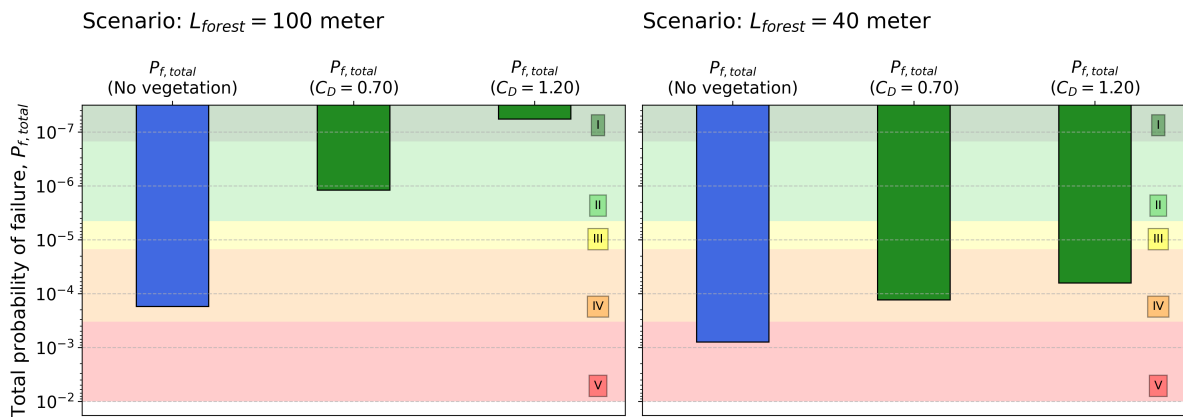
Figure 5.4: Total failure probability for the grass revetment due to wave-induced erosion with the according safety category

Figure 5.4 presents the results from the table above in a similar way as figure 2.7. It is observed that for the current situation, without a forest present on the foreshore, the assessed dike trajectory does not meet the required safety level, as it exceeds both the signal value as the lower limit (safety category IV). It is also observed that for the forest with a length of 100 meter (left), the total probability of the revetment is reduced by a significant amount, which improves the safety category from IV to I for the forest with a drag coefficient of 1.20, and to category II for the forest with a drag coefficient of 0.70.
For the shorter foreshore and forest (right) the same result is found for the situation without a forest, the dike section exceeds the signal value and lower limit, resulting just in safety category V. When a forest is placed on the foreshore, the total probability of failure is reduced for both the higher and lower drag scenarios, but both forests remain in safety category IV, meaning that the safety of the assessed revetment does not meet the required safety level, even with this relative short forest in front of the dike.

5.2. Sensitivity analysis

During the simulations each time a different value for the variable input is used in the model to calculate the probability of failure. A sensitivity analysis is performed to analyse what the contribution is of the variable input parameters. The sensitivity analysis method in the model keeps track of what the effect is of the changes in the input parameters to the outcome. So, when a small change in the value of an input parameter, results in a large change in the outcome, its contributions is large, and vice versa. The percentages of contribution for each variable that result from this analysis are similar to the α-values produced by the first order reliability method [FORM].
Keeping track of these changes results in the sensitivity of each parameter. Only parameters that are sampled from distributions, shown in figures 3.9 and 3.10, are taken into account in the sensitivity analysis, since a change of value is necessary. Therefore the effect of water level, foreshore length, and the bulk drag coefficient are not analysed. Although, their influence is still observed from the results for the probability of failure, and are discussed in the discussion (section 6).

The results analysed in this section are based on the plots in Appendix C and D, which present the results of the sensitivity analysis performed for each calculation. The contribution of each parameter is derived from these figures and put together in the tables, shown in Appendix E. From these tables the following pie charts summarize the contribution of the key parameters.

5.2.1. No forest

The scenario without a forest on the foreshore of the dike can also be referred to as the current situation of the dike. This scenario represent the load due to wave impact on a grass dike for multiple water levels with certain incoming waves. Therefore, the only analysed parameters for this scenario are the wave height, peak wave period and the duration of the load, since there are no variable vegetation parameters to analyse. In table E.1 and E.2 from Appendix E, the contribution of the parameters are shown for

each calculation per water level. For each input parameter, the average contribution is calculated by summing the contribution percentages divided by the number of water levels. The average contribution of the input parameter are shown in the pie charts of figure 5.5.

(a) Percentage of contribution per input parameter for the scenario without a forest (foreshore length of 100 meter)

(b) Percentage of contribution per input parameter for the scenario without a forest (foreshore length of 40 meter)
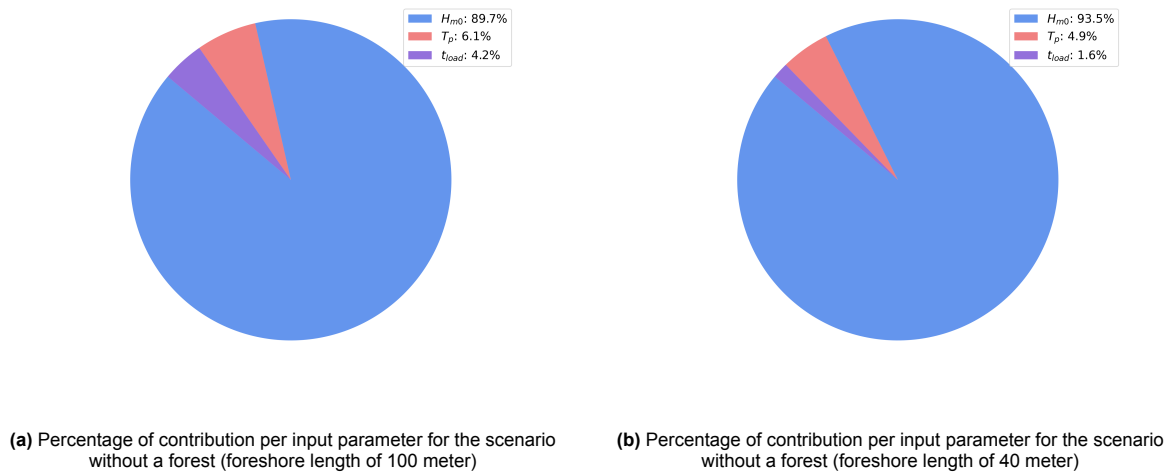
Figure 5.5: Pie charts for the results of the sensitivity analysis for the scenario without a forest

The pie charts show a significant contribution of the wave height on the outcome for wave impact on the grass revetment, which is expected as the wave height is a key parameter in the calculation of the resistance times against wave impact. Since the peak wave period depends extensively on the wave height, its small contribution could be explained by the fact that the influence of the wave period is part of the large contribution of the wave height. The load duration remains constant for the different water levels, as shown in table E.1 and E.2, and has a relative small contribution to the result.

Comparing the outcomes for two simulated forest lengths, it shows that the relative longer foreshore decreases the contribution of the wave height slightly, and increases the contribution of the other two parameters. The increase of the contribution of the load duration for a longer foreshore, could be related to the foreshore dissipating more wave energy, resulting in lower wave heights, which result in longer load duration needed to cause significant changes in the limit state function, and probability of failure.

5.2.2. Forest (drag coefficient = 1.2)

The analysis of the scenarios with a forest take the vegetation and forest parameters into account, so the forest length, frontal-surface area, and the height of the layers are added to the analysis. In Appendix C and D, the results from the simulations are presented in bar charts and pie charts. To come to a general conclusion, the results are taken together in the tables in Appendix E to analyse the effects for every simulation, and what the overall effects of the parameters are. The results from table E.5 and E.6 present the simulations for the 100 and 40 meter forest, accordingly. The contribution for the analysed parameters, where the layer-dependent parameters (frontal-surface area) are accumulated, are presented in the following pie charts.

The two tables in Appendix E, show that the higher the water level rises, the more distributed the percentage of contribution of the frontal-surface area becomes. So, for lower water levels the contribution is more concentrated on the lower layers of the tree, and for larger water levels, the contribution is more distributed. Shown more clearly in table E.6 for the simulations of the shorter forest, which highlights the dependency of the vegetation parameters on the forest length. This dependency on the forest length is observed in the analysis of the combined probability of failure, as shown in figure 5.3, where the longer forest has significantly more effect on the safety level of the assessed dike.

Looking at the pie charts in figures 5.6a and 5.6b, the frontal-surface area contributes the most to the outcome of the simulations with more than 50%, followed by the length of the forest that contributes around 20% to the outcome. The relative high contribution by the frontal-surface area can be due to the higher drag coefficient (C_D) of the tree, since bulk drag coefficient is multiplied with the frontal-surface

area in the vegetation term (equation: (2.15)) of the wave energy equation, increasing the amount of contribution of the frontal area. The bulk

The remaining vegetation parameters show relative low contributions to the outcome. For the height of the layer the contribution is relatively low, since the amount of contribution by the layer height is depending on the water level and the frontal-surface area of the layer, and directly part of a multiplication in the energy balance term. It can be seen as a secondary term, since its value is not directly used in the calculation, but it determines which frontal-surface area is present at which elevation.

5.2.3. Forest (drag coefficient = 0.7)

The analysis of the scenarios for the simulations with a bulk drag coefficient of 0.70, simulating a more flexible forest, creates the opportunity to not only compare the results for different forest lengths, but also to compare the effect of the bulk drag coefficient of the trees, since the bulk drag coefficient is not part of the analysed parameters. Appendix D and C show the results visualized in bar charts and pie chart to display the contribution for each parameter per simulated water level. To compare the overall results and analyse the effect of the parameters on the outcome, the results are collected in the tables in Appendix E and result in the following pie charts for the forest length of 100 and 40 meter, where the layer-dependent parameters are accumulated.

From the pie chart in figures 5.6c and 5.6d, the first observation is that the contribution of the frontal-surface area and the forest length decreased slightly with respect to the higher drag forest simulations. Together with a slight increase in the effect due to the wave height, tree height and bulk drag coefficient. The frontal area and the forest length remain the vegetation parameters with the highest contribution to the outcome, but the lower drag resulted in more contribution on the outcome by the wave height, due to less energy dissipation.
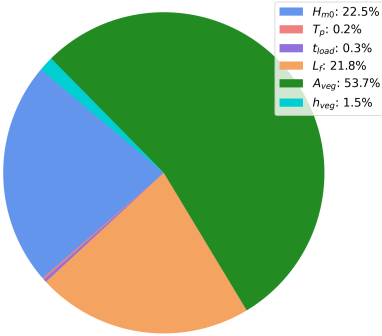
(a) Percentage of contribution per input parameter ($L_{forest} = 100$m and $C_D = 1.2$)
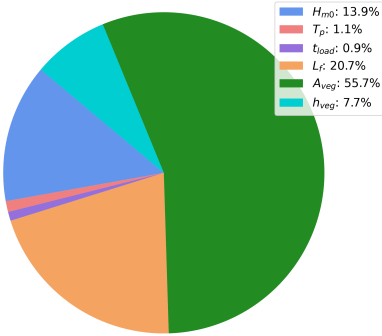
(b) Percentage of contribution per input parameter (($L_{forest} = 40$m and $C_D = 1.2$)
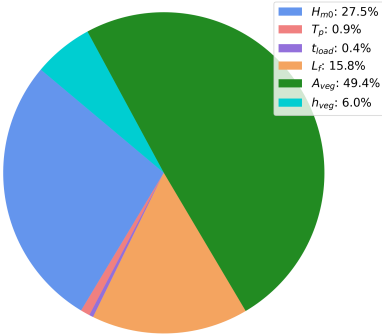
(c) Percentage of contribution per input parameter (($L_{forest} = 100$m and $C_D = 0.7$)
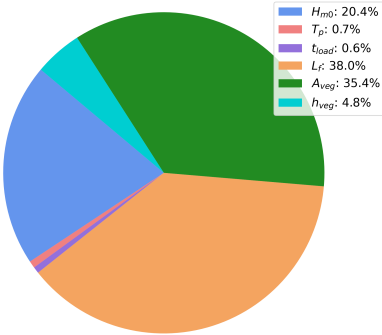
(d) Percentage of contribution per input parameter (($L_{forest} = 40$m and $C_D = 0.7$)

Figure 5.6: Pie charts for the results of the sensitivity analysis for the scenario with a forest

<div style="text-align: right">

6

Discussion

</div>

This chapter provides a critical analysis and interpretation of the findings presented in the previous chapters. The used methodology, results and findings of the simulations will be brought forward and discussed. This chapter works towards the final conclusion of the research into the potential of using riparian forest in dike design.

In Chapter 2 the dike design and assessment methods used in the Netherlands were studied in order to find how the use of forests could improve the safety level of existing dikes. Vegetated foreshores hold the potential to dissipate wave energy, and therefore hold the potential to reduce the failure probability related to wave attack on a dike, i.e. wave impact and wave load. Vegetated foreshores are not implemented in the current assessment, which created the opportunity to research and discuss its potential to improve dike design.

6.1. Model set-up

The results described in Chapter 5 point out the effects that different parameters have on the probability of failure. The methodology designed in this research focused on combining a wave attenuation model and the current used methods of calculating wave load due to wave impact and run-up. This connects the findings of previous studies towards the influence of vegetation on waves to the probability of failure of flood defense structures. Limitations of combining the two is that the current used methods implements the effects of foreshores in the calculation by taking it into account while generating the input for the assessment, and use the outcome directly on the structure. The designed model in this study has the foreshore effects in the calculation, the advantage is that it makes it possible to model vegetation on the foreshore and analyse the effects. The disadvantage is that it increases the computation time, because the wave energy balance differential equations are solved by iterating over the total foreshore length.

The designed model is based on several trade-offs. Modelling the vegetated foreshore with different layers of vegetation parameters over the height, connecting it to the calculations for the wave impact and run-up calculations, and performing Monte Carlo simulations made it a computational intensive model. Adjustments to the model can be made on several parts of the model to make it less intensive for computation.

First, the Monte Carlo simulation could be replaced by a different reliability analysis method, such as the first order reliability method (FORM). The disadvantage of FORM is that the input parameters need to have Normal-distributions, which was the reason that Monte Carlo was used in this thesis. The advantage of FORM is that it uses less samples to come to an accurate result, and that the sensitivity analysis is less intensive to compute. Another adjustment could be to add the calculation of the total probability of failure to the model. In this research the model produces the conditional probability of failure, and the total probability of failure is produced outside of it. This may increase the computation time slightly, but make it more user-friendly. An adjustment to decrease the runtime would be to implement thresholds for the wave load calculations. The wave height, or loading time, required for wave

load to occur can be used to skip a whole calculation if it is not large enough to induce erosion.

6.2. Probability of Failure

These effects of the foreshore length, and thereby forest length, are visible in every result of the calculation. In the conditional probability of failure in figure 5.1, it is shown that the failure probability is reduced significantly comparing by the longer and shorter forest. This is the result of the interaction between the foreshore and forest with the waves, the longer the foreshore, the more interaction between the waves and the foreshore, i.e. forest and bottom, can take place. The probabilities of zero for the longer forest, and the relative low probabilities for the shorter forest for the lower water levels, underline this theory. The influence by the forest length is also observed in the total failure probability of the dike revetment, showing that a long enough forest is able to improve the safety level from insufficient, to a safety level that meets the signal value, or meet it by a margin based on the drag coefficient of the forest. However, the opposite is found when the forest length is relative short. The influence of the forest is not sufficient to result in a safe grass revetment. This highlights the importance of the foreshore and forest length to the probability of failure due to erosion by wave attack.

Erosion due to wave run-up was not observed in the results for the scenario without a forest, indicating that the wave heights are to low for this failure mechanism to occur, and that it did not contribute to the total probability of failure for the assessed location. For dikes where higher water levels, and higher waves can occur, failure due to run-up can add to the total probability of failure for the assessed dike. Studies found that wave impact is dominant over wave run-up for the elevation levels below the highest still water level, and wave run-up above the highest still water level. As observed from the graphs, especially the conditional probability of failure, the effect of the forest on the probability of failure due to wave impact decreases as the water level increases. This could indicate that the effect of a forest on wave run-up is relative low, due to the larger waves needed for wave run-up, which needed more water depth to occur, while a higher water level shows a relative lower influence on the wave impact failure probability.

It is observed that the largest total probability of failure is not found for the highest water level. Due to the multiplication of the conditional failure probability (which is the highest for the highest water level) with the marginal probability (which becomes smaller when the water level increases) reduce the combined probability of failure for larger water levels. This means that the highest water level does not lead to the largest combined failure probability, since it occurs for the combination with the largest probabilities of occurrence. This points out the potential of using forests to prevent against wave load. When the largest combined failure probability is located at an elevation where the frontal-surface area of the tree is large, the total failure probability can be reduced significantly, as shown in the results.

For different failure mechanisms, such as erosion on the inner slope (as a result of wave overtopping), the influence of the trees are different. There the effect is affected by the freeboard, the vertical distance from still water level to the crest. For increasing water levels, the freeboard becomes smaller and overtopping occurs more frequent. For this failure mechanism, the largest total probability of failure will be found for higher water levels, so the largest frontal-surface area should be larger higher in the tree to be effective.

6.3. Sensitivity of parameters

In the results for the shorter forest, for the lower water levels between 1.70 and 2.30 mNAP, a decrease in failure probabilities for the shorter forests with larger drag (simulating a forest with stiffer trees), and stagnation of the failure probability for the lower drag forest (simulating more flexible trees) is observed in the lines in figures 5.2b and 5.3b. The elevation level where the decrease/stagnation in the lines occur, corresponds with tree layer where the largest frontal-surface area is located, demonstrating the effect of the frontal-surface area on the conditional and total probability of failure.

The effect of the frontal-surface area is also observed in the sensitivity analysis, as it is the parameter with the most significant contribution to the calculations of the limit state functions for every scenario. For the longer forest, it contributes for roughly 50 % to the outcome of the limit state calculations. Followed by the length of the forest, which has the second-largest contribution of around 15 to 25 %. This can be due to the fact that the length of the forest determines the amount of interaction between the waves and the foreshore/forest, as described above.

The sensitivity of the parameters is important in the process of dealing with uncertainty. Earlier studies show the relevance of dealing with uncertainty in the design and assessment of failure probability for different scenarios. For relative low water levels, this study shows that a forest contributes largely to the conditional probability of failure for lower water levels, while for relative high water levels, the contributions seems to decrease. The sensitivity of a parameter and its uncertainty are highly related to each other regarding the importance for design. Highly uncertain parameters, such as variation between frontal-surface area between different tree species, with a high contribution to the failure probability should be treated with more care than the highly uncertain parameters with a relative low contribution. Therefore, the uncertainty, or variability, in the frontal-surface area of the trees and the variability in the length of a forest should be considered as the most valuable design parameters of the forest, accompanied by the variability in the wave height. Since the bulk drag coefficient is not considered in the sensitivity analysis, no conclusions can be connected to the magnitude of contribution. However, from the graphs and results for the failure probability, the effect of the drag, and thereby partially the flexibility of the tree, highlights that an amount of contribution should be assigned to the bulk drag coefficient of the tree.

6.4. Vegetation in safety assessment

The results and findings described above in the failure probability and sensitivity analysis, indicate the potential that the vegetation has to increase the safety level, and thereby safety categories of a dike section. To incorporate vegetated foreshores in the safety assessment and design methodology, previous studies stated that to let the forests be an reliable addition, more reliability analysis and testing to engineering standards is required. The results of this study can contribute to this with the findings regarding the contribution of the parameters to the probability of failure.

The relative large contribution of the forest length and the frontal-surface area are considered as the most valuable parameters to be used in design and assessment. Having enough space for forests to grow, and having trees with the largest frontal-surface area in front of the elevation on the dike slope where the combined probability of failure becomes the largest can have a significant effect on the safety level of the dike. The bulk drag coefficient is probably the second-most important parameter, since the effect on the probability of failure is proven to be significant. However, the bulk drag coefficient is a parameter depending on several processes, one of them being the flexibility of the tree, which makes it less suitable as a design parameter, but not less important for the assessment of the safety level.

The large contribution by the forest length and frontal-surface area not only make it the most valuable parameter, but also the most vulnerable parameter. Some uncertainties, i.e. diseases and seasonal variability, will remain present, which results in the importance to implement securities, i.e. maintenance, in the design of a forest to keep it at the required safety level, which applies to all types of defense structure protections.

The input variables for the forest and trees, e.g. forest length, frontal-surface area, and vegetation height, are based on measurements. The forest length is based on the possible length normal to the dike trajectory and the parameters for the trees are based on measurements of 15-year old willow trees last cut 3 years back. Compared to the real situation, where diseases may occur and the willows are cut periodically, the results can be considered idealistic. The forest may lose its strength due to a disease or the frontal-surface area may be lost for severeal layers due to cutting of the branches. Implementing these factors in the model can be done by modelling different scenarios, that simulate the effect of a disease. To model the effect of cutting, scenarios can be created where the forest is distributed in different stretches of forest, e.g. cut recently, cut one year ago, and cut two years ago. This should give a more accurate result, but looking at the results in chapter 5, a forest with sufficient length has a margin before it does not meet the required safety level.

Using vegetated foreshores in front of the dike sections where it is possible, so when the safety level due to outer slope erosion is insufficient with regard to the required standard, and whether there is enough room for a forest to grow, has the potential to be a reliable, cost-effective and nature-friendly solution to increase the safety level. Using a forest on the foreshore, instead of harder revetment types, creates the opportunity to use forces of nature to protect against forces of nature.

7
Conclusion

This section combines the findings from the theoretical analysis and the probabilistic analysis using the created model, to conclude about the potential of using riparian forests to attenuate waves and optimize dike design.

To create a model that calculates failure mechanisms related to wave loads using the same method as currently used in the assessment of dike trajectories, the design and assessment standards were analysed. In the Netherlands, dikes are designed and assessed according to their level of safety against flooding. The safety level against flooding is distributed over the probabilities of failure for different dike failure mechanisms, that together form the probability of flooding. Vegetated foreshores hold the capability to dissipate wave energy, and can therefore reduce the failure probability due to wave-related failure mechanisms, such as erosion of the outer slope grass revetment due to wave impact and wave run-up. A grass revetment is eroded due to wave impact below the highest occurring still water level, and above this level by wave run-up.

Currently, vegetation is not incorporated in the methodology for design to, and assessment of, the safety level. To be implemented in detailed designs and assessments of river dikes with respect to wave load, the mechanism behind wave dampening due to vegetation has been studied. Vegetation fields on the foreshore of a dike, such as riparian forests, has been proven to be able to attenuate wave load by dissipating energy from the waves travelling through them. The wave energy balance is affected by three energy dissipating terms, a term due to breaking, due to bottom-friction, and due to vegetation. The parameters in the term due to vegetation are the frontal-surface area over the height of the vegetation, the ratio of the vegetation that is submerged, the bulk drag coefficient, and the length that the waves travel through the vegetation field.

This study combined the current-used methods to calculate erosion due to wave impact and run-up with a model to determine the wave energy dissipation for the described dissipation terms. The created model made it possible to analyse the effect of a forest on the probability of failure of the outer slope due to wave impact, and to analyse which parameters contribute most to this probability of failure.

In the end, to incorporate vegetation in the safety level calculation of a dike trajectory, insight in the contribution of the forest and tree parameters is necessary. The case study performed in this study showed that the largest contribution came from the frontal-surface area (50%), and that the largest reduction in failure probability for erosion of the outer slope was found when the largest amount of frontal-surface area was located at the same level as the level where the largest combined failure probability is found. For the 40 meter foreshore, the combined failure probability on the elevation level where the largest frontal-surface area is present, was decreased from $O(10^{-3})$ for the situation without a forest, to $O(10^{-4})$ for the forest with a bulk drag coefficient of 0.70 (relative flexible vegetation), and $O(10^{-5})$ for the forest with a bulk drag coefficient of 1.20 (relative stiff vegetation). For the 100m foreshore, the combined failure probability for the situation without a forest of $O(10^{-4})$, was decreased to zero for both bulk drag coefficients. This proofs that the elevation height of the largest frontal-surface area is an important

component for design and assessment of a dike.

It also shows that the magnitude of the effect on the probability of failure of the outer slope is strongly influenced by the length of the forest. The longer the forest, the more energy can be dissipated from the incoming waves by the frontal-surface area, and drag induced by the vegetation. Therefore, both the forest length and the frontal-surface area can be used to design a protective forest by adjusting them to increase the level of safety to the required level, or to determine if an existing forest can provide protection for a particular location if its dimensions are significantly large enough.

The fact that it can be used for the design of a safe dike section, but also for the assessment of a dike section, proves that vegetated foreshores can be suitable measures to be integrated into the current methods used in the Netherlands. Willows have been applied in the Noordwaard polder in the Netherlands (WitteveenBos et al. n.d.), which made it possible to raise the dike one meter less than originally designed and use a clay cover instead of stone revetment (WitteveenBos et al. n.d.).

Existing dike trajectories that do not meet the signal value in the previous large-scale safety assessment, and have enough space to grow a large enough forest on the foreshore can improve their safety level by growing a forest on the foreshore of the dike. When the forest is designed to have the largest frontal-surface on the same level as the largest combined probability of failure, the failure probability due to erosion of the outer slope can be reduced significantly. It should be taken into account that the results do not account for threats as diseases or the cutting of the branches, taking these into account probably results in lower probabilities of failure, but further research into this must provide more insight in these phenomena.

This research has shown that the use of riparian forests on the foreshore of a dike as a protective measure against wave attack, has the potential to increase the safety level significantly. Using the wave energy dissipating properties of a riparian forest and connect it to the current-used design and assessment methods for grass revetment erosion has the potential to be used for detailed designs and assessments, and to reduce the need for hard revetment types.

<div align="right">

8

</div>

Recommendations

This chapter outlines recommendations for future research and practical applications based on the results of this study. While this study has demonstrated the potential of riparian forests for wave attenuation and improved dike designs, several areas require further investigation to refine these strategies and improve the reliability for more general application. The recommendations aim to point out remaining knowledge gaps, improve methodological approaches and support the integration of vegetated foreshores into flood defence systems.

8.1. Model extension

The main driver behind the research to vegetation is that uncertainty makes it less reliable to incorporate vegetated foreshores in the design and assessment methods. This amount of uncertainty is reduced by performing more research to generate more knowledge and insight in the processes.

The findings from this study show the potential of applying forests as protective measure on the foreshore of dikes. The modelling technique used in this study is on several points simplified with regard to the situation in the real world. The created model uses a two-dimensional wave field, so waves travelling in straight lines through the forest. To extend the model, using a three-dimensional model to model the wave propagation through a riparian forest attacking the dikes outer slope, could provide different perspectives on the results from this study, and gather more detailed information to get the full picture on the grass revetment erosion process. A three-dimensional model can provide valuable insight in the effect of the angle of wave attack, which influences the length that the waves travel through the forest, and influence the magnitude of wave run-up load.

Another improvement of the model could be to perform more simulations in the Monte Carlo simulations by increasing the number of samples. This can result in smaller failure probabilities for the lower water levels, where in this study the results were zero. More samples make it possible to find smaller probabilities, as shown in the literature study in this research. For the assessed dike trajectory, the failure probabilities due to wave run-up all came out to be zero, due to the high water level required for erosion due to wave run-up to occur. The result that no run-up was found for the assessed location in this study, does not mean that this is the same for other dike trajectories in the Netherlands. The trajectories where higher waves occur, due to larger fetch lengths and/or deeper water in front of the dike, failure of the outer slope due to wave run-up can occur. Performing case studies on trajectories in the Netherlands where erosion due to wave impact and wave run-up occur both, creates more insight in the total failure mechanism for erosion of the grass revetment on the outer slope.

Continuing on the effect of wave run-up, as the wave run-up exceeds the crest level, the failure mechanism of overtopping occurs, leading to erosion of the inner slope. This failure mechanism is assessed with the discharge flowing over the top, or the accumulation of volumes flowing over the outer slope. Adding the wave overtopping failure mechanism to the model can be a valuable extension of the model as it can increase the number of potential locations in the Netherlands to use vegetated foreshores.

The wave energy dissipation term, and the related input parameters in this study are based on previous research towards willow trees. An extension of the model/study could be to test different types of riparian vegetation in large-scale wave flumes. Gathering more riparian vegetation data is useful to validate the model and test more hypothesis regarding the effects of bulk drag coefficients, and increase the reliability and create more foundation for applying riparian forests in dike design and assessment. The real world threats, e.g. diseases and cutting of the branches, were not in the scope of this research, but could influence the outcomes. Research into the influence of loss of forest due to a disease or loss of frontal-surface area for some stretches of the forest due to cutting can be modelled using different scenarios, and compare the results with findings of this research to provide more support for the results.

8.2. Reflection on policy

As described, the reliability of using vegetated foreshores has to be high enough for large scale application. The following studies and research are part of the timeline towards the point of implementation in the design and assessment methods for dikes in the Netherlands.

The start is the research that is, and will be conducted in the following years, aiming to identify the key parameters in the process, and create the necessary knowledge for the various types of riparian forests and there behaviour under different circumstances. Cooperated research between regulatory bodies, research institutions, and industry experts will create the required vegetation data and models to create design codes. The design codes are necessary to create a clear and general framework for application of vegetated foreshores in to the flood defense systems, similar to the codes that already exist for, e.g., breakwaters.

Pilot projects create a lot of potential future studies to validate the effectiveness of the design codes and use of vegetated foreshores. Monitoring and data collection from these projects provides critical information on the reduce wave load, erosion rates of the revetment, and the vegetation health.

The next step is that the existing hydrodynamic models used for design and assessment has to be adapted to incorporate the influence of vegetated foreshores on the model. Research with the adapted models in risk assessments, makes it possible to better assess the contribution of the overall safety against flooding of dike sections, and whether the design choice with a vegetated foreshore outperforms the other safety increasing options.

The last step is to incorporate the effects in national safety standards, to make it possible to make the use of vegetated foreshores more widely adopted in the design and large-scale safety assessments. As described in this last part, before arriving at this point the cooperated research and reliability increasing studies are of major importance to create the design codes for vegetated foreshores, and use their potential to create safer and greener dike trajectories in the Netherlands.

References

AHN (2019). *Actueel Hoogtebestand Nederland*. `https://ahn.arcgisonline.nl/ahnviewer/`. Accessed: 18 July 2024.

Arnold, G. et al. (2009). *Watermanagement in the Netherlands*. RWS WD.

Atmanspacher, Harald and Mike Martin (Aug. 2019). "Correlations and How to Interpret Them". In: *Information* 10, p. 272. DOI: `10.3390/info10090272`.

Battjes, J.A. (Jan. 1974). "SURF SIMILARITY". In: *Coastal Engineering Proceedings* 1 (14), p. 26. ISSN: 0589-087X. DOI: `10.9753/icce.v14.26`.

Bertotti, Luciana and Luigi Cavaleri (Jan. 2000). "Accuracy of Wind and Wave Evaluation in Coastal Regions". In: pp. 57–67. DOI: `10.1061/9780784400890.005`.

Bilkovic, Donna Marie et al. (2017). "Living shorelines : the science and management of nature-based coastal protection". In: CRC Press, Taylor & Francis. Chap. 8, p. 499. ISBN: 9781498740029.

BOI, Programmateam (2019). *Programmaplan BOI 2020 - 2023*. Tech. rep. Rijkswaterstaat Ministerie van Infrastructuur en Waterstaat.

Booij, N., R. Ris, and Leo Holthuijsen (Jan. 1999). "A third-generation wave model for coastal regions, Part I, Model description and validation". In: *J. Geophys. Res.* 104, pp. 7649–7656.

Bryan, Karin R. and Hannah E. Power (2020). "4 - Wave behaviour outside the surf zone". In: *Sandy Beach Morphodynamics*. Ed. by Derek W.T. Jackson and Andrew D. Short. Elsevier, pp. 61–86. ISBN: 978-0-08-102927-5. DOI: `https://doi.org/10.1016/B978-0-08-102927-5.00004-7`. URL: `https://www.sciencedirect.com/science/article/pii/B9780081029275000047`.

Burgers, T. (2014). *Nederlands grote rivieren: drie eeuwen strijd tegen overstromingen*. Matrijs, Utrecht.

Çete, Ceylan (2019). "Quantifying the effect of woody vegetation on the wave loads on a dike using remote sensing: Large scale physical model tests". In: URL: `https://api.semanticscholar.org/CorpusID:155661998`.

Dalrymple, Robert, James Kirby, and Paul Hwang (Feb. 1984). "Wave Diffraction Due to Areas of Energy Dissipation". In: *Journal of Waterway Port Coastal and Ocean Engineering-asce - J WATERW PORT COAST OC-ASCE* 110. DOI: `10.1061/(ASCE)0733-950X(1984)110:1(67)`.

de Bruijn, M. (2020). "Wave attenuation due to vegetation: Duursche Waarden (case study)". MA thesis. Delft University of Technology.

de Bruin, Huub, Goaitske de Vries, and Robert 't Hart (2016). *Voorschrift Toetsen op Veiligheid, Technisch Deel*. Tech. rep. Deltares.

de Waal, J.P. (2018). *Basisrapport WBI 2017 Versie 1.2*. Tech. rep. Rijkswaterstaat Water, Verkeer en Leefomgeving.

de Waal, J.P. and A. van Hoven (2015a). *Failure Mechanism Module Grass Wave Impact Zone Requirements and Functional Design*. Tech. rep. Deltares.

– (2015b). *Failure Mechanism Module Grass Wave Runup Zone Requirements and Functional Design*. Tech. rep. Deltares.

Deltares (2019). *Gebruikershandleiding Basis Module Gras Buitentalud*. Deltares. Boussinesqweg 1, Delft.

Diermanse, F., Ruben Jongejan, and Annemargreet de Leeuw (2016). *WBI - Onzekerheden*. Tech. rep. Ministerie van Infrastructuur en Milieu, Interprovinciaal Overleg, and Unie van Waterschappen.

E. Penning and V. Harezlak (2020). *Handleiding Vegetatiemonitor2.0*. Deltares. Boussinesqweg 1, Delft.

Eijgenraam, Carel (Apr. 2006). "Optimal safety standards for dike-ring areas". In.

Eyck, Bart van (1995). *Hoog water 1995 Rivierdijken*. `https://www.archieven.nl/nl/zoeken?mivast=0&mizig=269&miadt=2606&miview=gal&milang=nl&mizk_alle=van+Eyck+itteren`. Accessed: 14 August 2024.

Gerritsen, Herman (June 2005). "What Happened in 1953? The Big Flood in the Netherlands in Retrospect". In: *Philosophical transactions. Series A, Mathematical, physical, and engineering sciences* 363, pp. 1271–91. DOI: `10.1098/rsta.2005.1568`.

Gibson, William H (2011). "Probabilistic Methods for Slope Analysis and Design". In: URL: `https://www.researchgate.net/publication/282853927`.

Hasselmann, K., T.P. Barnett, et al. (1973). "Measurements of wind-wave growth and swell decay during the Joint North Sea Wave Project (JONSWAP)." In: *Ergaenzungsheft zur Deutschen Hydrographischen Zeitschrift, Reihe A*.

Hasselmann, K. and J.I. Collins (1968). "Spectral Dissipation of Finite-depth Gravity Waves Due to Turbulent Bottom Friction'". In: *Journal of Marine Research* 26 (1). URL: `www.journalofmarineresearch.org`.

HWBP (2023). *HWBP 'voor sterke dijken'*. [Accessed on October 26th, 2023]. URL: `https://www.hwbp.nl/`.

IPLO (2023). *BOI-programma 2023-2035*. `https://iplo.nl/thema/water/waterveiligheid/programma-projecten-waterveiligheid/boi-programma-2023-2035/`. Accessed: 13 August 2024.

Jongejan, R.B. and E.O.F. Calle (June 2013). "Calibrating semi-probabilistic safety assessments rules for flood defences". In: *Georisk* 7 (2), pp. 88–98. ISSN: 17499518. DOI: `10.1080/17499518.2013.790731`.

Jongejan, R.B., F. Diermanse, et al. (2020). "Reliability-based partial factors for flood defenses". In: *Reliability Engineering & System Safety* 193, p. 106589. ISSN: 0951-8320. DOI: `https://doi.org/10.1016/j.ress.2019.106589`. URL: `https://www.sciencedirect.com/science/article/pii/S0951832019300717`.

Jonkman, S.N. (Jan. 2007). "Loss of Life Estimation in Flood Risk Assessment: Theory and Applications". In.

Jonkman, S.N., R.E. Jorissen, et al. (Apr. 2021). "Lecture notes CIE5314 Flood Defences". In.

Jonkman, S.N., H. G. Voortman, et al. (Mar. 2018). "Developments in the management of flood defences and hydraulic infrastructure in the Netherlands". In: *Structure and Infrastructure Engineering* 14.7, pp. 895–910. DOI: `10.1080/15732479.2018.1441317`. URL: `https://doi.org/10.1080/15732479.2018.1441317`.

Kalloe, S.A. et al. (Mar. 2022). "Quantifying Frontal-Surface Area of Woody Vegetation: A Crucial Parameter for Wave Attenuation". In: *Frontiers in Marine Science* 9. ISSN: 22967745. DOI: `10.3389/fmars.2022.820846`.

Keijser, Mischa (2021). *Sapiens*. `https://mischakeijser.com/series/sapiens`. Accessed: 12 August 2024.

Kobayashi, Nobuhisa, Andrew W. Raichle, and Toshiyuki Asano (1993). "Wave Attenuation by Vegetation". In: *Journal of Waterway, Port, Coastal, and Ocean Engineering* 119.1, pp. 30–48. DOI: `10.1061/(ASCE)0733-950X(1993)119:1(30)`. eprint: `https://ascelibrary.org/doi/pdf/10.1061/%28ASCE%290733-950X%281993%29119%3A1%2830%29`. URL: `https://ascelibrary.org/doi/abs/10.1061/%28ASCE%290733-950X%281993%29119%3A1%2830%29`.

Kok, Matthijs et al. (2016). *Grondslagen voor hoogwaterbescherming*. 1st ed. Ministerie van Infrastructuur en Milieu and ENW.

Kruse, GAM (2010). "Studie voor richtlijnen klei op dijktaluds in het rivierengebied [Study for guidelines for clay on dike slopes in riverine areas]". In: *Report No. 1202512*.

M. Duits (2020). *Hydra-NL Gebruikershandleiding (versie 2.8)*. HKV lijn in water BV. Botter 11-29, Lelystad.

Mendez, Fernando J. and Inigo J. Losada (2004). "An empirical model to estimate the propagation of random breaking and nonbreaking waves over vegetation fields". In: *Coastal Engineering* 51.2, pp. 103–118. ISSN: 0378-3839. DOI: `https://doi.org/10.1016/j.coastaleng.2003.11.003`. URL: `https://www.sciencedirect.com/science/article/pii/S0378383903001182`.

Möller, I. and T. Spencer (Mar. 2002). "Wave dissipation over macro-tidal saltmarshes: Effects of marsh edge typology and vegetation change". In: vol. 36. Coastal Education Research Foundation Inc., pp. 506–521. DOI: `10.2112/1551-5036-36.sp1.506`.

Muijs, J. A. (1999). "Grass cover as a dike revetment". In: URL: `https://api.semanticscholar.org/CorpusID:127009125`.

Oestges, Claude and Danielle Vanhoenacker-Janvier (Apr. 2001). "A physical-statistical shadowing correlation model and its application to low-Earth-orbit systems". In: *Vehicular Technology, IEEE Transactions on* 50, pp. 416–421. DOI: `10.1109/25.923053`.

Quartel, S. et al. (Feb. 2007). "Wave attenuation in coastal mangroves in the Red River Delta, Vietnam". In: *Journal of Asian Earth Sciences* 29 (4), pp. 576–584. ISSN: 13679120. DOI: `10.1016/j.jseaes.2006.05.008`.

RWS (2017). *Handreiking ontwerpen met overstromingskansen*. Tech. rep. Rijkswaterstaat Water, Verkeer en Leefomgeving.

– (2022a). "Nationaal Deltaprogramma 2023". In.

– (n.d.). *Ruimte voor de rivieren*. `https://www.rijkswaterstaat.nl/water/waterbeheer/bescherming-tegen-het-water/maatregelen-om-overstromingen-te-voorkomen/ruimte-voor-de-rivieren`. Accessed: 14 August 2024.

– (2022b). *Schematiseringshandleiding grasbekleding*. Tech. rep. Rijkswaterstaat, Water Verkeer en Leefomgeving.

RWS, Kennisplatform Risicobenadering, and Deltares (2016). *Achtergrondrapport Ontwerpinstrumentarium 2014*. Rijkswaterstaat Water, Verkeer en Leefomgeving.

Saltelli, Andrea and Paola Annoni (Jan. 2010). "Sensitivity Analysis". In: DOI: `10.1007/978-3-642-04898-2_509`.

Saltelli, Andrea, M. Ratto, et al. (Jan. 2008). *Global Sensitivity Analysis. The Primer*. Vol. 304. ISBN: 9780470059975. DOI: `10.1002/9780470725184.ch6`.

Schiereck, G.J. and H.J. Verhagen (2019). *Introduction to bed, bank and shore protection: Revised edition*. English. Delft Academic Press. ISBN: 978-90-6562-4413.

Schoonees, T. et al. (2019). "Hard Structures for Coastal Protection, Towards Greener Designs". English. In: *Estuaries and Coasts* 42.7. Special Issue: Integrating Ecosystems and Coastal Engineering Practice, pp. 1709–1729. ISSN: 1559-2723. DOI: `10.1007/s12237-019-00551-z`.

Schüttrumpf, Holger (Jan. 2001). "Wellenüberlaufströmung bei Seedeichen – Experimentelle und Theoretische Untersuchungen". In.

Sekhavatian, Arash and A. Choobbasti (Dec. 2018). "Comparison of Point Estimate and Monte Carlo probabilistic methods in stability analysis of a deep excavation". In: *International Journal of Geo-Engineering* 9. DOI: `10.1186/s40703-018-0089-8`.

Sobol', I.M (2001). "Global sensitivity indices for nonlinear mathematical models and their Monte Carlo estimates". In: *Mathematics and Computers in Simulation* 55.1. The Second IMACS Seminar on Monte Carlo Methods, pp. 271–280. ISSN: 0378-4754. DOI: `https://doi.org/10.1016/S0378-4754(00)00270-6`. URL: `https://www.sciencedirect.com/science/article/pii/S0378475400002706`.

Suzuki, T (2011). "Wave dissipation over vegetation fields". English. PhD thesis. Delft University of Technology. ISBN: 978-94-91211-44-7.

TAW (2000). *From probability of exceedance to probability of flooding*. Tech. rep. Technical Advisory Committee for Flood Defence in The Netherlands.

Temmerman, Stijn et al. (Dec. 2013). "Ecosystem-based coastal defence in the face of global change". In: *Nature* 504, pp. 79–83. DOI: `10.1038/nature12859`.

Thornton, Ed and R. Guza (Jan. 1983). "Transformation of Wave Height Distribution". In: *Journal of Geophysical Research* 88, pp. 5925–5938. DOI: `10.1029/JC088iC10p05925`.

Tockner, Klement and Jack A. Stanford (Sept. 2002). *Riverine flood plains: Present state and future trends*. DOI: `10.1017/S037689290200022X`.

van Baars, Stefan (Jan. 2004). "Peat Dike Failure in the Netherlands". In.

– (Jan. 2009). "The Causes and Mechanisms of Historical Dike Failures in the Netherlands". In.

van der Krogt, M.G. (2022). "Reliability updating for slope stability: Improving dike safety assessments using performance information". In.

van der Meer, J.W. et al. (2018). *EurOtop, 2018. Manual on wave overtopping of sea defences and related structures. An overtopping manual largely based on European research, but for worldwide application*. Tech. rep. URL: `www.overtopping-manual.com`.

van Wesenbeeck, B.K. et al. (Dec. 2022). "Wave attenuation through forests under extreme conditions". In: *Scientific Reports* 12 (1). ISSN: 20452322. DOI: `10.1038/s41598-022-05753-3`.

van Wesenbeeck, Bregje K. et al. (Mar. 2014). "Damming deltas: A practice of the past? Towards nature-based flood defenses". In: *Estuarine, Coastal and Shelf Science* 140, pp. 1–6. ISSN: 02727714. DOI: `10.1016/j.ecss.2013.12.031`.

van Zelst, Vincent T.M. et al. (Dec. 2021). "Cutting the costs of coastal protection by integrating vegetation in flood defences". In: *Nature Communications* 12 (1). ISSN: 20411723. DOI: `10.1038/s41467-021-26887-4`.

VegetationChart (2020). *VegetatieMonitor*. `https://vegetatiemonitor.rijkswaterstaat.nl/#/veld`. Accessed: 12 July 2024.

Vergouwe, Ronny et al. (2014). *De veiligheid van Nederland in kaart*. Tech. rep. Deltares.

Vuik, V. (2019). "Building safety with nature Salt marshes for flood risk reduction". PhD thesis. ISBN: 9789463324700. DOI: `10.4233/uuid:9339474c-3c48-437f-8aa5-4b908368c17e`. URL: `https://doi.org/10.4233/uuid:9339474c-3c48-437f-8aa5-4b908368c17e`.

Vuik, V., H.Y. Suh Heo, et al. (Jan. 2018). "Stem breakage of salt marsh vegetation under wave forcing: A field and model study". In: *Estuarine, Coastal and Shelf Science* 200, pp. 41–58. ISSN: 02727714. DOI: `10.1016/j.ecss.2017.09.028`.

Vuik, V., S. van Vuren, et al. (Sept. 2018). "Assessing safety of nature-based flood defenses: Dealing with extremes and uncertainties". In: *Coastal Engineering* 139, pp. 47–64. ISSN: 03783839. DOI: `10.1016/j.coastaleng.2018.05.002`.

WitteveenBos, Deltares, and EcoShape (n.d.). *Factsheet Wave attenuation with willow woodland*. `https://ocw.tudelft.nl/wp-content/uploads/FactSheets_Willows_for_Noordwaard.pdf`. Accessed: 14 August 2024.

Software and Data Sources

A.1. Hydra-NL

Hydra-NL (M. Duits 2020) is a probabilistic software program that models the statistics for hydraulic loads in the Netherlands, such as the water level or wave conditions. The output of the program is used for the assessment of the primary flood defences and dike trajectories in the Netherlands, and therefore is consistent with the Assessment- and Design Instrument (*BOI: Beoordelings- en Ontwerpinstrumentarium*). *Hydra-NL* is able to deliver the hydraulic load based on the probability of exceedance, including uncertainty consistent with BOI. The hydraulic loads consist of: the water level, wave height, peak wave period, hydraulic load level (to determine minimum crest height), overtopping discharge (for given crest height and dike profile), and wave conditions for given revetment types and water levels (for assessment of the revetment of the outer slope) (M. Duits 2020).
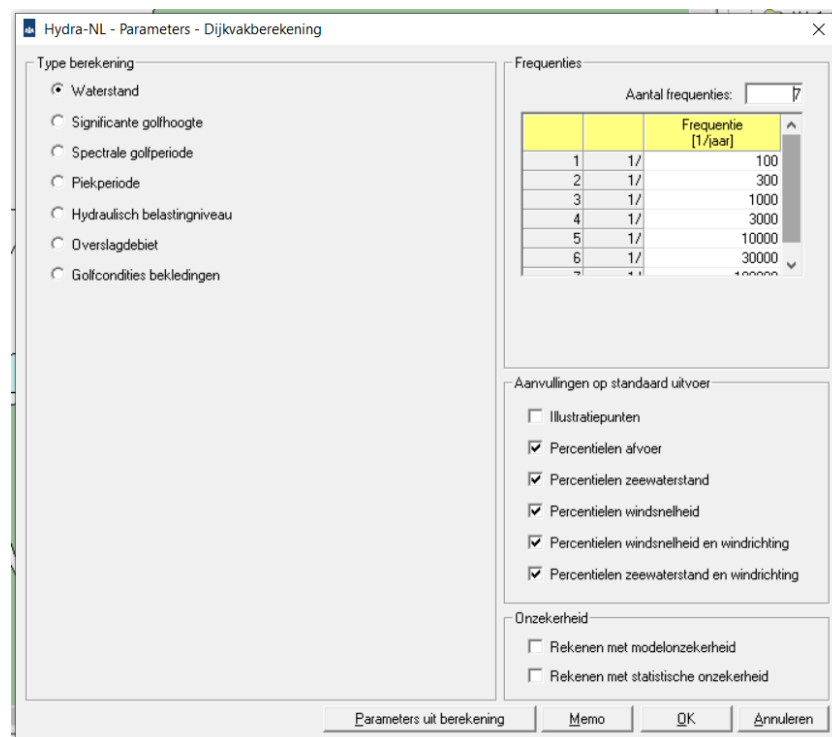
Figure A.1: Interface input Hydra-NL software

The software uses the following calculations steps to calculate the hydraulic load (M. Duits 2020):

1. Load and select the *Boundary conditions* for the location for which the assessment of hydraulic loads is calculated. These boundary conditions contain all the data regarding bathymetry, fetch lengths and hydraulic data for the specific location and need to be downloaded from the data files connected to the *Hydra-NL* software, delivered together with the set-up file for the *Hydra-NL* software.

2. The *Dike trajectory calculation* menu gives the possibility to select all the sections for which the calculation can be made, and one should select the option *Parameters*.

3. Within the *Parameters* menu (displayed in figure A.1, the following calculation input must be selected:

    (a) Type of hydraulic load (e.g. water level, wave height, etc.)
    (b) At least 5 probabilities of exceedance
    (c) Select *No additions to standard output*
    (d) Switch off *Calculation with model uncertainty*
    (e) Switch off *Calculate with statistical uncertainty*

4. Return to the dike trajectory screen by *OK*.

5. Give the calculation a name, select the desired location(s) and *Start* the calculation.

6. The calculation results can be reviewed by selecting *Output* from the *Calculation* menu, the output is shown in a HTML-file as shown in figure A.2, and can also be saved to an Excel-file.
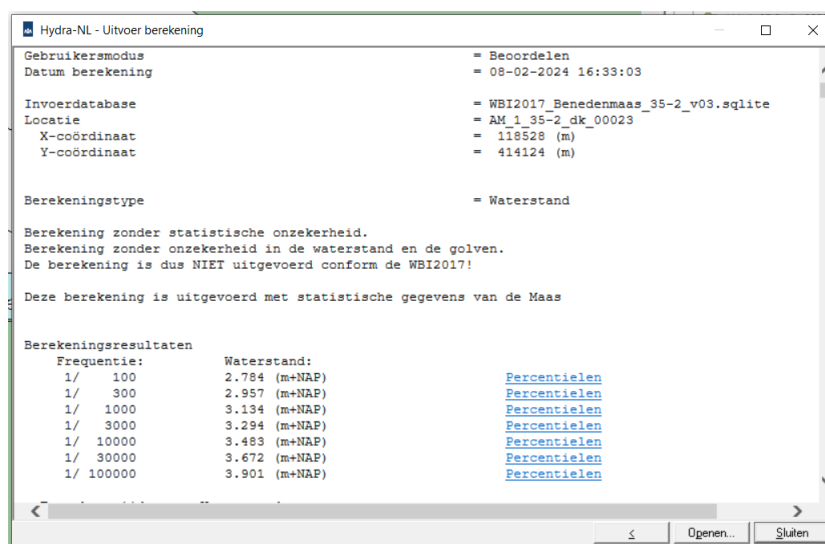
Figure A.2: Interface results Hydra-NL software

The output from *Hydra-NL* is used as input for the Attenuation-Erosion model, and the software program BM Gras Buitentalud as part of the validation of the AE model. Since both the model and BM need the durationline as input, another software connect to the BOI is used to determine this for each location, and is also dependent on the output of *Hydra-NL*.

A.2. Basis Module Gras Buitentalud

BM (Basis Module) Gras Buitentalud is a software program designed in line with BOI, to assess the failure mechanism due to erosion of the outer slope. Erosion of the outer slope occurs because of wave impact and wave run-up. *BM Gras* is able to calculate the load for specified evaluation levels using the same method as the Attenuation-Erosion model, which makes it possible to use *BM Gras* as a validation method for the model.

Figure A.3: Interface input BM Outer Slope software

To determine the failure fraction due to wave impact, the following steps shall be taken:

1. Select *Wave Impact* as calculation method
2. Fill in the *general parameters*: Δ_z, H_{m0}, h_{min} and h_{max}. The lay-out of this screen is shown in figure A.3.
3. Fill in the *construction- and strength parameters*: c_a, c_b, c_c, f_{sand}, d_{tot}, and the upper- and lower level where the slope is covered with grass revetment.
4. On the tab *Hydraulic load*, load the durationline with according wave height H_{m0}.
5. Before the calculation can be performed, the program validates if all input parameters are valid by clicking *Validation* in the *Calculation* menu.
6. When all input is validated, click *Start* in the same *Calculation* menu to calculate the failure fraction due to wave impact.
7. The results will show up in the *Results* tab that will appear, as shown in figure A.4, from where the results can be copied to Excel-files for further analysis.

Figure A.4: Interface results BM Outer Slope software

For determination of the cumulative overload due to wave run-up, the following steps shall be taken:

1. Select *Wave Run-up* as calculation method
2. Fill in the *general parameters*: evaluation level h_{eval}, C_u, g and deselect *scaling*. The lay-out of this screen is shown in figure A.3.
3. Fill in the *strength parameters*: u_c, D_{crit}, α_{mz}, α_{sz}.
4. On the tab *Geometry* and fill in the dike geometry and orientation for the location that the calculation is made for.
5. On the tab *Hydraulic load*, load the durationline with according wave heights H_{m0}, spectral wave period T_{m0}, and direction of the incoming waves with respect to the dike normal.

6. Before the calculation can be performed, the program validates if all input parameters are valid by clicking *Validation* in the *Calculation* menu.

7. When all input is validated, click *Start* in the same *Calculation* menu to calculate the cumulative overload due to wave run-up.

8. The results will show up in the *Results* tab that will appear, as shown in figure A.4, from where the results can be copied to Excel-files for further analysis.

A.3. Actueel Hoogtebestand Nederland (AHN)

To gather the geometry of the different dike sections, the levee height with respect to NAP ($mNAP$) has to be obtained in order to assess the probability of failure for the dike. The Current Altitude file of the Netherlands (*Actueel Hoogtebestand Nederland (AHN)*) is a online storage containing detailed and precise altitude data points for every square meter in the Netherlands, up to 5 centimeter accurate. The data is collected using laser technology attached to helicopters and airplanes, to collect the 3D-altitude information.
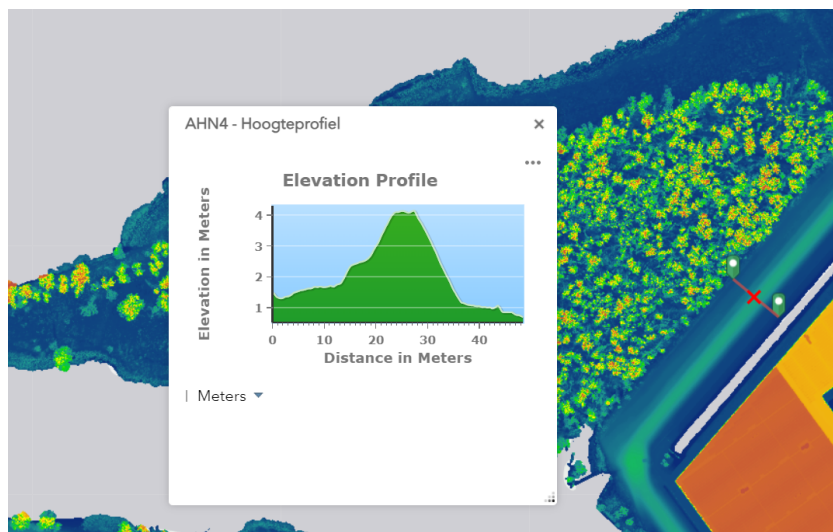
Figure A.5: Interface AHN

The user interface is shown in figure A.5 for a dike section in the Netherlands. The unit for the output parameters can be specified to get results on the right scale (e.g. meter, kilometer, inches, etc.). The data can be exported to CSV files to create elevation overviews as shown in figure A.6. The geometry collected from AHN is used as input for the Attenuation-Erosion model and *BM Gras Buitentalud*.
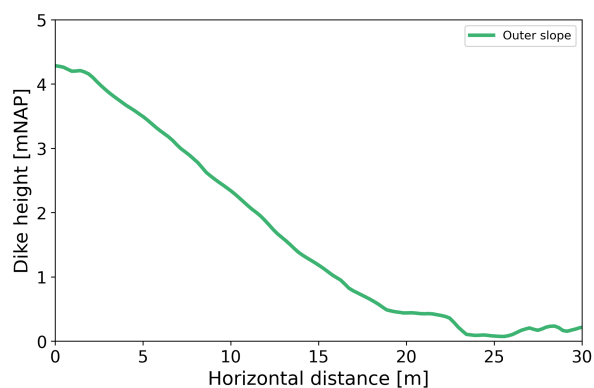
Figure A.6: Converted AHN data for dike trajectory 10.3 (converted using Python)

A.4. Vegetatiemonitor 2.0

The Department of Waterways and Public Works (*Rijkswaterstaat*) is responsible for monitoring the condition of the vegetation in the total river areas for the Meuse, Rhine and Rhinebranches (Waal, Lower Rhine, Lek and IJssel, and compare it to the vegetation chart (*vegetatielegger*). The Vegetation Chart consists of survey maps and rules, and contributes to a safe flow and the improvement of the water quality of the Dutch rivers and strengthen river nature. The Vegetationmonitor 2.0 is an online view program that delivers information and data about vegetation in the area to make it possible to (i) classify the existing vegetation on a specified location, and (ii) compare it to the allowed roughness according to the rules of the Vegetation Chart.
The Vegetationmonitor 2.0 offers three main functionalities:

1. **Chart layers**: different chart layers can be viewed on an interactive map using a Google Earth Engine (GGE) to view the data projected on day-by-day updated satellite images. On top of the satellite imaging, the year-average vegetation charts can be layed on top to perform visual compare and analyse changes (E. Penning and V. Harezlak 2020).

2. **Analysis**: For individual plots and vegetation layer polygons, separate analyses can be performed to quantify changes relative to the Vegetation Chart per plot or vegetation layer polygon.

3. **Download**: Export functions allow the results of the polygon analysis to be downloaded as a pdf. Multiple map layers can be downloaded as GeoTIFF for further processing as required (E. Penning and V. Harezlak 2020).

The user interface of the Vegetationmonitor 2.0 showing the Vegetation Chart on top of the Google Earth satellite image is shown in figure A.7. This information is used for this research to analyse what the forest dimensions in front of a dike section are allowed to be.

Figure A.7: Interface Vegetation Monitor

B

Combined failure probability

The model produces the conditional probability of failure given the occurrence of that water level $P(F|h)$. F is the failure due to wave load, i.e. impact or run-up, and h is the particular water level. The conditional probability of failure is relative high, because the probability of occurrence of the water level is part of it. The calculation to go from the conditional probability of failure due to wave load for a certain water level $P(F|h)$, needs to marginal probability of occurrence of that water level $P(h)$ to determine to the combined probability of failure $P(F|h)P(h)$. Calculating the combined probability of failure for every water level, with vertical step size Δz between each two levels, and integrating over all the levels gives the total probability of failure P_f for the dike slope due to the modelled failure mechanism, as shown in the equation below.

$$P_f = \int P(F|h)P(h)\Delta z \tag{B.1}$$

The marginal probability of occurrence of a certain water level differs for each water level. From Hydra-NL, the water levels with their probability of non-exceedance are collected, as presented in table 3.3. With this data, the marginal probability of occurrence of each water level can be determined following the steps below.

1. Calculate the probability of non-exceedance ($P_{non-exceed} = 1 - P_{non-exceed}$), which is equal to the cumulative density function (CDF).
2. Interpolate the CDF to get a value for each water level in the interpolated conditional probability of failure produced by the model.
3. Use inverse accumulation (accumulated values are calculated back to their individual value) to go from the CDF to the PDF. The PDF displays the marginal probability of occurrence for each water level $P(h)$, needed to calculate the combined probability of failure for each water level.

In the following figures, these steps are shown for the results of the case study, as described in chapter 5. Figure B.1 displays the data collected from Hydra-NL, as described in Appendix A, representing the probability of non-exceedance for each water level. Figure B.2, shows the probability of non-exceedance for the same water levels, which is equal to the cumulative density function (CDF). Interpolating the CDF results using the same step size as for the conditional probability of failure results in figure B.3.
In figure B.4, the CDF is calculated back to the PDF, which represents the marginal probability of occurrence for each water level $P(h)$, and since the conditional failure probability in chapter 5 is interpolated for the same water levels, the combined failure probabilities can be calculated, to produce the total probability of failure for each calculation.
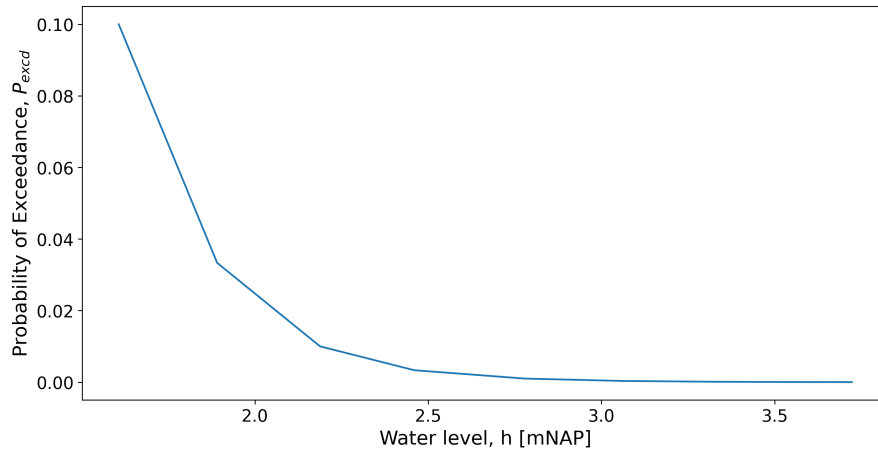
Figure B.1: Probability of exceedance for the water levels of trajectory 10.3
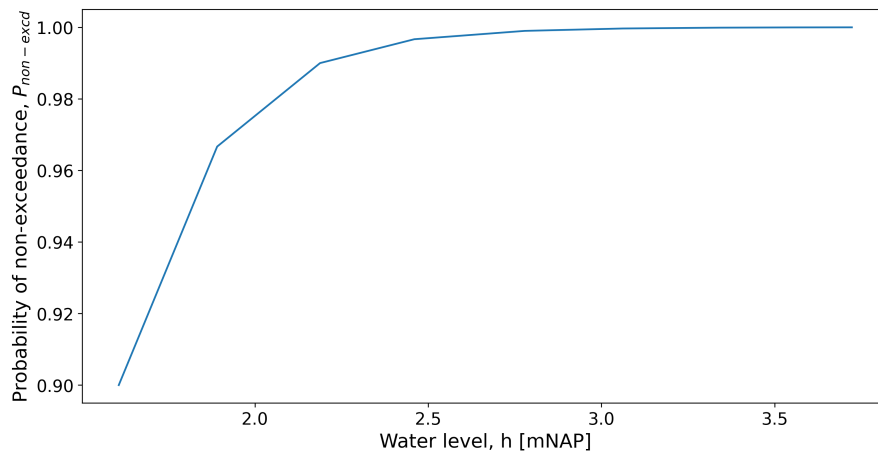
Figure B.2: Probability of non-exceedance (CDF) for the water levels of trajectory 10.3
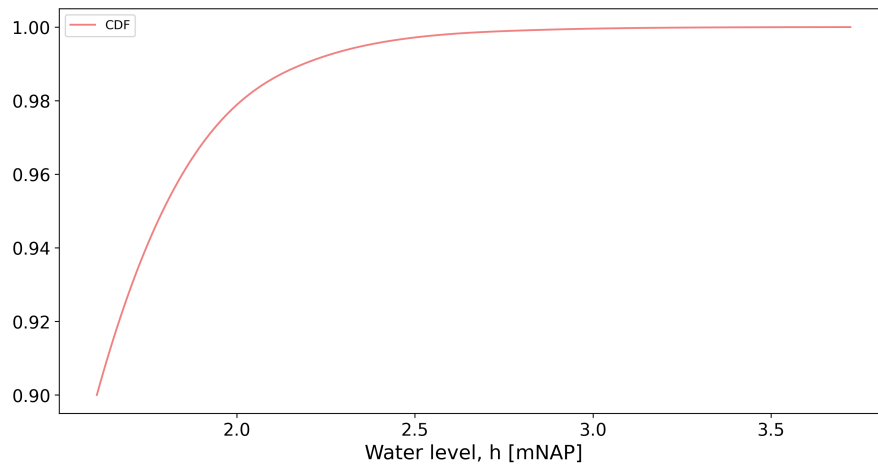
Figure B.3: Interpolated CDF for the water levels of trajectory 10.3
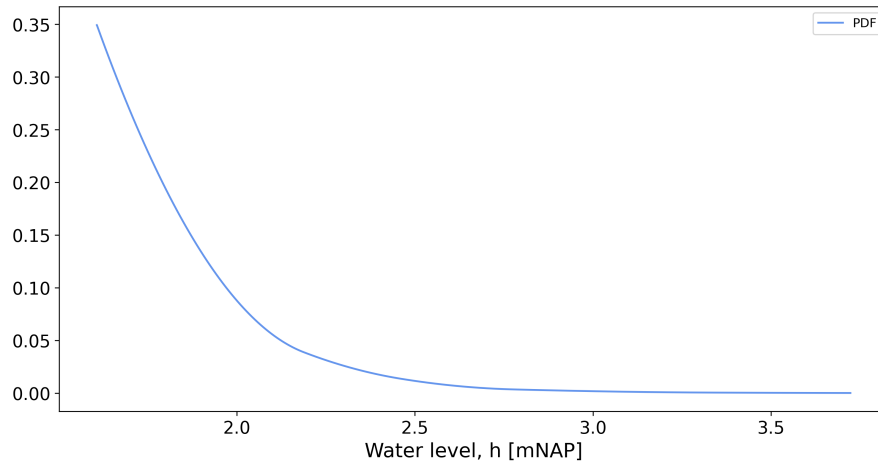
Figure B.4: Interpolated PDF (marginal probability of occurrence $P(h)$) for the water levels of trajectory 10.3

Sensitivity Analysis results (forest length = 40 meter)

C.1. Sensitivity indices
C.1.1. Without vegetation
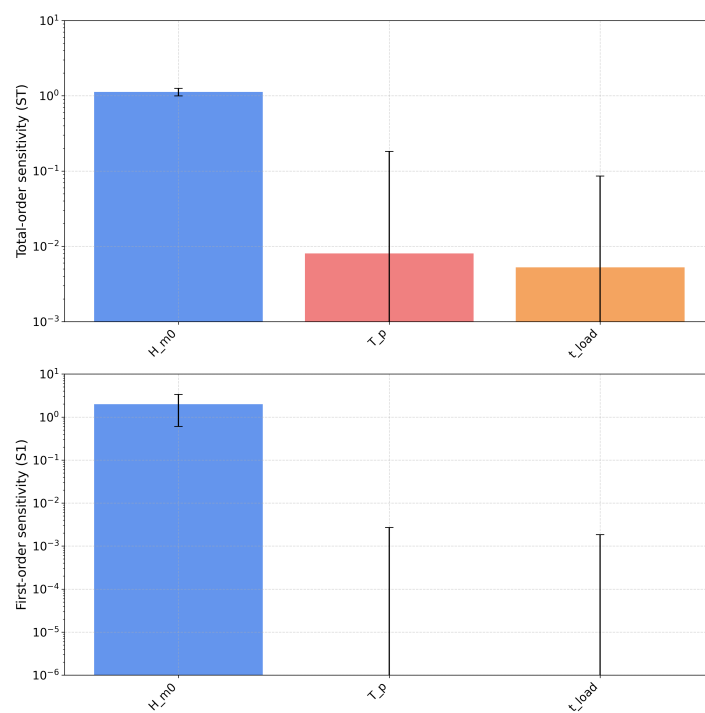
Figure C.1: Sensitivity Indices (No vegetation) $R = 10$ years
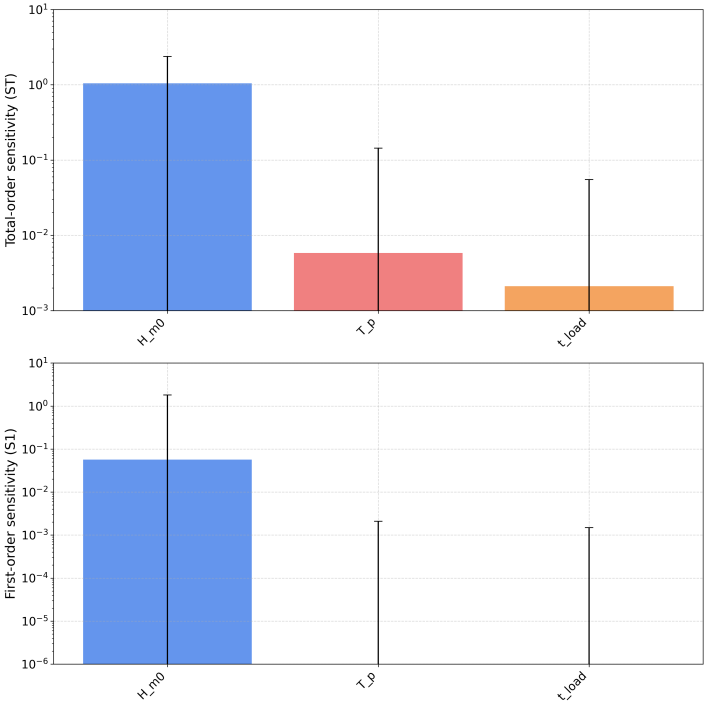
Figure C.2: Sensitivity Indices (No vegetation) $R = 30$ years
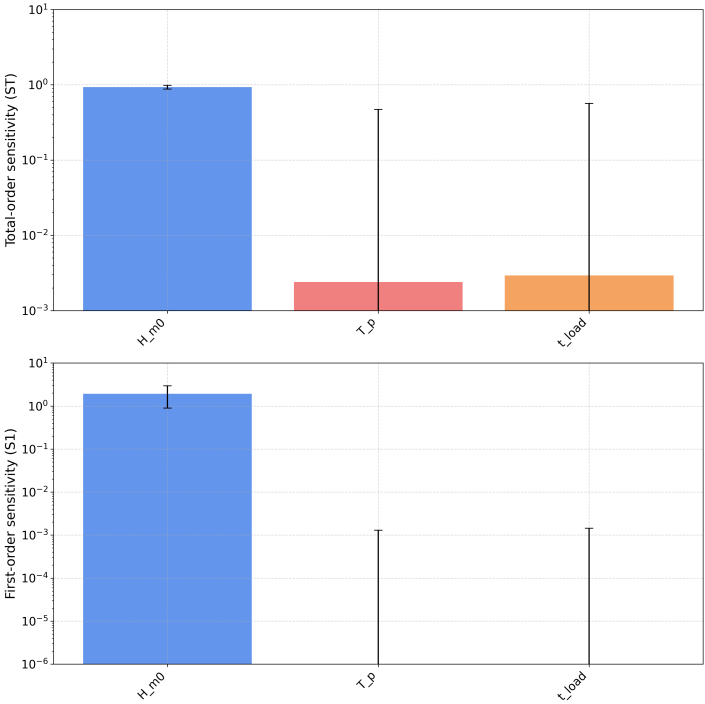
Figure C.3: Sensitivity Indices (No vegetation) $R = 100$ years
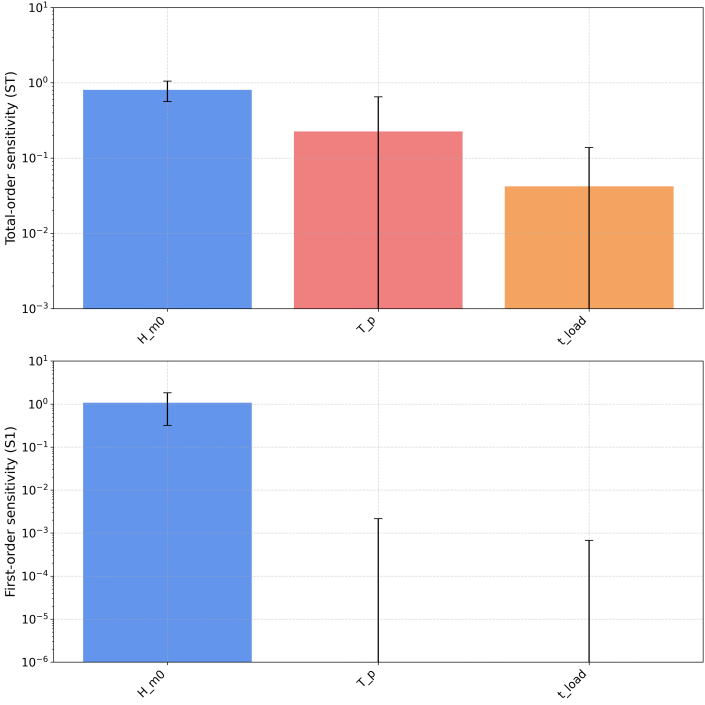
Figure C.4: Sensitivity Indices (No vegetation) $R = 300$ years
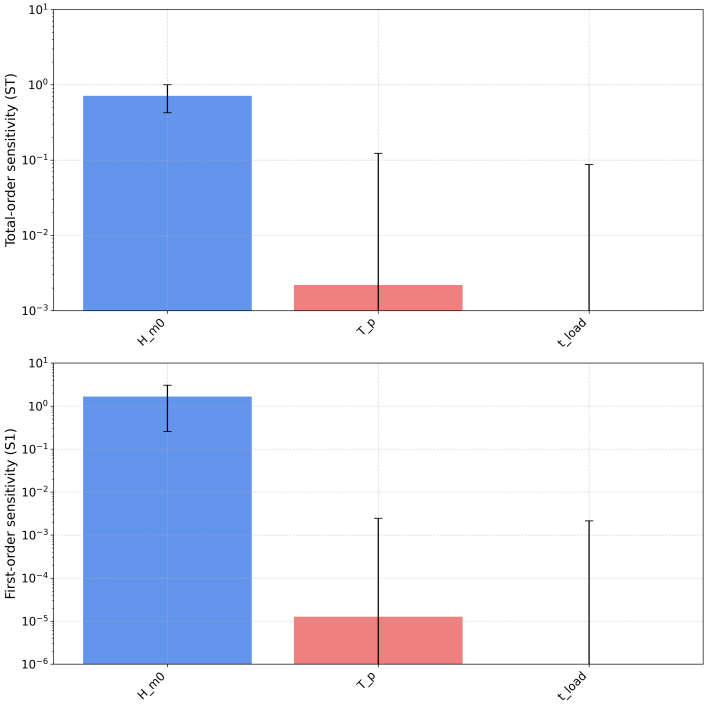
Figure C.5: Sensitivity Indices (No vegetation) $R = 1000$ years
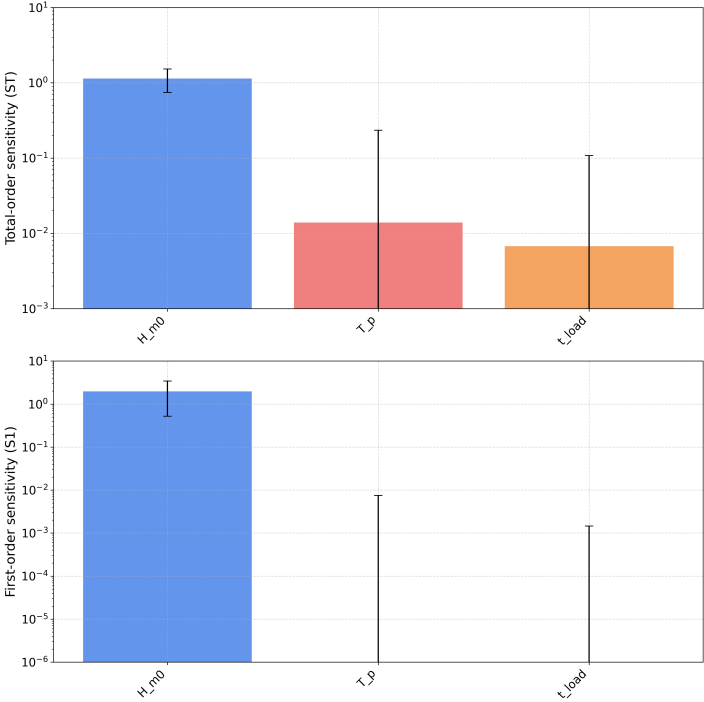
Figure C.6: Sensitivity Indices (No vegetation) $R = 3000$ years
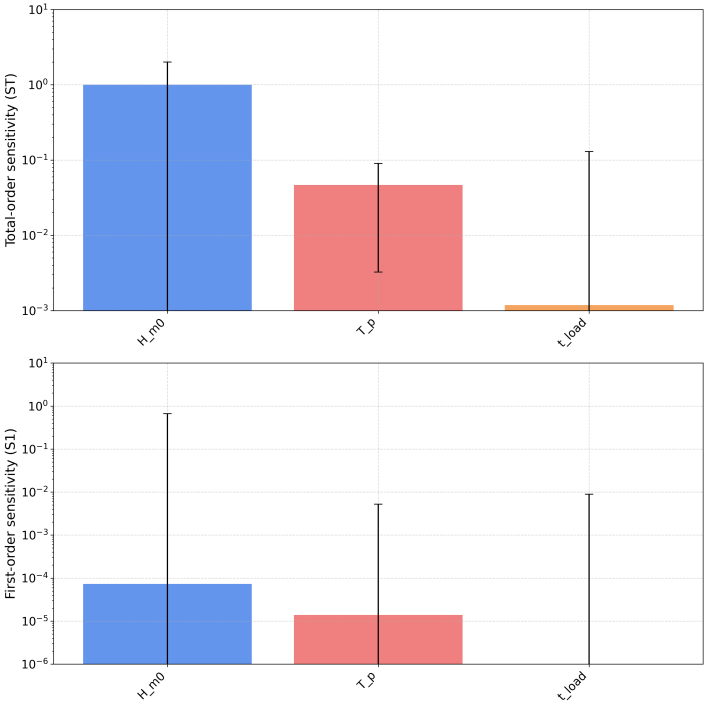
Figure C.7: Sensitivity Indices (No vegetation) $R = 10000$ years
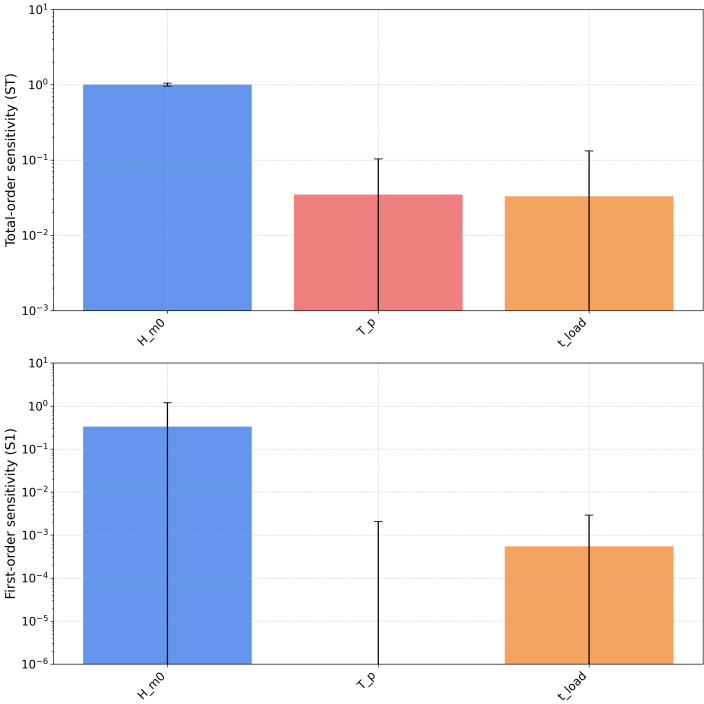
Figure C.8: Sensitivity Indices (No vegetation) $R = 30000$ years
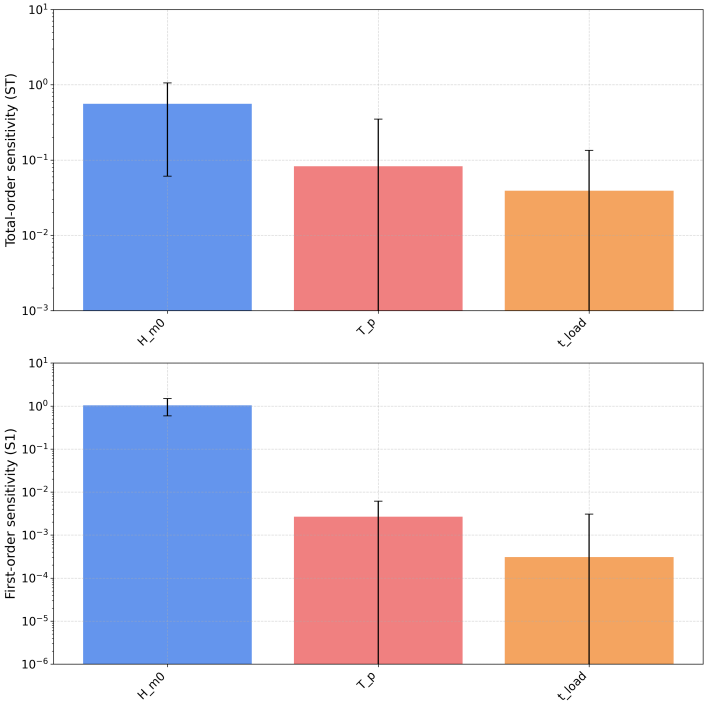
Figure C.9: Sensitivity Indices (No vegetation) $R = 100000$ years

C.1.2. With vegetation

(a) Sensitivity Indices (Vegetation: $C_D = 0.70$

(b) Sensitivity Indices (Vegetation: $C_D = 1.20$
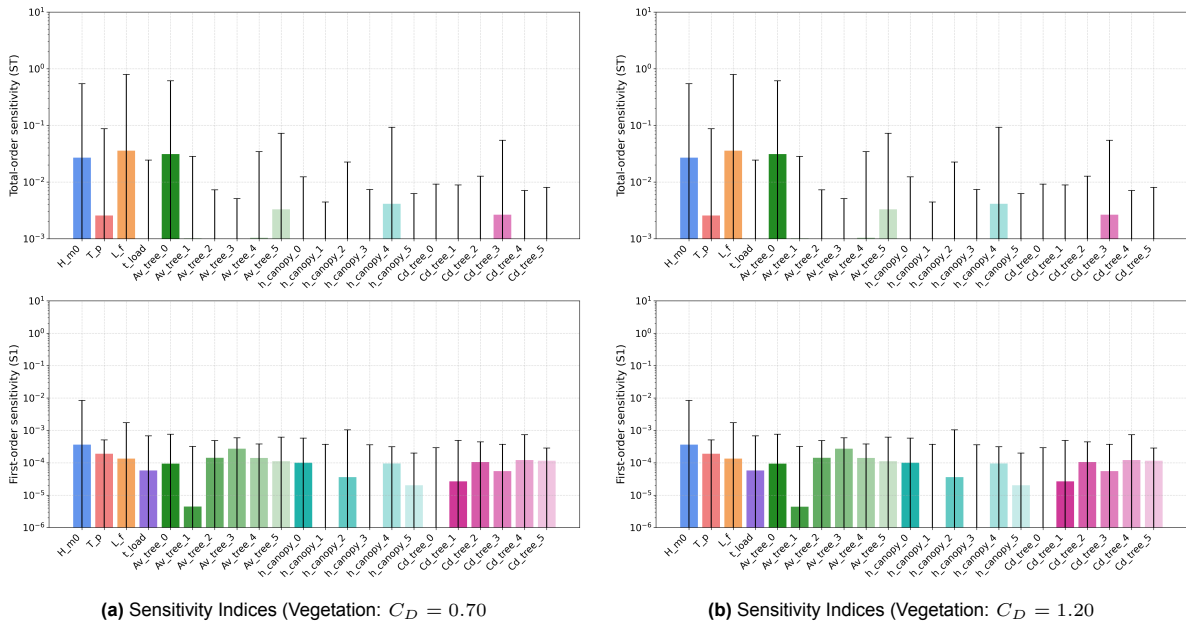
Figure C.10: Sensitivity Indices for the situation with vegetation and $R = 10$ years

(a) Sensitivity Indices (Vegetation: $C_D = 0.70$

(b) Sensitivity Indices (Vegetation: $C_D = 1.20$
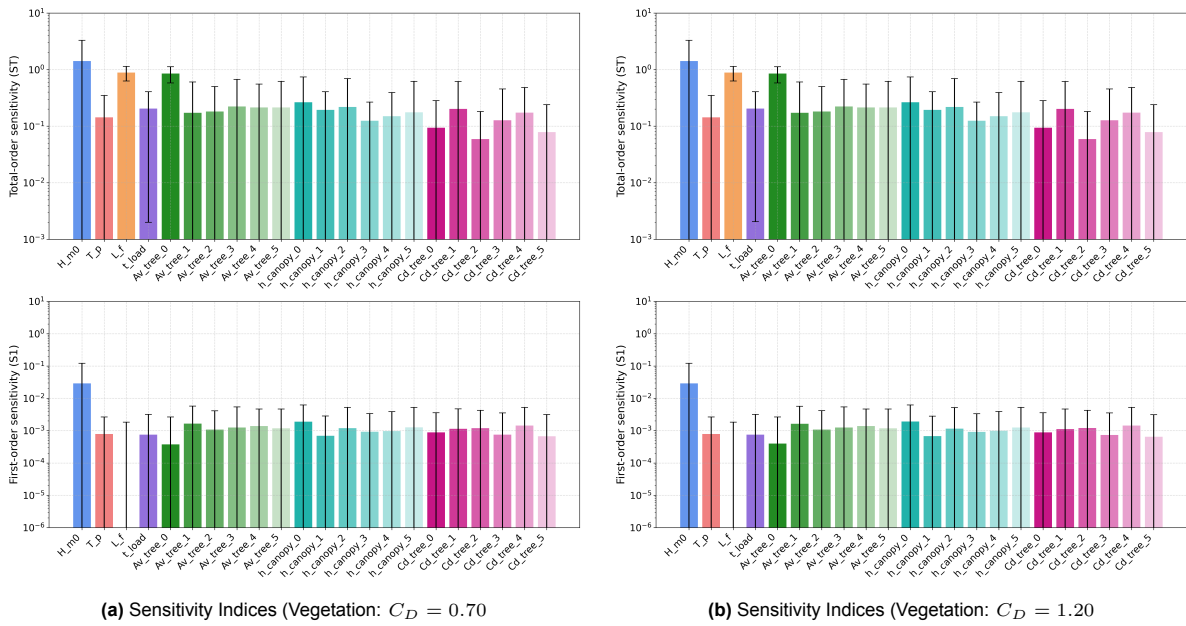
Figure C.11: Sensitivity Indices for the situation with vegetation and $R = 30$ years

(a) Sensitivity Indices (Vegetation: $C_D = 0.70$

(b) Sensitivity Indices (Vegetation: $C_D = 1.20$
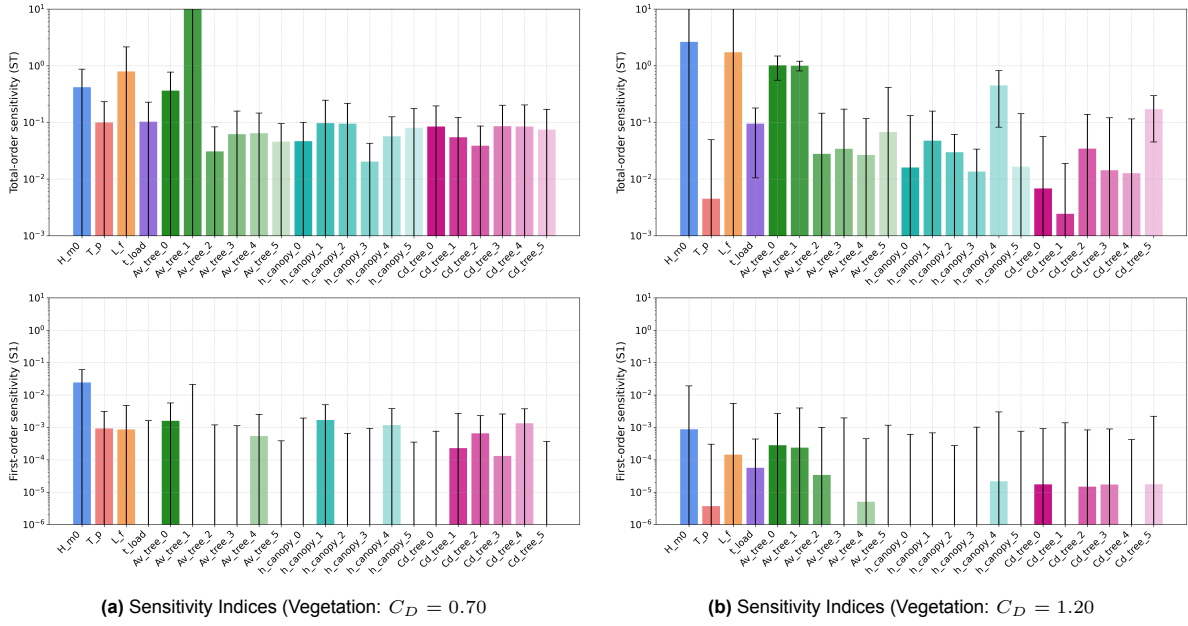
Figure C.12: Sensitivity Indices for the situation with vegetation and $R = 100$ years

(a) Sensitivity Indices (Vegetation: $C_D = 0.70$

(b) Sensitivity Indices (Vegetation: $C_D = 1.20$
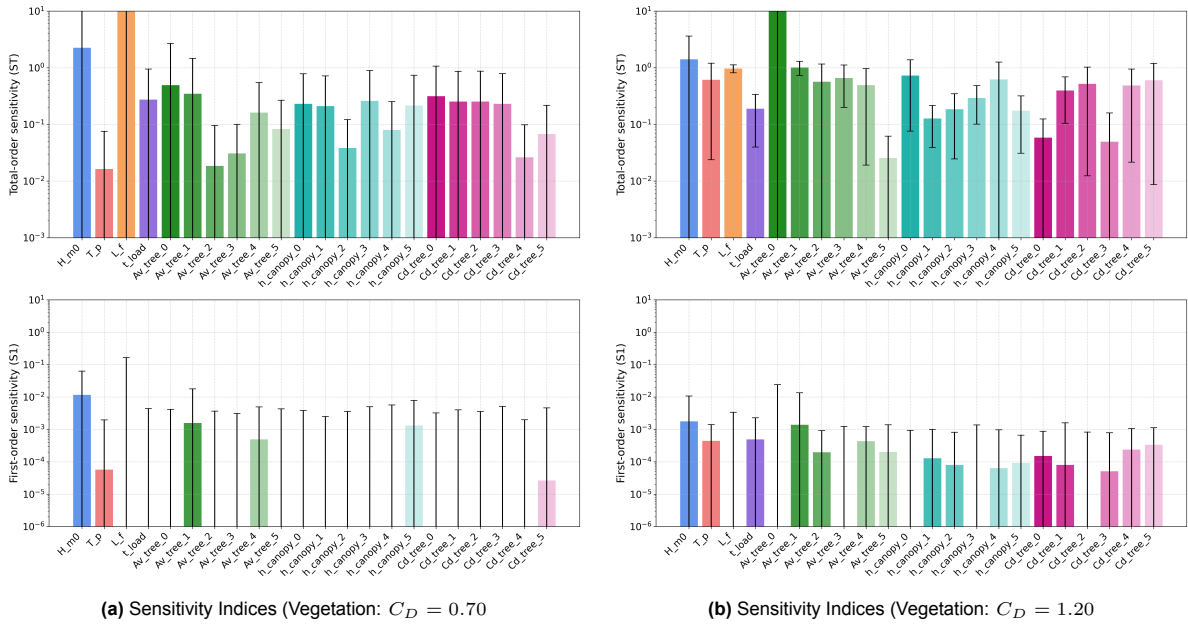
Figure C.13: Sensitivity Indices for the situation with vegetation and $R = 300$ years

(a) Sensitivity Indices (Vegetation: $C_D = 0.70$

(b) Sensitivity Indices (Vegetation: $C_D = 1.20$
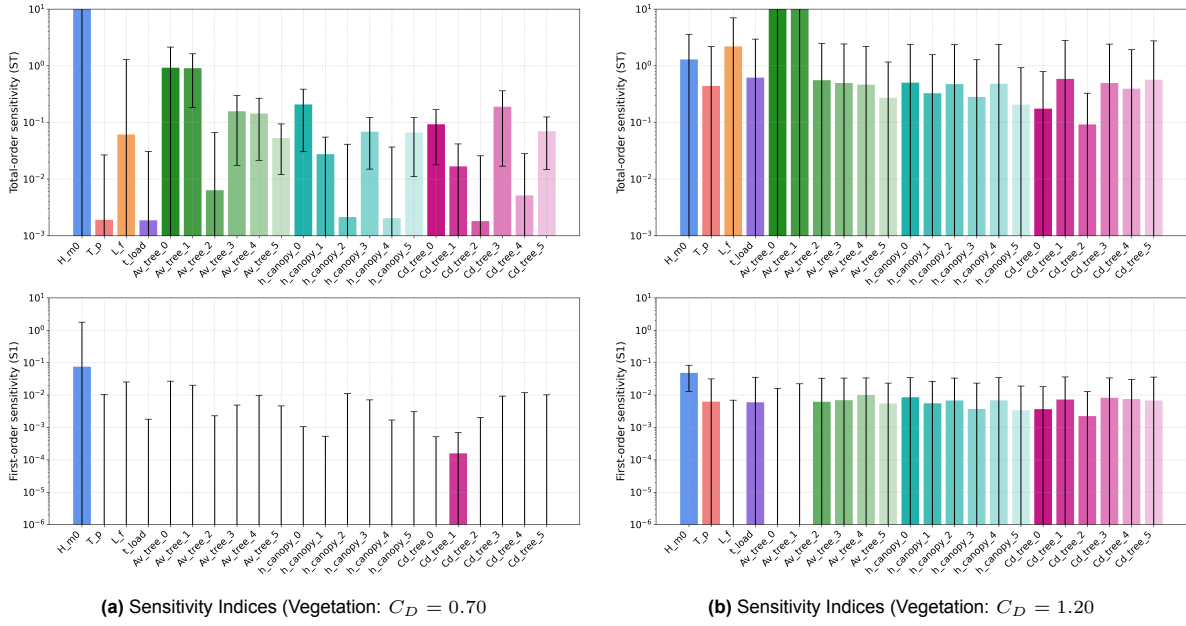
Figure C.14: Sensitivity Indices for the situation with vegetation and $R = 1000$ years

(a) Sensitivity Indices (Vegetation: $C_D = 0.70$

(b) Sensitivity Indices (Vegetation: $C_D = 1.20$
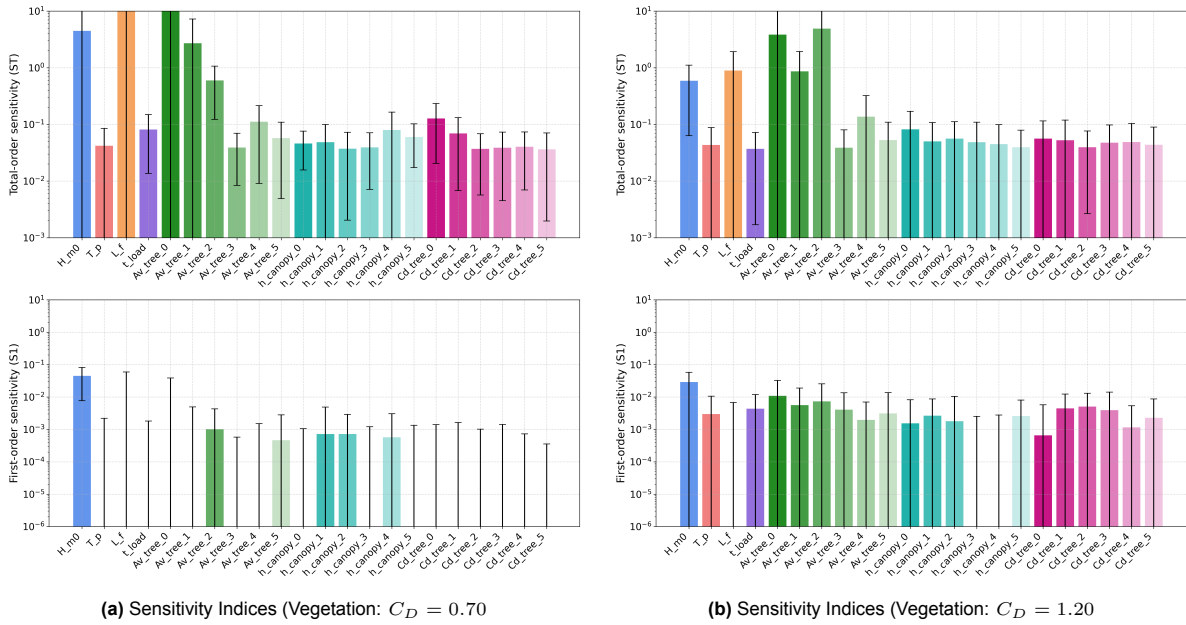
Figure C.15: Sensitivity Indices for the situation with vegetation and $R = 3000$ years

(a) Sensitivity Indices (Vegetation: $C_D = 0.70$

(b) Sensitivity Indices (Vegetation: $C_D = 1.20$
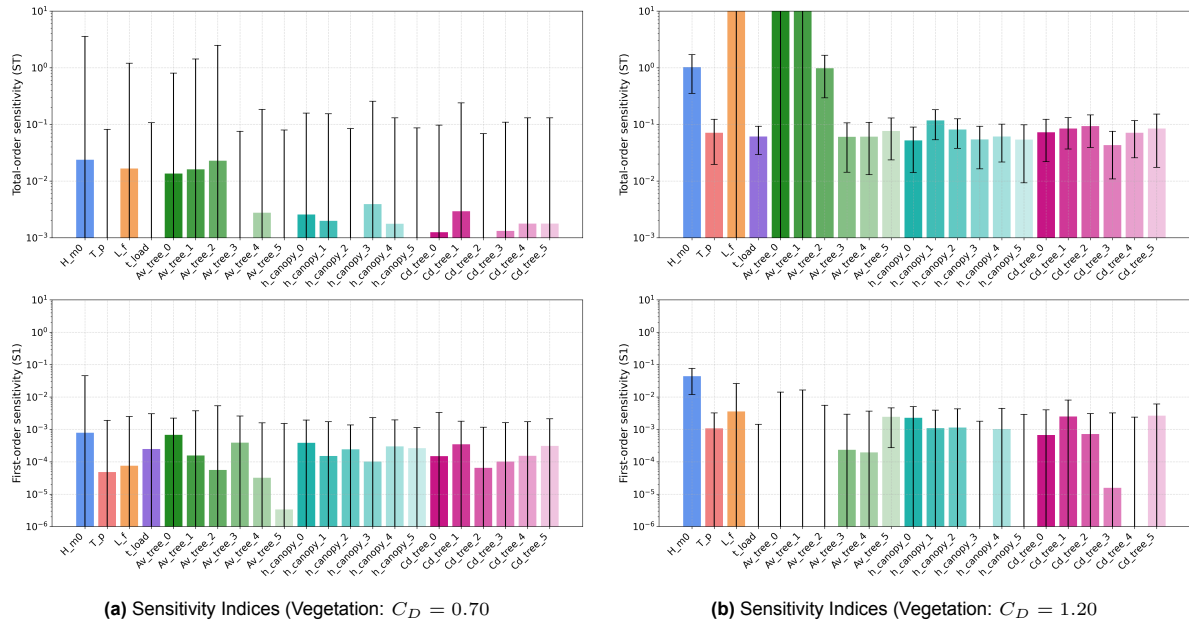
Figure C.16: Sensitivity Indices for the situation with vegetation and $R = 10000$ years

(a) Sensitivity Indices (Vegetation: $C_D = 0.70$

(b) Sensitivity Indices (Vegetation: $C_D = 1.20$
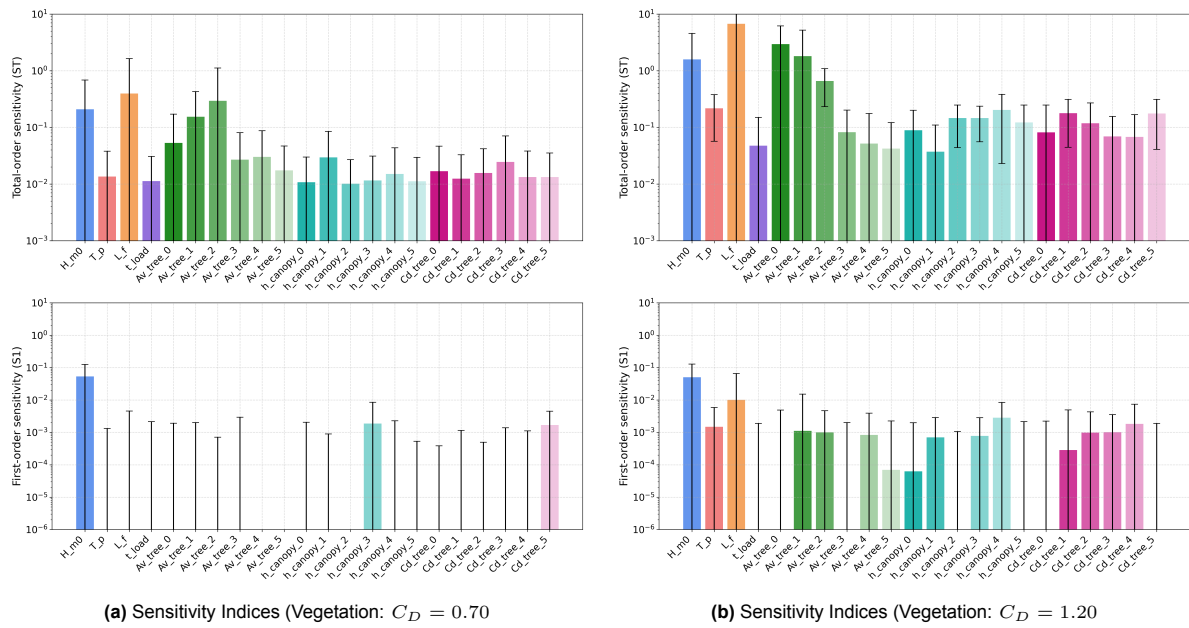
Figure C.17: Sensitivity Indices for the situation with vegetation and $R = 30000$ years

(a) Sensitivity Indices (Vegetation: $C_D = 0.70$

(b) Sensitivity Indices (Vegetation: $C_D = 1.20$
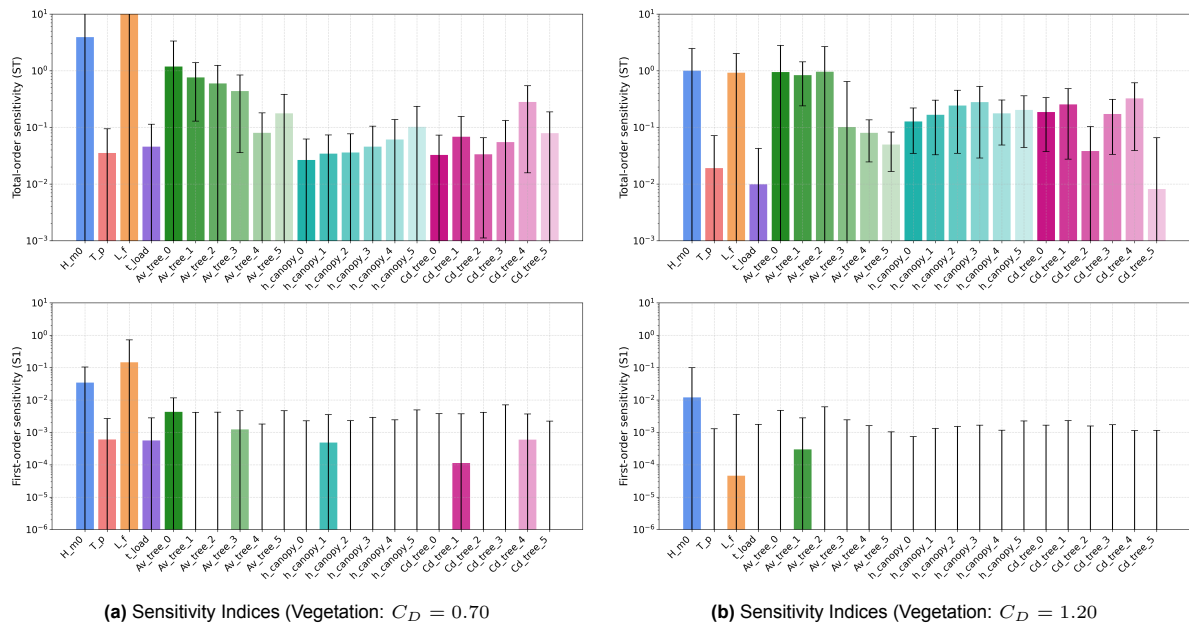
Figure C.18: Sensitivity Indices for the situation with vegetation and $R = 100000$ years

C.2. Pie charts
C.2.1. Without vegetation
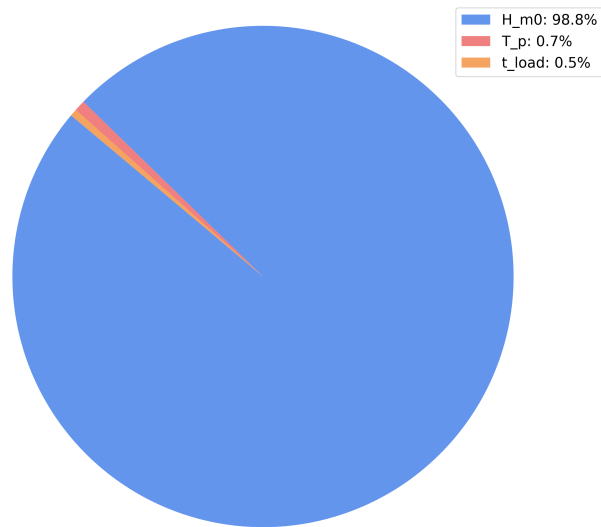
Figure C.19: Pie chart (No vegetation) $R = 10$ years
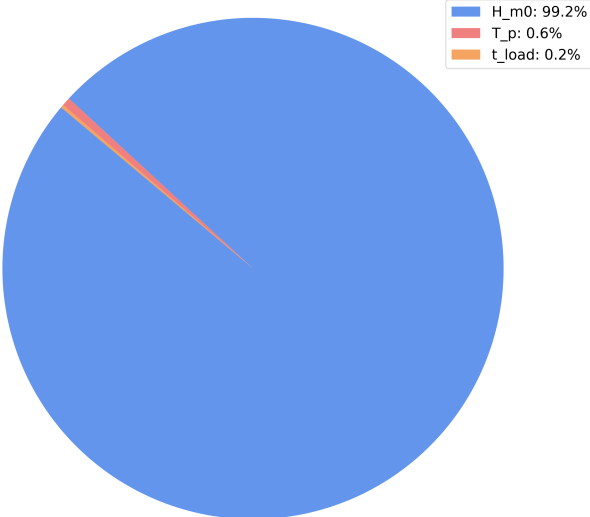
Figure C.20: Pie chart (No vegetation) $R = 30$ years
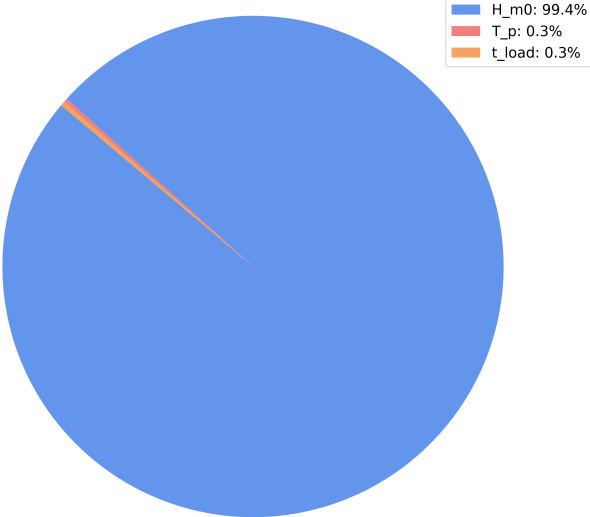
Figure C.21: Pie chart (No vegetation) $R = 100$ years
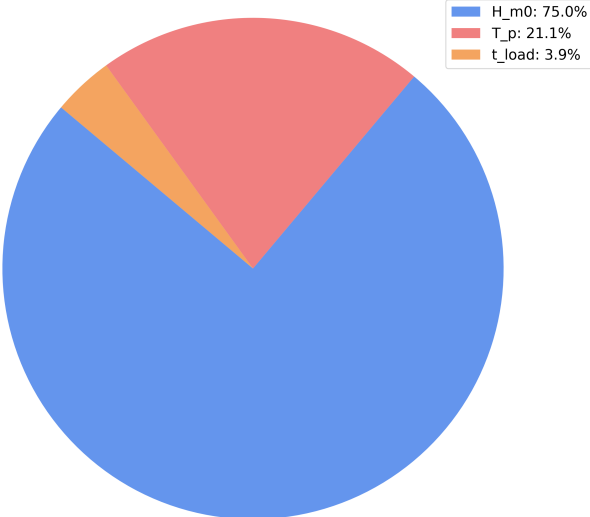
Figure C.22: Pie chart (No vegetation) $R = 300$ years
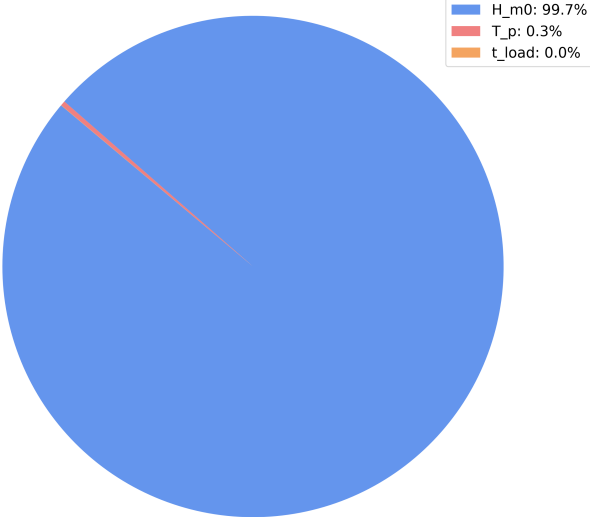
Figure C.23: Pie chart (No vegetation) $R = 1000$ years
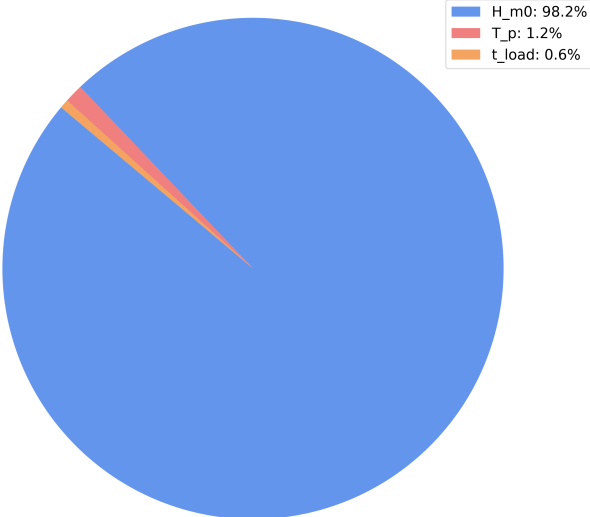
Figure C.24: Pie chart (No vegetation) $R = 3000$ years
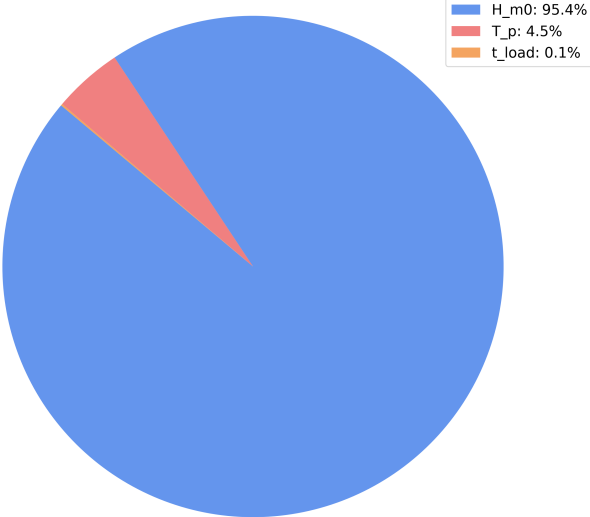
Figure C.25: Pie chart (No vegetation) $R = 10000$ years
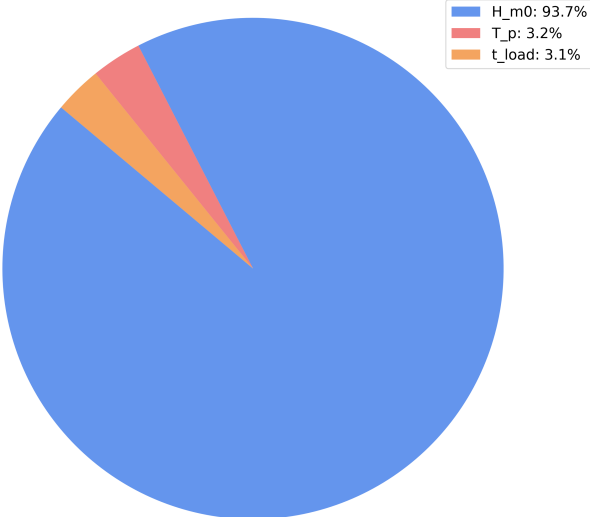
Figure C.26: Pie chart (No vegetation) $R = 30000$ years
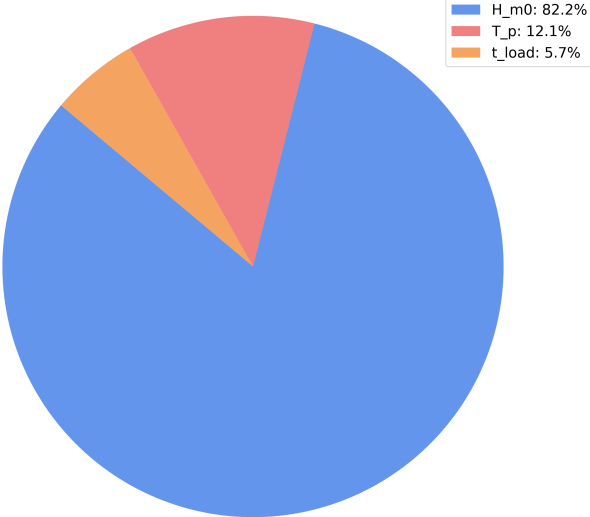
Figure C.27: Pie chart (No vegetation) $R = 100000$ years

C.2.2. With vegetation
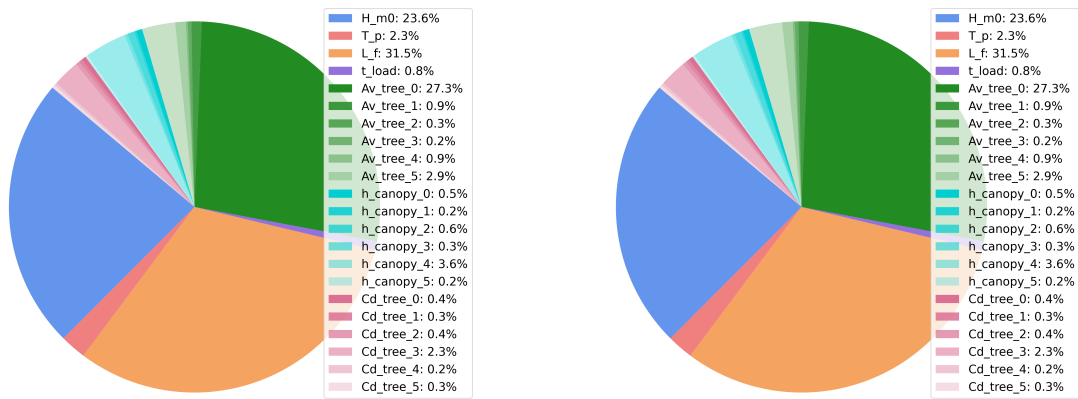
(a) Pie chart (No vegetation) $C_D = 0.70$

(b) Pie chart (No vegetation) $C_D = 1.20$

Figure C.28: Pie chart for the situation without vegetation and $R = 10$ years
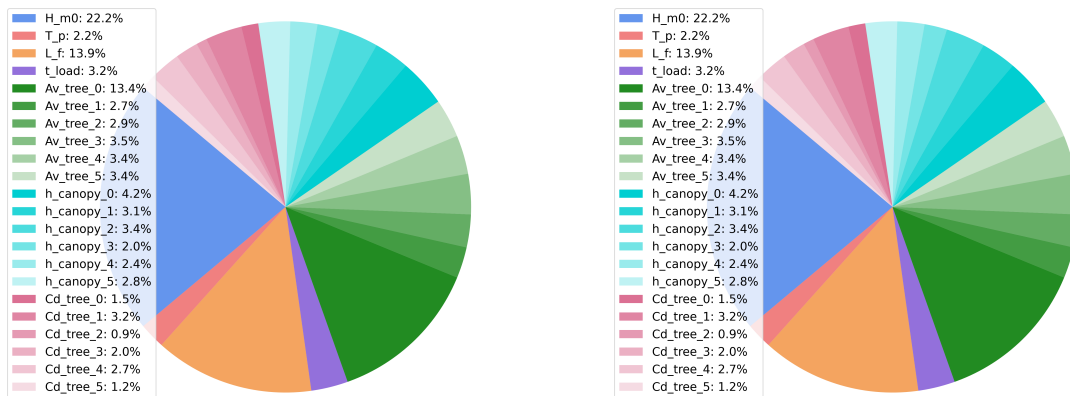
(a) Pie chart (No vegetation) $C_D = 0.70$

(b) Pie chart (No vegetation) $C_D = 1.20$

Figure C.29: Pie chart for the situation without vegetation and $R = 30$ years
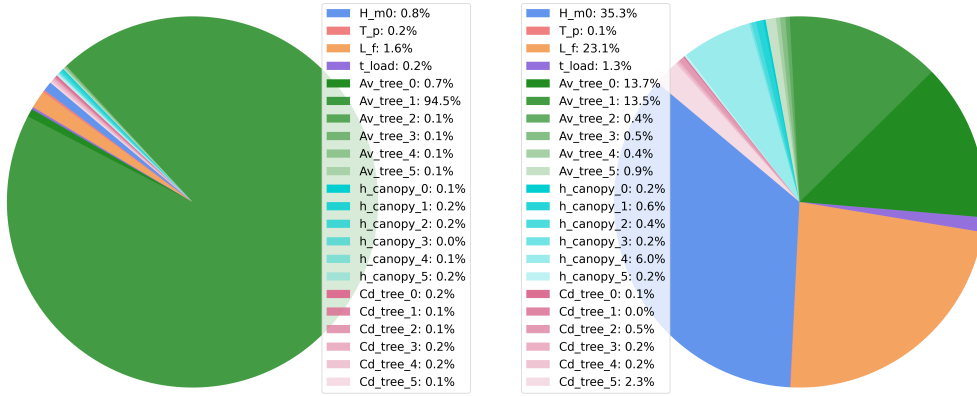
(a) Pie chart (No vegetation) $C_D = 0.70$

(b) Pie chart (No vegetation) $C_D = 1.20$

Figure C.30: Pie chart for the situation without vegetation and $R = 100$ years
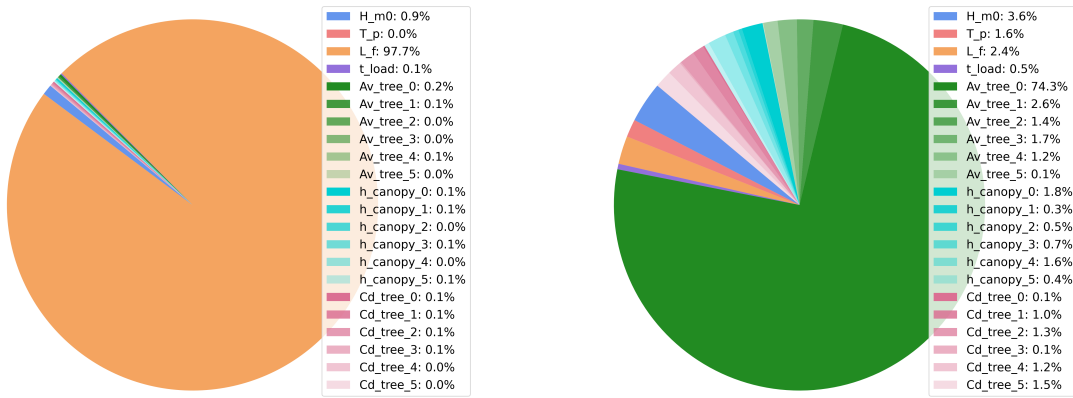
(a) Pie chart (No vegetation) $C_D = 0.70$

(b) Pie chart (No vegetation) $C_D = 1.20$

Figure C.31: Pie chart for the situation without vegetation and $R = 300$ years
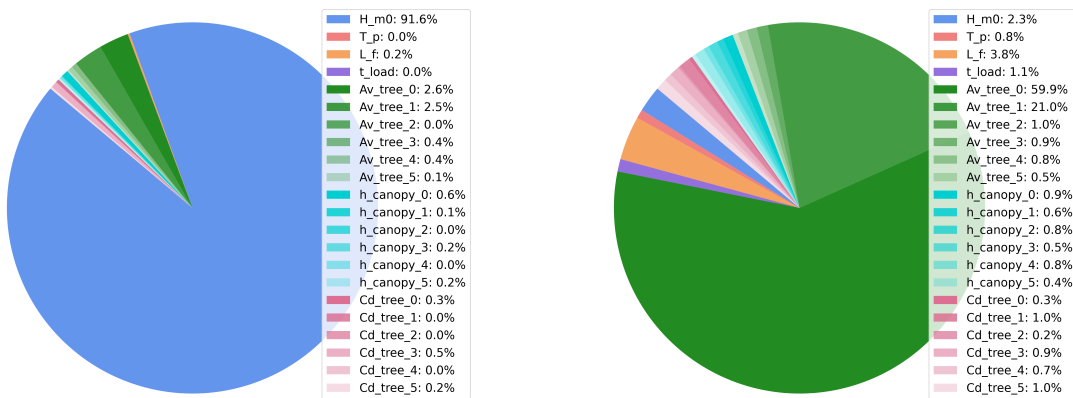
(a) Pie chart (No vegetation) $C_D = 0.70$

(b) Pie chart (No vegetation) $C_D = 1.20$

Figure C.32: Pie chart for the situation without vegetation and $R = 1000$ years
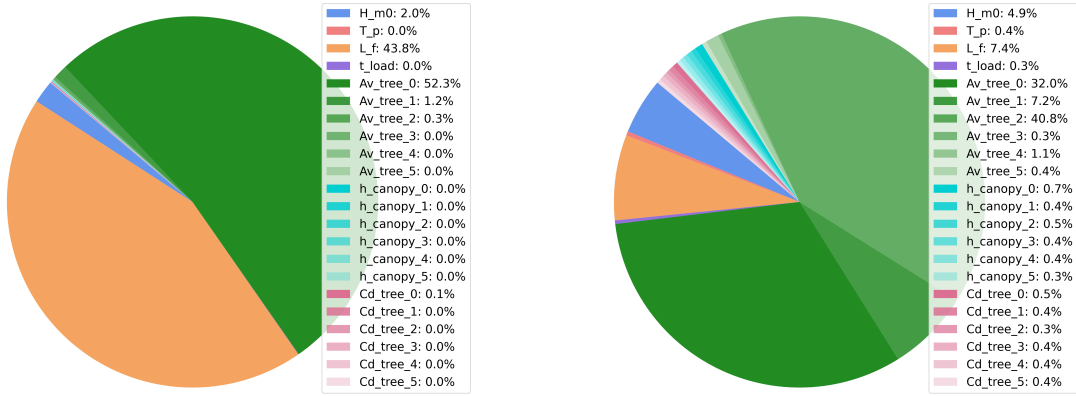
(a) Pie chart (No vegetation) $C_D = 0.70$

(b) Pie chart (No vegetation) $C_D = 1.20$

Figure C.33: Pie chart for the situation without vegetation and $R = 3000$ years
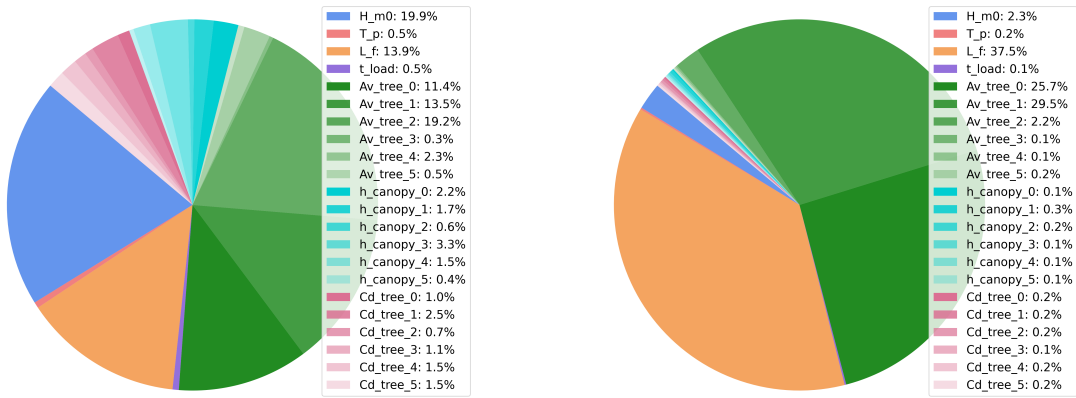
(a) Pie chart (No vegetation) $C_D = 0.70$

(b) Pie chart (No vegetation) $C_D = 1.20$

Figure C.34: Pie chart for the situation without vegetation and $R = 10000$ years
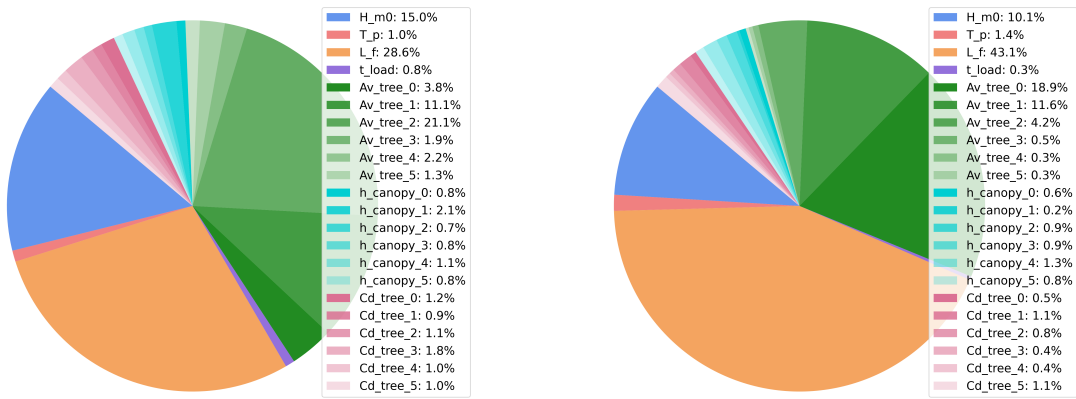
(a) Pie chart (No vegetation) $C_D = 0.70$

(b) Pie chart (No vegetation) $C_D = 1.20$

Figure C.35: Pie chart for the situation without vegetation and $R = 30000$ years
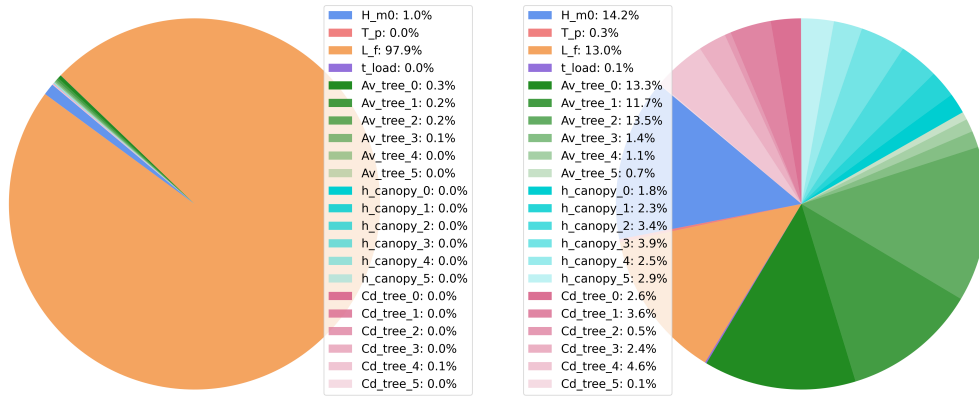
(a) Pie chart (No vegetation) $C_D = 0.70$

(b) Pie chart (No vegetation) $C_D = 1.20$

Figure C.36: Pie chart for the situation without vegetation and $R = 100000$ years

D

Sensitivity Analysis results (forest length = 100 meter)

D.1. Sensitivity indices

D.1.1. Without vegetation
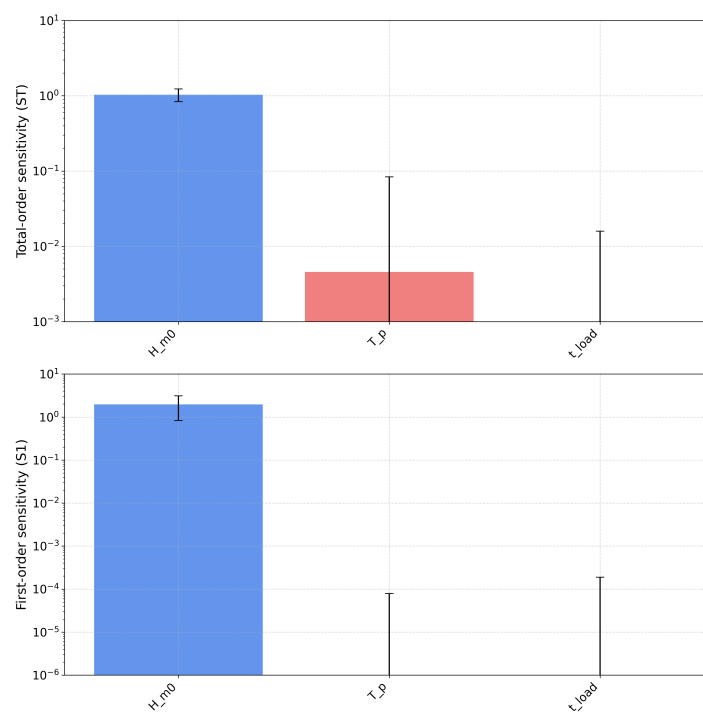
Figure D.1: Sensitivity Indices (No vegetation) $R = 10$ years
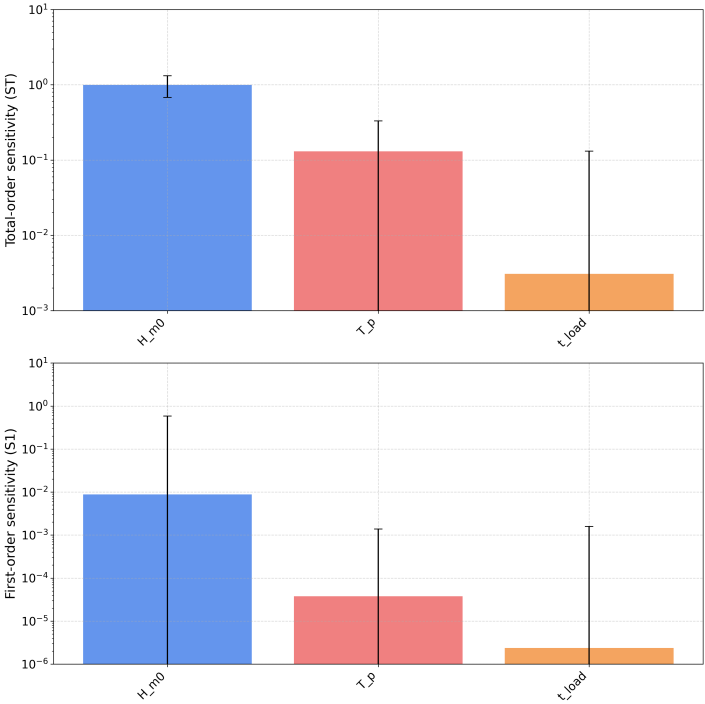
Figure D.2: Sensitivity Indices (No vegetation) $R = 30$ years
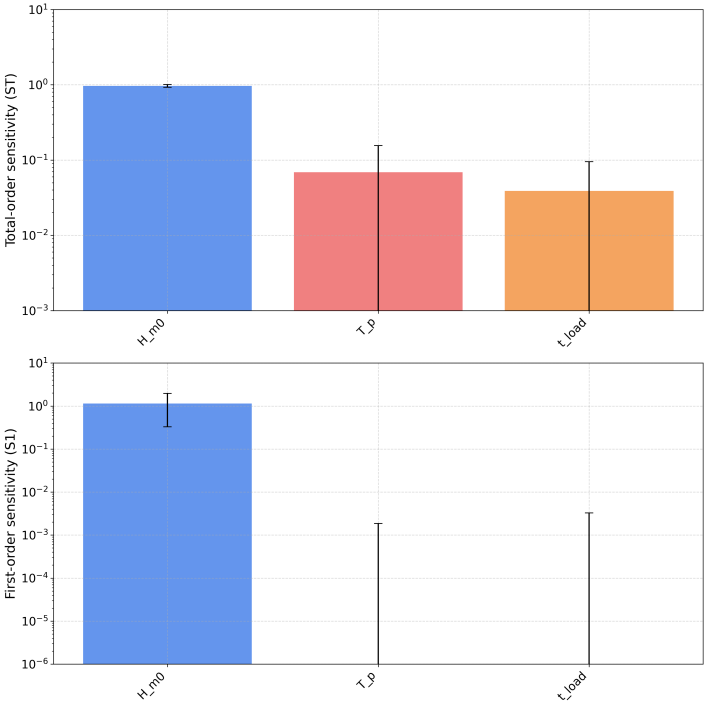
Figure D.3: Sensitivity Indices (No vegetation) $R = 100$ years
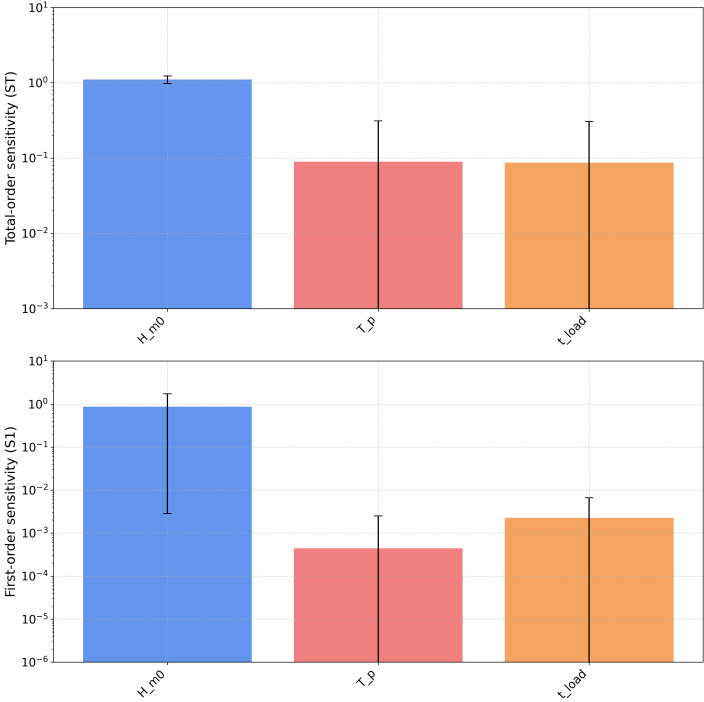
Figure D.4: Sensitivity Indices (No vegetation) $R = 300$ years
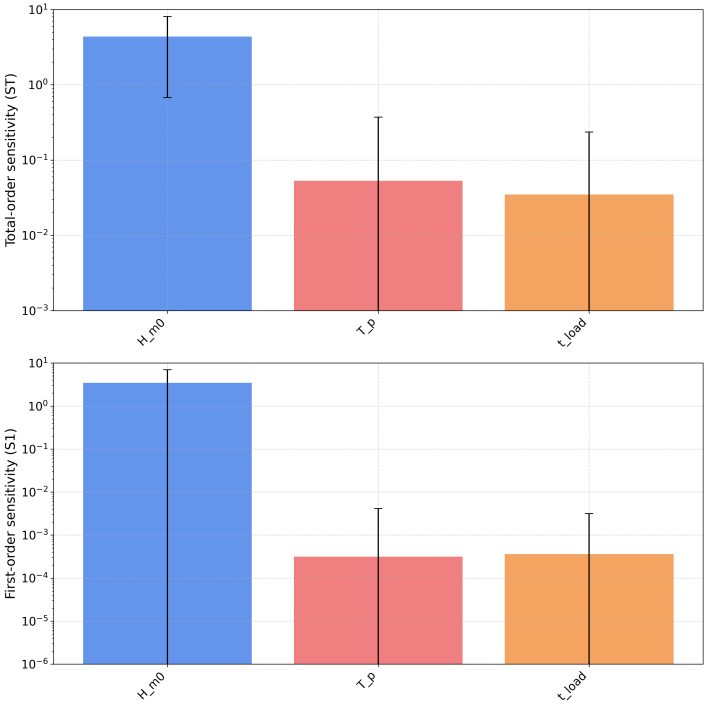
Figure D.5: Sensitivity Indices (No vegetation) $R = 1000$ years
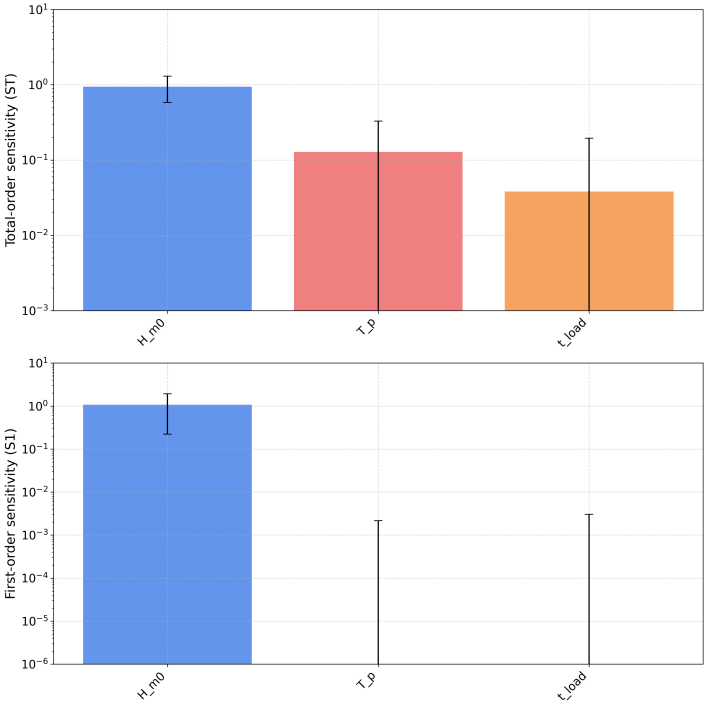
Figure D.6: Sensitivity Indices (No vegetation) $R = 3000$ years
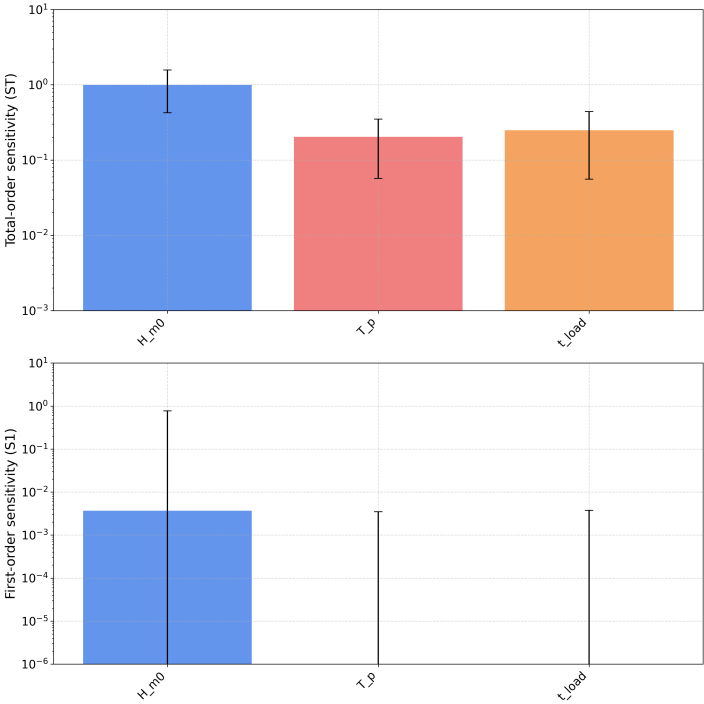
Figure D.7: Sensitivity Indices (No vegetation) $R = 10000$ years
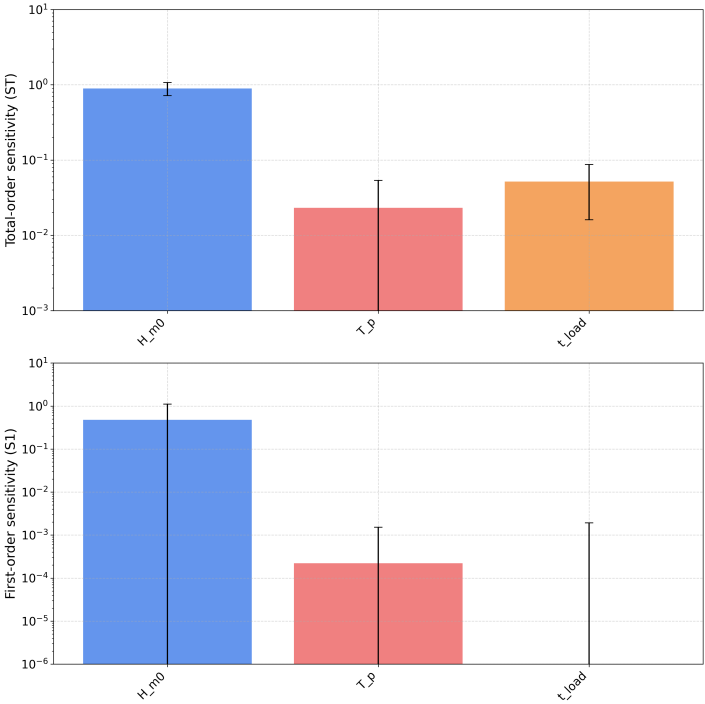
Figure D.8: Sensitivity Indices (No vegetation) $R = 30000$ years
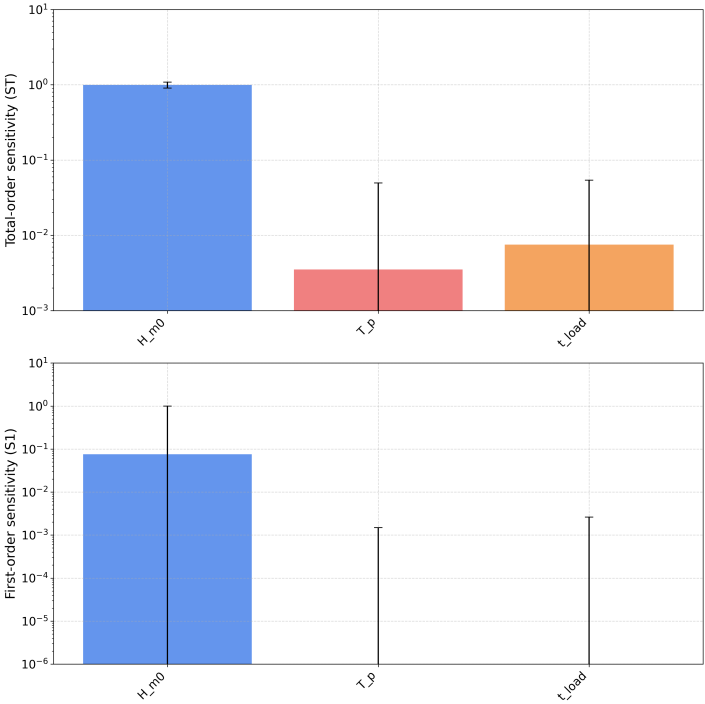
Figure D.9: Sensitivity Indices (No vegetation) $R = 100000$ years

D.1.2. With vegetation

(a) Sensitivity Indices (Vegetation: $C_D = 0.70$)

(b) Sensitivity Indices (Vegetation: $C_D = 1.20$)
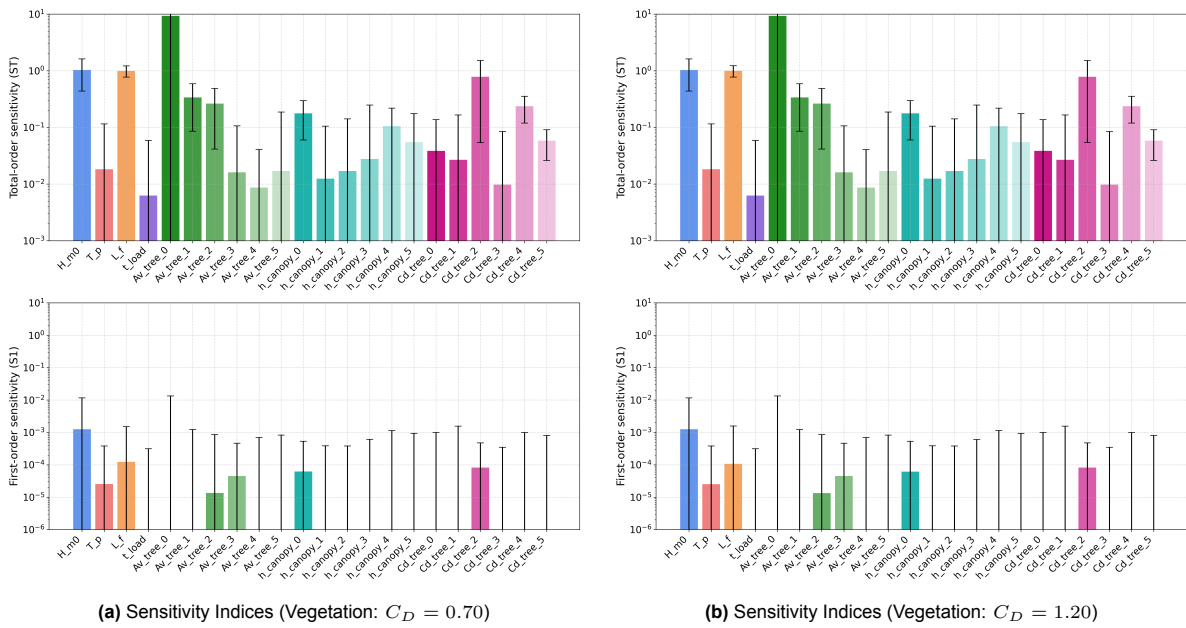
Figure D.10: Sensitivity Indices for the situation with vegetation and $R = 10$ years

(a) Sensitivity Indices (Vegetation: $C_D = 0.70$)

(b) Sensitivity Indices (Vegetation: $C_D = 1.20$)
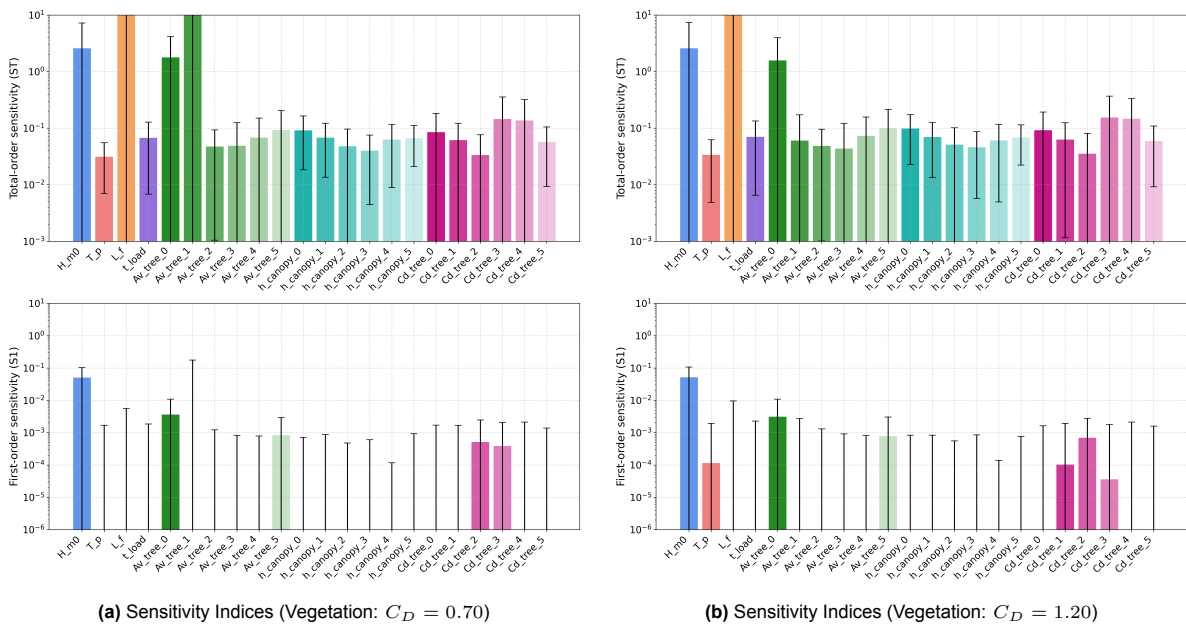
Figure D.11: Sensitivity Indices for the situation with vegetation and $R = 30$ years

(a) Sensitivity Indices (Vegetation: $C_D = 0.70$)

(b) Sensitivity Indices (Vegetation: $C_D = 1.20$)
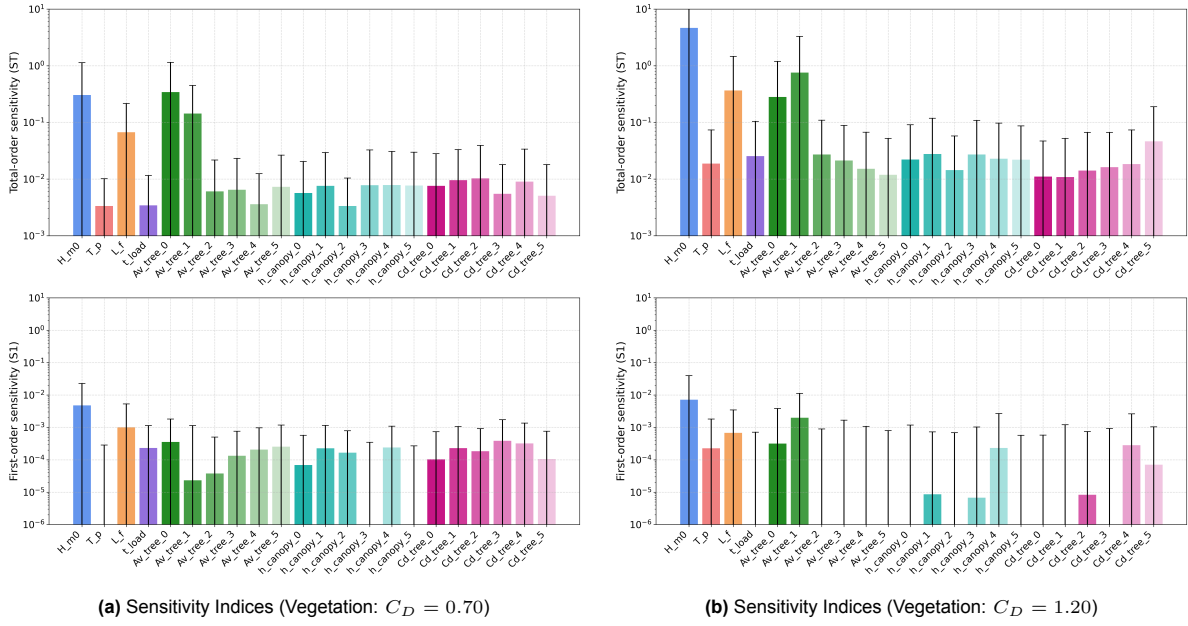
Figure D.12: Sensitivity Indices for the situation with vegetation and $R = 100$ years

(a) Sensitivity Indices (Vegetation: $C_D = 0.70$)

(b) Sensitivity Indices (Vegetation: $C_D = 1.20$)
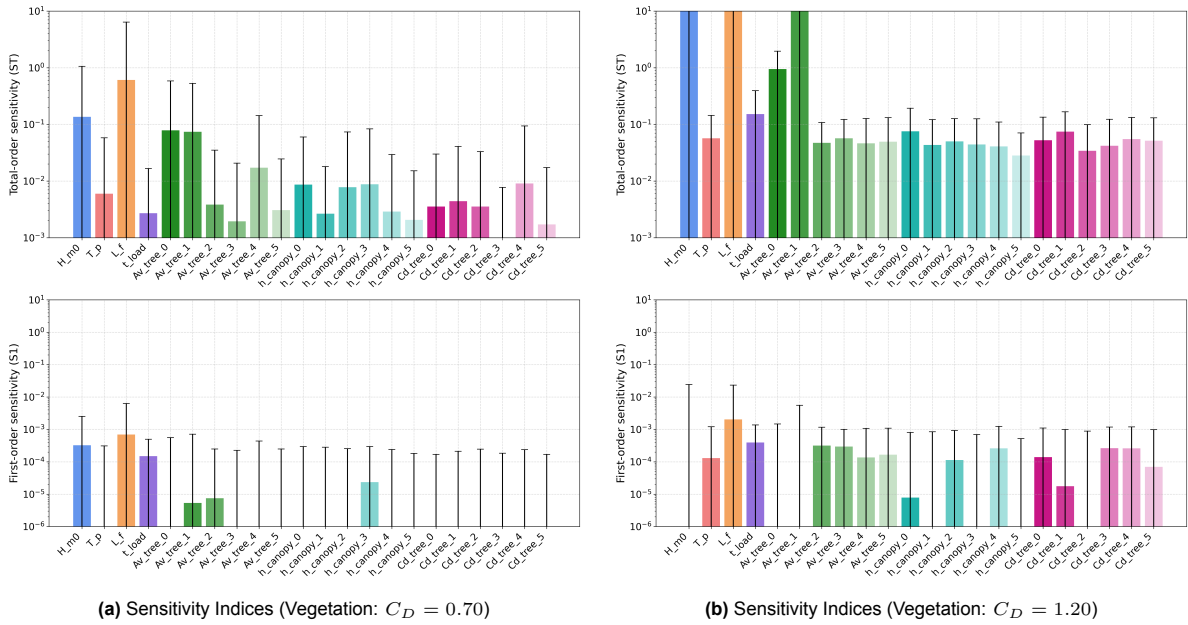
Figure D.13: Sensitivity Indices for the situation with vegetation and $R = 300$ years

(a) Sensitivity Indices (Vegetation: $C_D = 0.70$)

(b) Sensitivity Indices (Vegetation: $C_D = 1.20$)
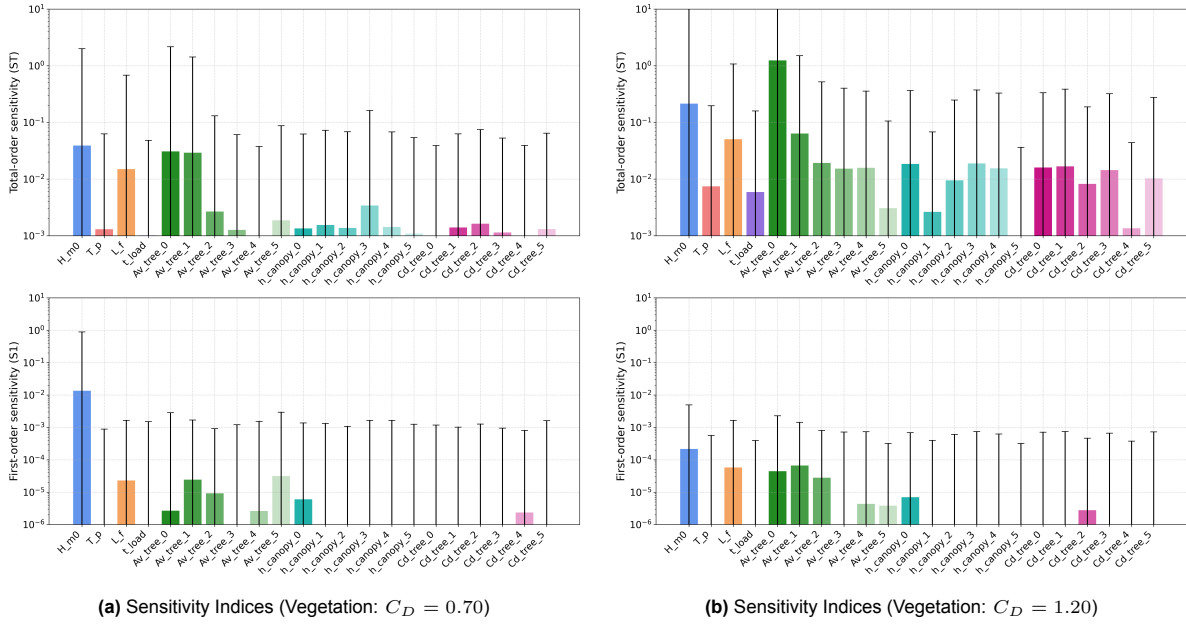
Figure D.14: Sensitivity Indices for the situation with vegetation and $R = 1000$ years

(a) Sensitivity Indices (Vegetation: $C_D = 0.70$)

(b) Sensitivity Indices (Vegetation: $C_D = 1.20$)
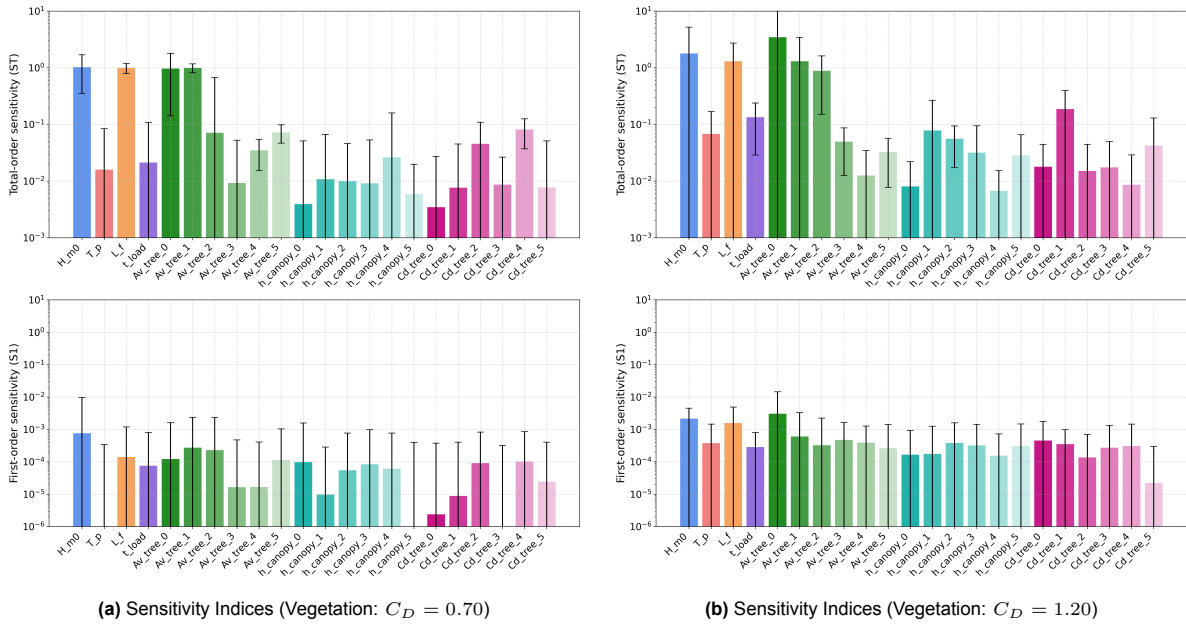
Figure D.15: Sensitivity Indices for the situation with vegetation and $R = 3000$ years

(a) Sensitivity Indices (Vegetation: $C_D = 0.70$)

(b) Sensitivity Indices (Vegetation: $C_D = 1.20$)
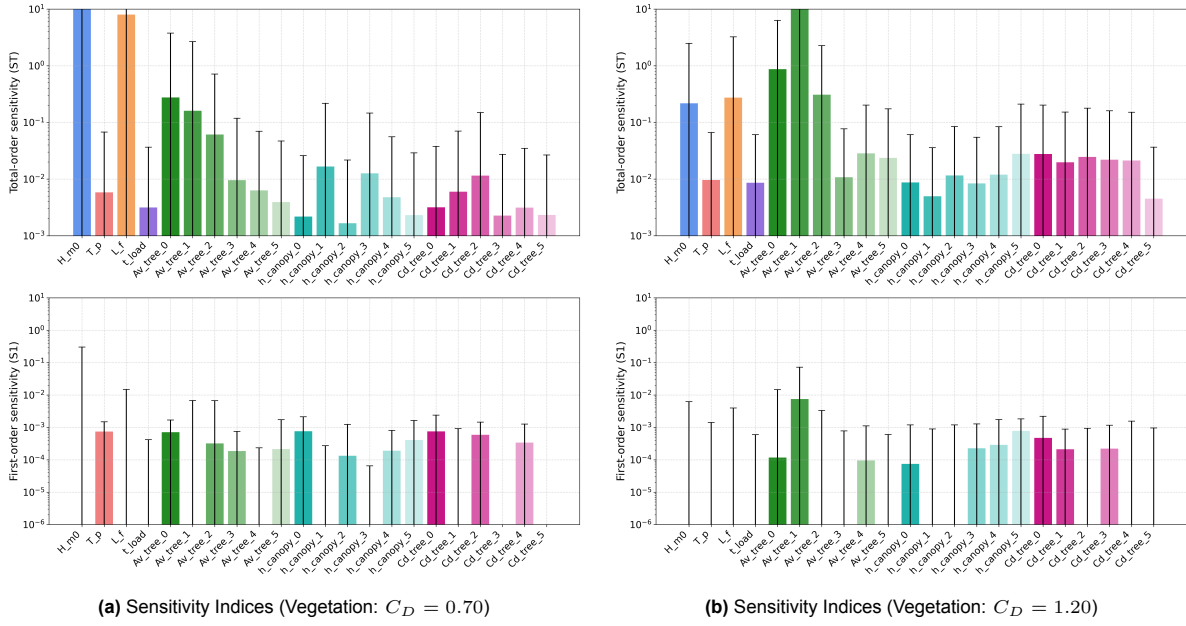
Figure D.16: Sensitivity Indices for the situation with vegetation and $R = 10000$ years

(a) Sensitivity Indices (Vegetation: $C_D = 0.70$)

(b) Sensitivity Indices (Vegetation: $C_D = 1.20$)
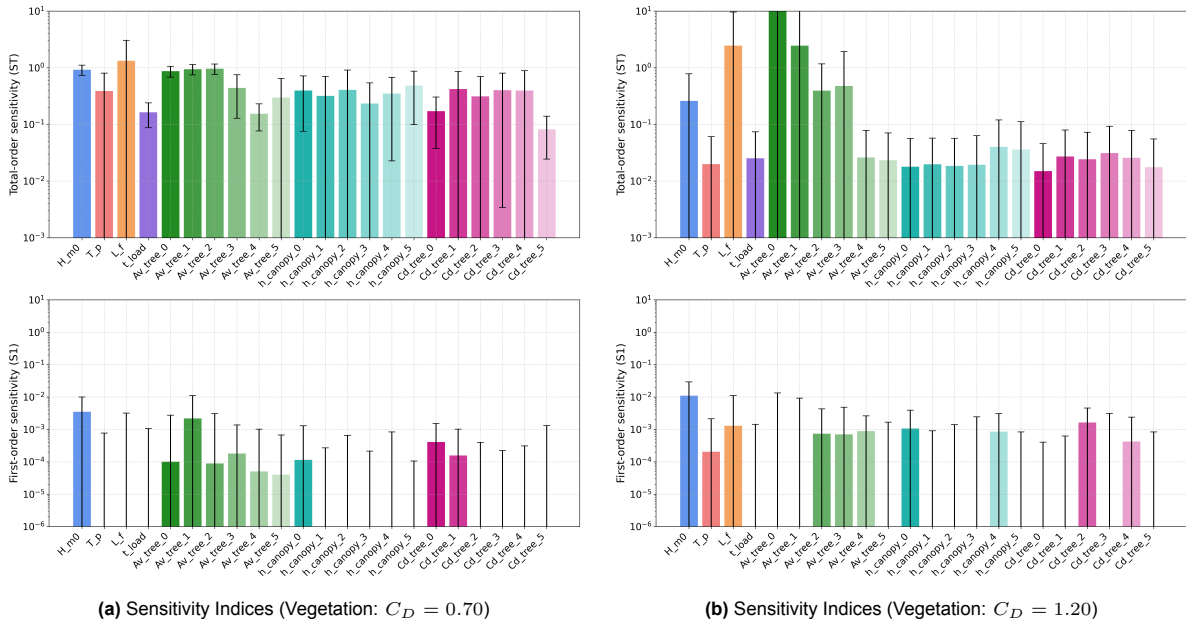
Figure D.17: Sensitivity Indices for the situation with vegetation and $R = 30000$ years

(a) Sensitivity Indices (Vegetation: $C_D = 0.70$)

(b) Sensitivity Indices (Vegetation: $C_D = 1.20$)
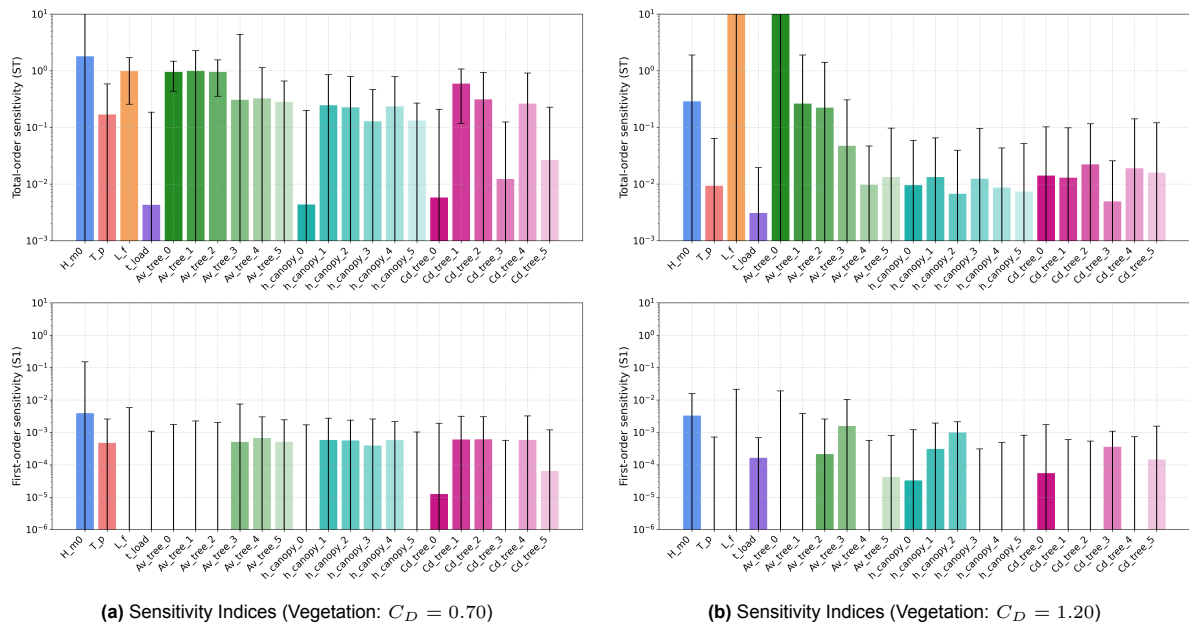
Figure D.18: Sensitivity Indices for the situation with vegetation and $R = 100000$ years

D.2. Pie charts
D.2.1. Without vegetation
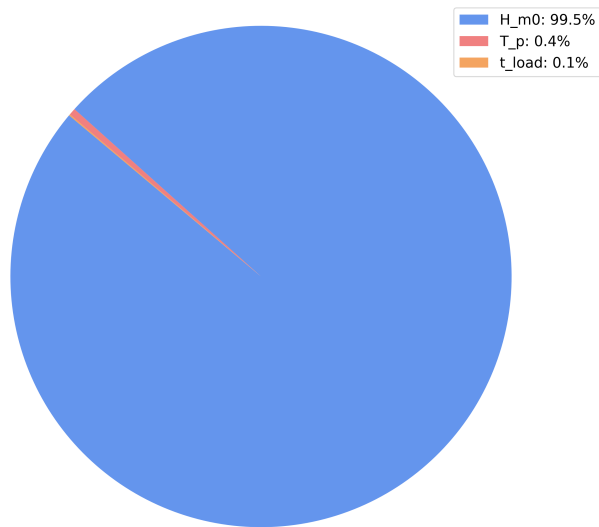
Figure D.19: Pie chart (No vegetation) $R = 10$ years
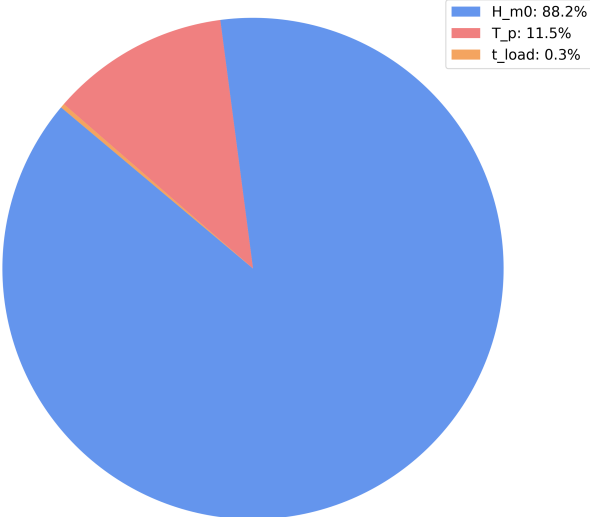
Figure D.20: Pie chart (No vegetation) $R = 30$ years
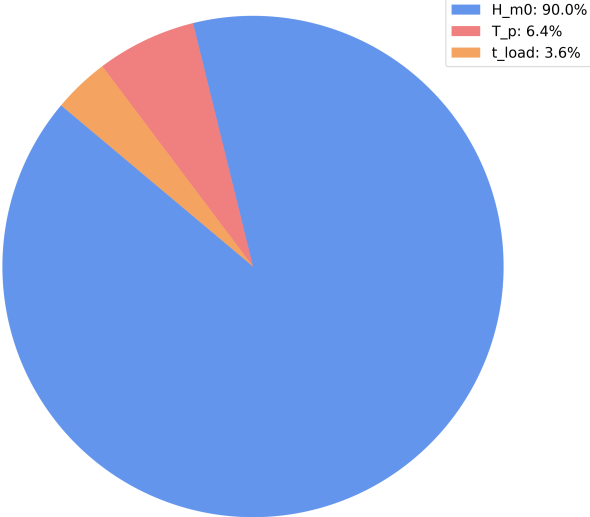
Figure D.21: Pie chart (No vegetation) $R = 100$ years
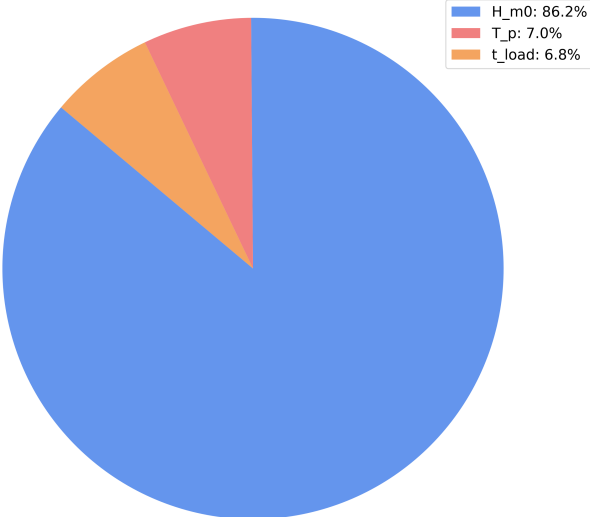
Figure D.22: Pie chart (No vegetation) $R = 300$ years
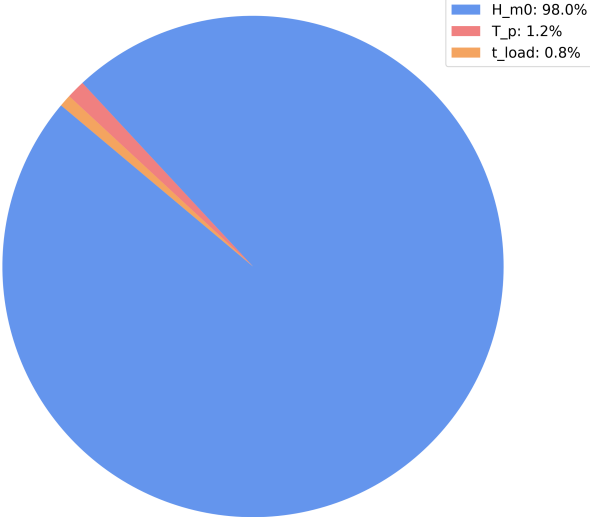
Figure D.23: Pie chart (No vegetation) $R = 1000$ years
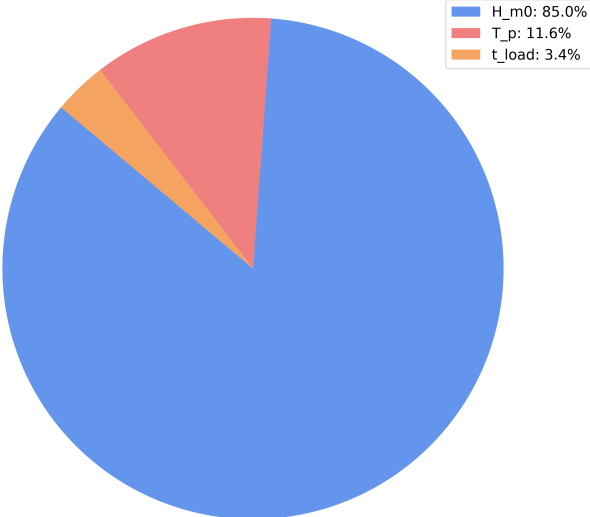
Figure D.24: Pie chart (No vegetation) $R = 3000$ years
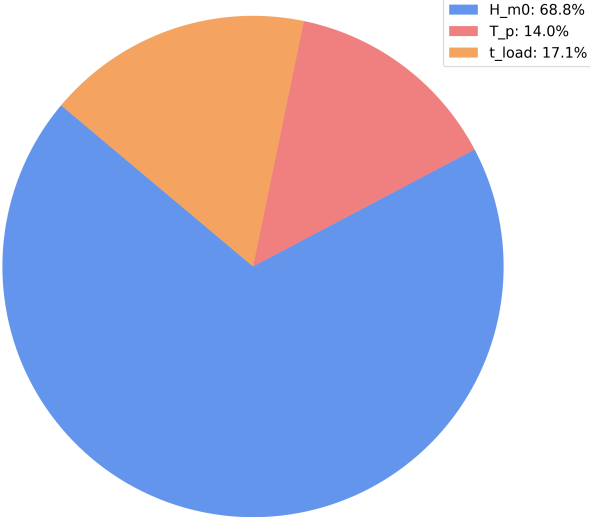
Figure D.25: Pie chart (No vegetation) $R = 10000$ years
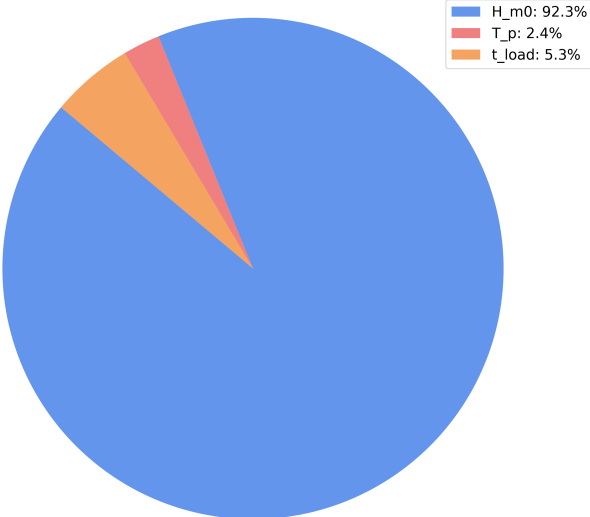
Figure D.26: Pie chart (No vegetation) $R = 30000$ years
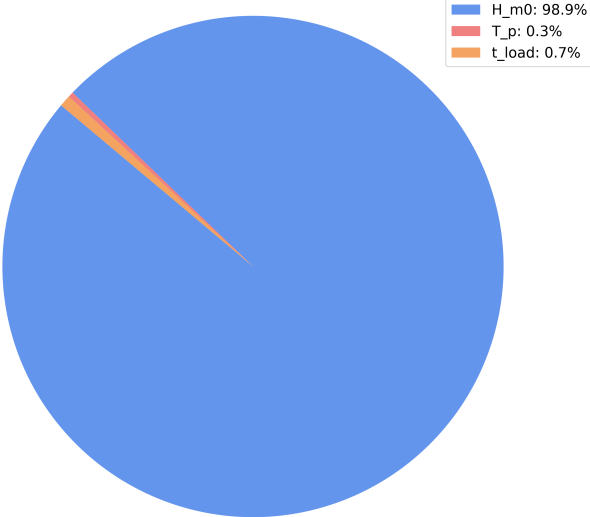
Figure D.27: Pie chart (No vegetation) $R = 100000$ years

D.2.2. With vegetation

(a) Pie chart (No vegetation: $C_D = 0.70$)

(b) Pie chart (No vegetation: $C_D = 1.20$)
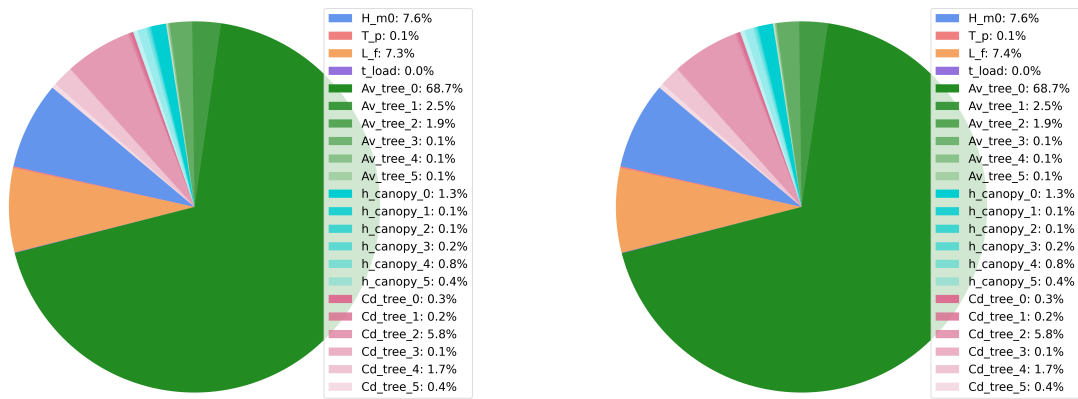
Figure D.28: Pie chart for the situation without vegetation and $R = 10$ years

(a) Pie chart (No vegetation: $C_D = 0.70$)

(b) Pie chart (No vegetation: $C_D = 1.20$)
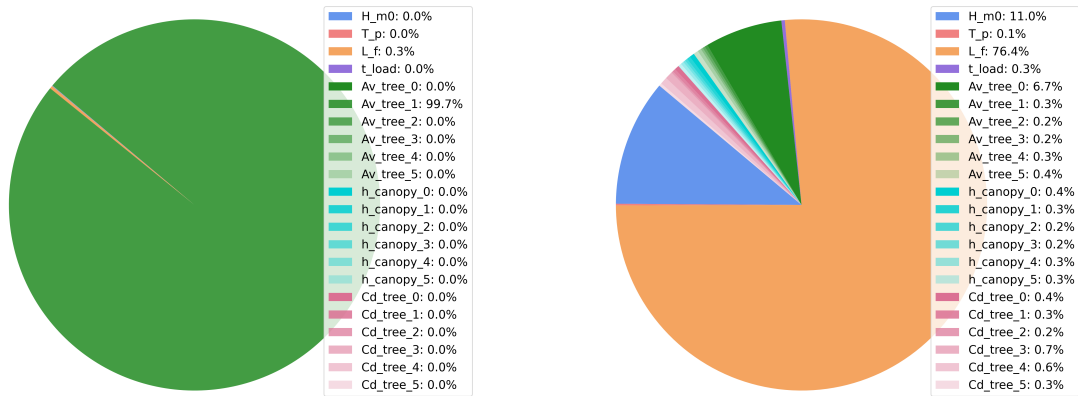
Figure D.29: Pie chart for the situation without vegetation and $R = 30$ years
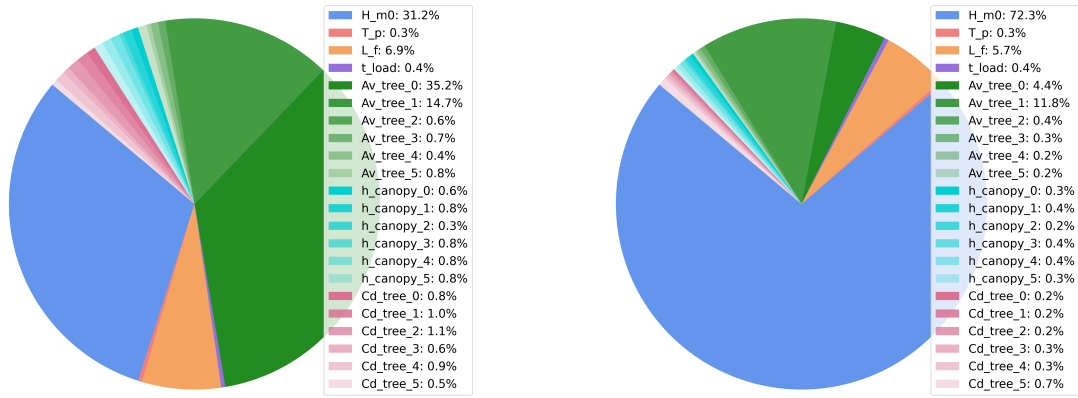
(a) Pie chart (No vegetation: $C_D = 0.70$)

(b) Pie chart (No vegetation: $C_D = 1.20$)

Figure D.30: Pie chart for the situation without vegetation and $R = 100$ years
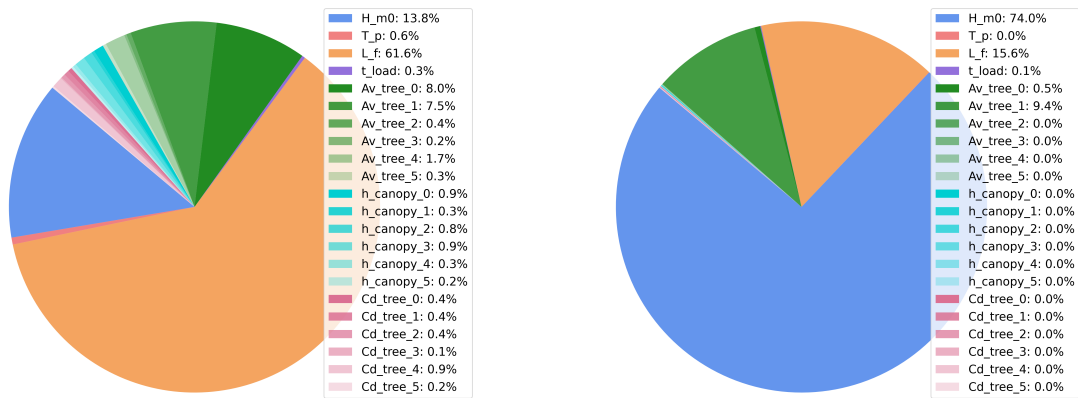
(a) Pie chart (No vegetation: $C_D = 0.70$)

(b) Pie chart (No vegetation: $C_D = 1.20$)

Figure D.31: Pie chart for the situation without vegetation and $R = 300$ years
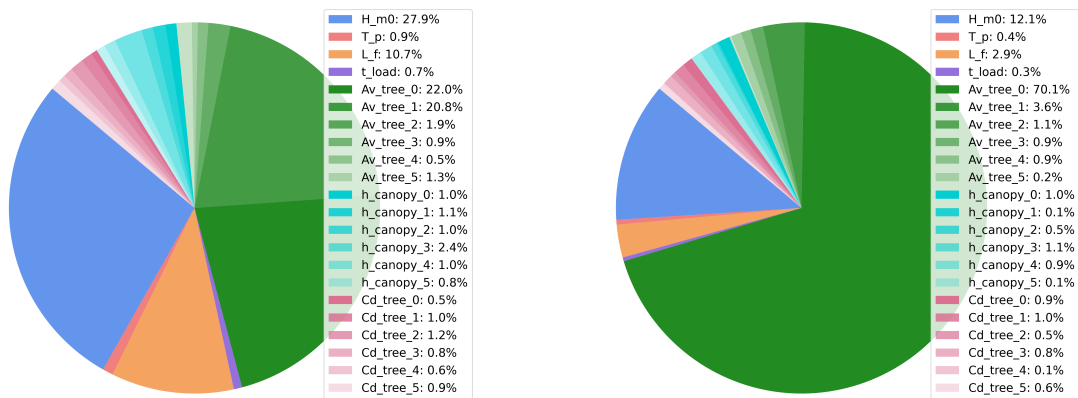
(a) Pie chart (No vegetation: $C_D = 0.70$)

(b) Pie chart (No vegetation: $C_D = 1.20$)

Figure D.32: Pie chart for the situation without vegetation and $R = 1000$ years
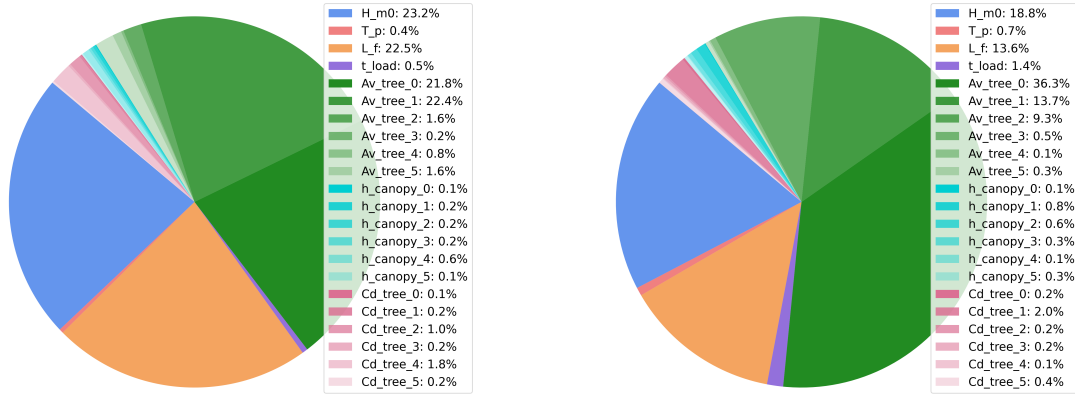
(a) Pie chart (No vegetation: $C_D = 0.70$)

(b) Pie chart (No vegetation: $C_D = 1.20$)

Figure D.33: Pie chart for the situation without vegetation and $R = 3000$ years
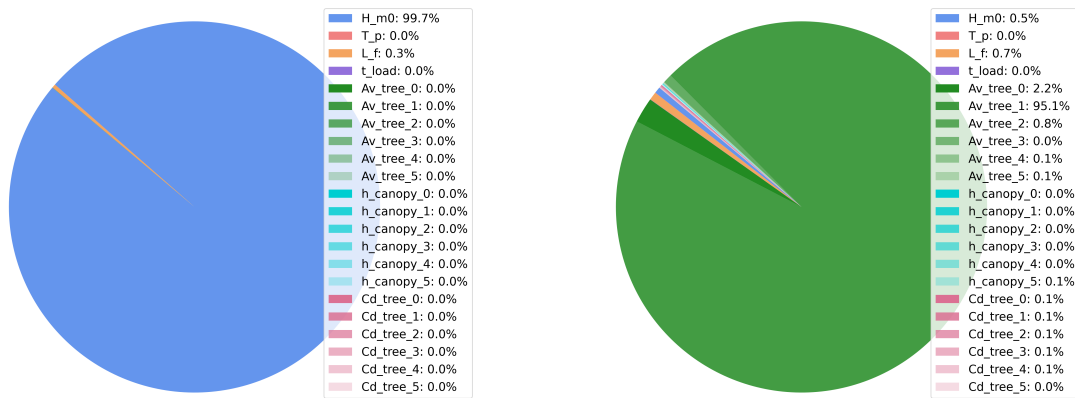
(a) Pie chart (No vegetation: $C_D = 0.70$)

(b) Pie chart (No vegetation: $C_D = 1.20$)

Figure D.34: Pie chart for the situation without vegetation and $R = 10000$ years
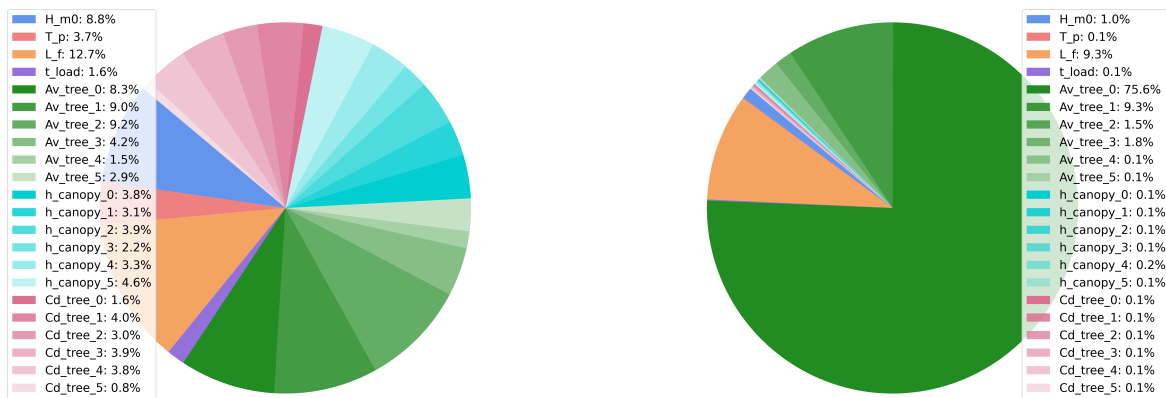
(a) Pie chart (No vegetation: $C_D = 0.70$)

(b) Pie chart (No vegetation: $C_D = 1.20$)

Figure D.35: Pie chart for the situation without vegetation and $R = 30000$ years
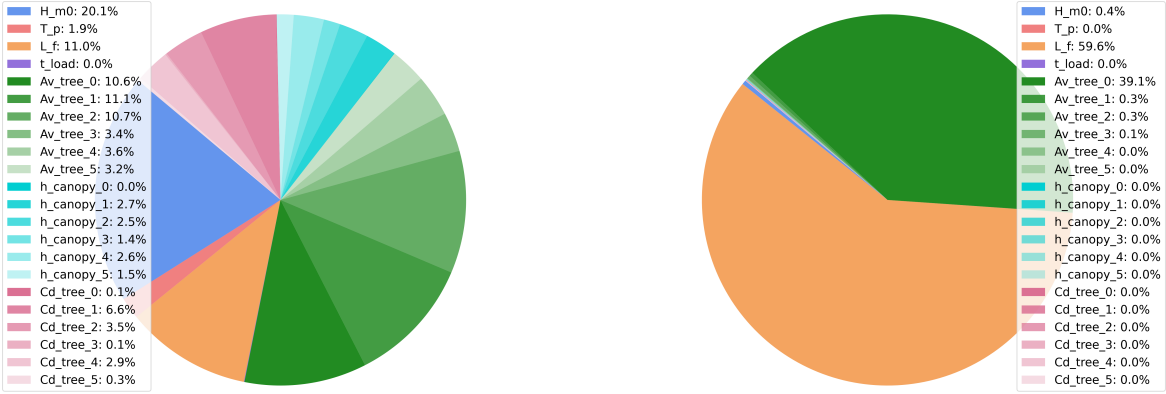
(a) Pie chart (No vegetation: $C_D = 0.70$)

(b) Pie chart (No vegetation: $C_D = 1.20$)

Figure D.36: Pie chart for the situation without vegetation and $R = 100000$ years

Sensitivity Analysis tables

E.1. Tables scenario no forest

Parameter	Unit	Elevation level	1.607	1.891	2.188	2.46	2.779	3.062	3.341	3.551	3.723	[mNAP]
		Return period	10	30	100	300	1,000	3,000	10,000	30,000	100,000	[1/years]
												Avg.
H_m0	[m]		99.5%	88.2%	90.0%	86.2%	98.0%	85.0%	68.8%	92.3%	98.9%	89.7%
T_p	[s]		0.4%	11.5%	6.4%	7.0%	1.2%	11.6%	14.0%	2.4%	0.3%	6.1%
t_load	[h]		0.1%	0.3%	3.6%	6.8%	0.8%	3.4%	17.1%	5.3%	0.7%	4.2%

Figure E.1: sensitivity indices (S_i) for the scenario without vegetation ($L_{forest} = 100$ meter)

Parameter	Unit	Elevation level	1.607	1.891	2.188	2.46	2.779	3.062	3.341	3.551	3.723	[mNAP]
		Return period	10	30	100	300	1,000	3,000	10,000	30,000	100,000	[1/years]
												Avg.
H_m0	[m]		98.8%	99.2%	99.4%	75.0%	99.7%	98.2%	95.4%	93.7%	82.2%	93.5%
T_p	[s]		0.7%	0.6%	0.3%	21.1%	0.3%	1.2%	4.5%	3.2%	12.1%	4.9%
t_load	[h]		0.5%	0.2%	0.3%	3.9%	0.0%	0.6%	0.1%	3.1%	5.7%	1.6%

Figure E.2: sensitivity indices (S_i) for the scenario without vegetation ($L_{forest} = 40$ meter)

E.1.1. Tables scenario forest (Cd = 0.70)

Parameter	Unit	Elevation level	1.607	1.891	2.188	2.46	2.779	3.062	3.341	3.551	3.723	[mNAP]
		Return period	10	30	100	300	1,000	3,000	10,000	30,000	100,000	[1/years]
												Avg.
H_m0	[m]		7.6%	0.0%	31.2%	13.8%	27.9%	23.2%	99.7%	8.8%	20.1%	25.8%
T_p	[s]		0.1%	0.0%	0.3%	0.6%	0.9%	0.4%	0.0%	3.7%	1.9%	0.9%
t_load	[h]		0.0%	0.0%	0.4%	0.3%	0.7%	0.5%	0.0%	1.6%	0.0%	0.4%
L_f	[m]		7.3%	0.3%	6.9%	61.6%	10.7%	22.5%	0.3%	12.7%	11.0%	14.8%
Av_tree_0	[m/tree]		68.7%	0.0%	35.2%	8.0%	22.0%	21.8%	0.0%	8.3%	10.6%	19.4%
Av_tree_1	[m/tree]		2.5%	99.7%	14.7%	7.5%	20.8%	22.4%	0.0%	9.0%	11.1%	20.9%
Av_tree_2	[m/tree]		1.9%	0.0%	0.6%	0.4%	1.9%	1.6%	0.0%	9.2%	10.7%	2.9%
Av_tree_3	[m/tree]		0.1%	0.0%	0.7%	0.2%	0.9%	0.2%	0.0%	4.2%	3.4%	1.1%
Av_tree_4	[m/tree]		0.1%	0.0%	0.4%	1.7%	0.5%	0.8%	0.0%	1.5%	3.6%	1.0%
Av_tree_5	[m/tree]		0.1%	0.0%	0.8%	0.3%	1.3%	1.6%	0.0%	2.9%	3.2%	1.1%
h_tree_0	[m]		1.3%	0.0%	0.6%	0.9%	1.0%	0.1%	0.0%	3.8%	0.0%	0.9%
h_tree_1	[m]		0.1%	0.0%	0.8%	0.3%	1.1%	0.2%	0.0%	3.1%	2.7%	0.9%
h_tree_2	[m]		0.1%	0.0%	0.3%	0.8%	1.0%	0.2%	0.0%	3.9%	2.5%	1.0%
h_tree_3	[m]		0.2%	0.0%	0.8%	0.9%	2.4%	0.2%	0.0%	2.2%	1.4%	0.9%
h_tree_4	[m]		0.8%	0.0%	0.8%	0.3%	1.0%	0.6%	0.0%	3.3%	2.6%	1.0%
h_tree_5	[m]		0.4%	0.0%	0.8%	0.2%	0.8%	0.1%	0.0%	4.6%	1.5%	0.9%

Figure E.3: sensitivity indices (S_i) for the scenario without vegetation ($L_{forest} = 100$ meter)

	Elevation level	1.607	1.891	2.188	2.46	2.779	3.062	3.341	3.551	3.723	[mNAP]
	Return period	10	30	100	300	1,000	3,000	10,000	30,000	100,000	[1/years]
Parameter	Unit										Avg.
H_m0	[m]	23.6%	22.2%	0.8%	0.9%	91.6%	2.0%	19.9%	15.0%	1.0%	19.7%
T_p	[s]	2.3%	2.2%	0.2%	0.0%	0.0%	0.0%	0.5%	1.0%	0.0%	0.7%
L_f	[m]	31.5%	13.9%	1.6%	97.7%	0.2%	43.8%	13.9%	28.6%	97.9%	36.6%
t_load	[h]	0.8%	3.2%	0.2%	0.1%	0.0%	0.0%	0.5%	0.8%	0.0%	0.6%
Av_tree_0	[m/tree]	27.3%	13.4%	0.7%	0.2%	2.6%	52.3%	11.4%	3.8%	0.3%	12.4%
Av_tree_1	[m/tree]	0.9%	2.7%	94.5%	0.1%	2.5%	1.2%	13.5%	11.1%	0.2%	14.1%
Av_tree_2	[m/tree]	0.3%	2.9%	0.1%	0.0%	0.0%	0.3%	19.2%	21.1%	0.2%	4.9%
Av_tree_3	[m/tree]	0.2%	3.5%	0.1%	0.0%	0.4%	0.0%	0.3%	1.9%	0.1%	0.7%
Av_tree_4	[m/tree]	0.9%	3.4%	0.1%	0.1%	0.4%	0.0%	2.3%	2.2%	0.0%	1.0%
Av_tree_5	[m/tree]	2.9%	3.4%	0.1%	0.0%	0.1%	0.0%	0.5%	1.3%	0.0%	0.9%
h_tree_0	[m]	0.5%	4.2%	0.1%	0.1%	0.6%	0.0%	2.2%	0.8%	0.0%	0.9%
h_tree_1	[m]	0.2%	3.1%	0.2%	0.1%	0.1%	0.0%	1.7%	2.1%	0.0%	0.8%
h_tree_2	[m]	0.6%	3.4%	0.2%	0.0%	0.0%	0.0%	0.6%	0.7%	0.0%	0.6%
h_tree_3	[m]	0.3%	2.0%	0.0%	0.1%	0.2%	0.0%	3.3%	0.8%	0.0%	0.7%
h_tree_4	[m]	3.6%	2.4%	0.1%	0.0%	0.0%	0.0%	1.5%	1.1%	0.0%	1.0%
h_tree_5	[m]	0.2%	2.8%	0.2%	0.1%	0.2%	0.0%	0.4%	0.8%	0.0%	0.5%

Figure E.4: sensitivity indices (S_i) for the scenario without vegetation ($L_{forest} = 40$ meter)

E.1.2. Tables scenario forest (Cd = 1.20)

	Elevation level	1.607	1.891	2.188	2.46	2.779	3.062	3.341	3.551	3.723	[mNAP]
	Return period	10	30	100	300	1,000	3,000	10,000	30,000	100,000	[1/years]
Parameter	Unit										Avg.
H_m0	[m]	7.6%	11.0%	72.3%	74.0%	12.1%	18.8%	0.5%	1.0%	0.4%	22.0%
T_p	[s]	0.1%	0.1%	0.3%	0.0%	0.4%	0.7%	0.0%	0.1%	0.0%	0.2%
t_load	[h]	0.0%	0.3%	0.4%	0.1%	0.3%	1.4%	0.0%	0.1%	0.0%	0.3%
L_f	[m]	7.4%	76.4%	5.7%	15.6%	2.9%	13.6%	0.7%	9.3%	59.6%	21.2%
Av_tree_0	[m/tree]	68.7%	6.7%	4.4%	0.5%	70.1%	36.3%	2.2%	75.6%	39.1%	33.7%
Av_tree_1	[m/tree]	2.5%	0.3%	11.8%	9.4%	3.6%	13.7%	95.1%	9.3%	0.3%	16.2%
Av_tree_2	[m/tree]	1.9%	0.2%	0.4%	0.0%	1.1%	9.3%	0.8%	1.5%	0.3%	1.7%
Av_tree_3	[m/tree]	0.1%	0.2%	0.3%	0.0%	0.9%	0.5%	0.0%	1.8%	0.1%	0.4%
Av_tree_4	[m/tree]	0.1%	0.3%	0.2%	0.0%	0.9%	0.1%	0.1%	0.1%	0.0%	0.2%
Av_tree_5	[m/tree]	0.1%	0.4%	0.2%	0.0%	0.2%	0.3%	0.1%	0.1%	0.0%	0.2%
h_tree_0	[m]	1.3%	0.4%	0.3%	0.0%	1.0%	0.1%	0.0%	0.1%	0.0%	0.4%
h_tree_1	[m]	0.1%	0.3%	0.4%	0.0%	0.1%	0.8%	0.0%	0.1%	0.0%	0.2%
h_tree_2	[m]	0.1%	0.2%	0.2%	0.0%	0.5%	0.6%	0.0%	0.1%	0.0%	0.2%
h_tree_3	[m]	0.2%	0.2%	0.4%	0.0%	1.1%	0.3%	0.0%	0.1%	0.0%	0.3%
h_tree_4	[m]	0.8%	0.3%	0.4%	0.0%	0.9%	0.1%	0.0%	0.2%	0.0%	0.3%
h_tree_5	[m]	0.4%	0.3%	0.3%	0.0%	0.1%	0.3%	0.1%	0.1%	0.0%	0.2%

Figure E.5: sensitivity indices (S_i) for the scenario without vegetation ($L_{forest} = 100$ meter)

	Elevation level	1.607	1.891	2.188	2.46	2.779	3.062	3.341	3.551	3.723	[mNAP]
	Return period	10	30	100	300	1,000	3,000	10,000	30,000	100,000	[1/years]
Parameter	Unit										Avg.
H_m0	[m]	23.6%	22.2%	35.3%	3.6%	2.3%	4.9%	2.3%	10.1%	14.2%	13.2%
T_p	[s]	2.3%	2.2%	0.1%	1.6%	0.8%	0.4%	0.2%	1.4%	0.3%	1.0%
t_load	[h]	0.8%	3.2%	1.3%	0.5%	1.1%	0.3%	0.1%	0.3%	0.1%	0.9%
L_f	[m]	31.5%	13.9%	23.1%	2.4%	3.8%	7.4%	37.5%	43.1%	13.0%	19.5%
Av_tree_0	[m/tree]	27.3%	13.4%	13.7%	74.3%	59.9%	32.0%	25.7%	18.9%	13.3%	30.9%
Av_tree_1	[m/tree]	0.9%	2.7%	13.5%	2.6%	21.0%	7.2%	29.5%	11.6%	11.7%	11.2%
Av_tree_2	[m/tree]	0.3%	2.9%	0.4%	1.4%	1.0%	40.8%	2.2%	4.2%	13.5%	7.4%
Av_tree_3	[m/tree]	0.2%	3.5%	0.5%	1.7%	0.9%	0.3%	0.1%	0.5%	1.4%	1.0%
Av_tree_4	[m/tree]	0.9%	3.4%	0.4%	1.2%	0.8%	1.1%	0.1%	0.3%	1.1%	1.0%
Av_tree_5	[m/tree]	2.9%	3.4%	0.9%	0.1%	0.5%	0.4%	0.2%	0.3%	0.7%	1.0%
h_tree_0	[m]	0.5%	4.2%	0.2%	1.8%	0.9%	0.7%	0.1%	0.6%	1.8%	1.2%
h_tree_1	[m]	0.2%	3.1%	0.6%	0.3%	0.6%	0.4%	0.3%	0.2%	2.3%	0.9%
h_tree_2	[m]	0.6%	3.4%	0.4%	0.5%	0.8%	0.5%	0.2%	0.9%	3.4%	1.2%
h_tree_3	[m]	0.3%	2.0%	0.2%	0.7%	0.5%	0.4%	0.1%	0.9%	3.9%	1.0%
h_tree_4	[m]	3.6%	2.4%	6.0%	1.6%	0.8%	0.4%	0.1%	1.3%	2.5%	2.1%
h_tree_5	[m]	0.2%	2.8%	0.2%	0.4%	0.4%	0.3%	0.1%	0.8%	2.9%	0.9%

Figure E.6: sensitivity indices (S_i) for the scenario without vegetation ($L_{forest} = 40$ meter)